Master thesis and internship[BR]- Master's thesis : Modal analysis of a footbridge using the OMAX method[BR]- Integration internship

Auteur : Purpura, Laura
Promoteur(s) : Denoel, Vincent
Faculté : Faculté des Sciences appliquées
Diplôme : Master en ingénieur civil en aérospatiale, à finalité spécialisée en "aerospace engineering"
Année académique : 2022-2023
URI/URL : http://hdl.handle.net/2268.2/16755

Modal analysis of a footbridge using the OMAX method

Author:
Laura Purpura
Promoter:
Vincent Denoël

Jury members:
Christophe Collette
Grigorios Dimitriadis
Hüseyin Güner (V2i)

I

Acknowledgement

I would like to thank my promoters Vincent Denoël and Hüseyin Güner for their constant help and advice throughout my project, as well as the V2i staff for their help in explaining concepts, giving advice or helping realise the measurement campaigns.

I would also like to thank the jury members who took their time to evaluate this project.

This work would not be achieved without the help of my family and friends and particularly the ones who made part of the measurement campaign and helped me proofreading my work, so that I am also thankful for their help.

I am grateful for these years that brought me knowledge in various subjects, experience throughout my implication in the student association *La Centrale Des Cours - FSA* and for the numerous beautiful people that I met.

Résumé

Nom et prénom: PURPURA Laura
Titre du travail de fin d'études: Analyse modale d'une passerelle piétonne en utilisant la méthode OMAX
Section: Ingénieur en aérospatiale
Année académique: 2022-2023
Promoteurs: Vincent Denoël (ULiège) & Hüseyin Güner (V2i)

L'identification des propriétés modales d'une passerelle piétonne caractérisant son comportement vibratoire peut être réalisée grâce à des méthodes d'identification modale. L'analyse modale opérationnelle avec des forces extérieures (OMAX), prenant en compte les forces ambiantes et artificielles, présente de nombreux avantages par rapport à d'autres méthodes d'identification classiques. En effet, elle permet de couvrir une plus large bande de fréquences et d'analyser les données même quand du bruit est présent dans le système. Le but de cette thèse est donc d'étudier l'effet d'un niveau de bruit croissant sur l'identification des propriétés modales. Cela a pu être réalisé en appliquant l'algorithme d'identification de sous-espaces combinée (CSI) développée dans le livre *Subspace identification for linear systems: theory - implementation - applications* par P. Van Overschee.

Afin de tester cet algorithme, un modèle simplifié de la passerelle piétonne suspendue de Tilff a été développé sur Matlab. Des forces artificielles ainsi que des forces ambiantes ont été appliquées sur ce modèle et sa réponse a été calculée grâce à la méthode de Newmark. Deux types de bruits ont été testés: un bruit aléatoire en bande limitée et un bruit induit par des piétons marchant sur la passerelle. Comme la méthode OMAX fait l'hypothèse que le bruit est un bruit blanc Gaussien, le second cas a permis de tester l'algorithme quand le bruit était coloré (des composantes en fréquence sont dominantes). En effet, la force induite par les piétons peut être décrite comme la somme de signaux sinusoïdaux. Lorsque le bruit était hors de la bande de fréquence d'intérêt (autour d'une des fréquences de résonance de la passerelle), les propriétés modales étaient proches de la valeur identifiée avec 0% de bruit. Cependant, lorsque le bruit était dans la bande de fréquence d'intérêt, une modification du coefficient d'amortissement a pu être observée. Pour un bruit blanc, le coefficient d'amortissement décroissait au fur et à mesure que le niveau de bruit croissait. Pour le bruit induit par les piétons, le même comportement a pu être observé excepté le fait que plus le nombre de piétons augmentait, plus l'influence du piéton additionnel était moindre (montrant donc un effet de saturation). Concernant la fréquence, appliquer un bruit dans la bande de fréquence d'intérêt a causé des variations dans la fréquence identifiée contrairement au cas où le bruit était blanc. En effet, quand l'hypothèse que le bruit doit être blanc n'est pas respectée, l'algorithme considère le bruit comme un pôle de la matrice d'état A et il apparaît donc comme un pôle réel dans les diagrammes de stabilisation.

Finalement, une campagne de mesures détaillée sur le site de la passerelle de Tilff a été réalisée avec l'aide d'un shaker et de piétons marchant d'un côté à l'autre de la passerelle. L'algorithme CSI a permis d'obtenir des résultats cohérents avec une autre méthode d'identification expérimentale classique lorsqu'il n'y avait pas de bruit (piétons) dans le système. Des résultats cohérents avec la partie numérique ont été également été trouvés quand les piétons ont été ajoutés. Cependant, à la place d'évoluer vers des valeurs plus faibles, le coefficient d'amortissement évoluait vers des valeurs plus élevées. De plus, dans un système réel, le bruit n'est pas uniquement causé par les piétons mais aussi le vent, l'eau ou le traffic sous la passerelle.

Summary

Name and firstname: PURPURA Laura
Title of the Master's thesis: Modal analysis of a footbrige using the OMAX method
Section: Aerospace engineering
Academic year: 2022-2023
Promoters: Vincent Denoël (ULiège) & Hüseyin Güner (V2i)

The identification of the modal properties of a footbridge characterising its vibration behaviour can be realised thanks to modal identification methods. The Operational Modal Analysis with eXogenous forces (OMAX) method, taking both ambient and artificial excitations into account shows several advantages over classical identification methods. Indeed, it allows to cover a wider frequency range and to analyse the data even when noise is present in the system. The goal of this thesis was to study the effect of an increasing level of noise on the identification of the modal properties. This could be realised by applying the Combined Subspace Identification (CSI) algorithm developed in the book *Subspace identification for linear systems: theory - implementation - applications* by P. Van Overschee.

In order to test this algorithm, a simplified numerical model of Tilff cable-stayed footbridge was developed in Matlab. Both artificial and ambient forces were applied to that model and its response was computed with a Newmark integration method. Two types of noise were tested: a limited band random noise and the noise induced by some pedestrians walking on the footbridge. As the OMAX method makes the assumption that the noise should be a Gaussian white sequence, the second case allowed to test the algorithm when the noise was couloured (dominant frequency components). Indeed, the force induced by the pedestrians can be described by a sum of sine signals. When noise was outside the frequency range of interest (around one of the eigenfrequency of the footbridge), the modal properties were close to the identified value at 0% noise. However, when noise was inside the frequency range of interest, a modification of the damping ratio could be observed. For the random white noise, the damping ratio decreased as the level of noise increased. For the noise induced by the pedestrians, the same behaviour was observed excepted the fact that as more pedestrians were added, the influence of the added pedestrian decreased (showing a saturation behaviour). Concerning the frequency, applying a noise in the frequency range of interest would cause variations in the identified frequency contrary to the case when noise was white. Indeed, when the white noise assumption is violated, the algorithm considers noise as poles of the state matrix A and they thus appear as real poles on the stabilisation diagrams.

Finally, a detailed measurement campaign on the site of the Tilff footbridge was realised with the use of a shaker and pedestrians walking back and forth on the footbridge. The CSI algorithm provided consistent results with another classical experimental modal analysis when there was no noise (pedestrians) on the system. When the pedestrians were added, consistent results with the numerical part were found. However, instead of converging towards lower values, the damping converged towards higher values. Moreover, in a real system, the noise is not only caused by the pedestrians but also by the wind, the water or the traffic underneath the footbridge.

Nomenclature

β, γ — Parameters of Newmark method

$.^{\dagger}$ — Moore-Penrose pseudo-inverse

$.^{T}$ — Transpose of vector

$\frac{\Delta T}{T}$ — Periodicity error

Γ_i — Extended observability matrix

$\ddot{\mathbf{x}}$ — Acceleration

$\dot{\mathbf{x}}$ — Velocity

$\mathbf{C}^*$ — Generalised damping matrix

$\mathbf{F}_p$ — Force imposed by the pedestrians

$\mathbf{K}^*$ — Generalised stiffness matrix

$\mathbf{M}^*$ — Generalised mass matrix

$\mathbf{P}^*_{shaker}$ — Generalised force imposed by the shaker

$\mathbf{x}$ — Displacement

$\overline{\Gamma_i}$ — Extended observability matrix without the first l rows

ρ — Residuals

$\underline{\Gamma_i} = \Gamma_{i-1}$ — Extended observability matrix without the last l rows

A, B, C, D — Dynamical system matrices

c_{critic} — Critical damping ratio

F_p^v — Vertical pedestrian load

F_{amb} — Ambient forces

F_{art} — Artificial forces

H — Square root of the power spectral density or amplitude spectral density

h — Time step

l — Number of rows of the output data y

l_X — Length of element X

m — Number of rows of the input data u

n_p — Number of pedestrians on the footbridge

O_i — Observability matrix

P_i — Nodal forces

P_X — Random pressure applied on element X

$P_{shaker}(t)$ — Force imposed by the shaker

Q — Quality factor

R_f — Matrix of future outputs

R_p — Matrix of past inputs and outputs

R_u — Matrix of future inputs

R_{fp} — Matrix of perpendicular future outputs

R_{pp} — Matrix of perpendicular past inputs and outputs

Re — Real part operator

S — Matrix containing the singular values on its diagonal

U — Left singular vectors

V — Right singular vectors

$\alpha_{i,v}$ — Dynamical load factor

δ — Dirac delta

$\boldsymbol{\Phi}$ — Modal form/Mode shapes

$\mathbf{C}$ — Damping matrix

$\mathbf{K}$ — Stiffness matrix

$\mathbf{M}$ — Mass matrix

ω — Angular velocity

φ — Phase angle of the ith harmonic relative to the first harmonic

ζ — Damping ratio

f — Frequency

f_s — Pacing rate of the pedestrian

i	Number of block rows used in the Hankel matrices	CSI	Combined Subspace Identification
k	Pedestrian number	DOFs	Degrees of freedom
n	Order of the identified system	DSI	Deterministic Subspace Identification
T	Period	EMA	Experimental Modal Analysis
t_0	Initial phase shift of the pedestrian	FRF	Frequency Response Function
u	Inputs of the system	LHS	Left Hand Side
v_p	Forward speed of the pedestrian	OMA	Operational Modal Analysis
W	Weight of the pedestrian	OMAX	Operational Modal Analysis with eXogenous forces
x_0	Initial position of the pedestrian		
x_p	Instant position of the pedestrian	PSD	Power Spectral Density
x_{end}	Right extremity of the model of the footbridge	RHS	Right Hand Side
x_{start}	Left extremity of the model of the footbridge	rms	Root mean square
		SSI	Stochastic Subspace Identification
y	Responses of the system	svd	Singular value decomposition

Contents

Introduction

Recent improvements in design and manufacturing methods and a more efficient use of structural materials allow engineers to design slender and lighter structures such as footbridges. However, these are prone to higher levels of vibration due to ambient forces such as wind or pedestrians. For example, footbridges can be used for marathons where a large group of people would load the footbridge to higher levels causing possible structural disorders. The comfort of pedestrians must also be guaranteed under more usual loading. Therefore, it is as important to study the behaviour of the structure before its construction as to make verifications after construction. Indeed, reality is often different from simulations, and this can be revealed by dynamic testing experiments on the structure after it has been built.

The behaviour of the structure can be characterised by its modal properties or modal parameters: 1) the *eigenfrequencies* corresponding to the frequencies at which the system will oscillate, 2) the *damping ratios* showing how much the mode excited by a certain eigenfrequency is damped out and 3) the *mode shapes* showing how the structure deforms when excited at a certain eigenfrequency.

In order to identify these parameters, several approaches of dynamic testing exist. These are called modal identification or modal analysis techniques. In this work the modal analysis of a footbridge using the Operational Modal Analysis with eXogenous (OMAX) forces method will be performed. The OMAX method is a combination between Experimental Modal Analysis (EMA) and Operational Modal Analysis (OMA), so that both unmeasured ambient forces and measured artificial forces are taken into account. All these methods will be presented **Section 1** as well as their advantages, disadvantages and some applications.

The main goal of this thesis is to show what is the effect of adding an increasing level of noise on the identified modal properties, thanks to an algorithm that will take both known artificial forces and unknown ambient forces into account. To do so, the method will be applied to a numerical model but also to a real footbridge: Tilff cable-stayed footbridge in Liège, Belgium. This work is thus separated in two main sections:

Section 2 will start by the analysis of the results of a preliminary measurement campaign that was held on the Tilff cable-stayed footbridge in order to roughly extract its modal properties. These estimated properties will allow to build a simplified numerical model of a footbridge. This model will be used to test the influence of an increasing noise level on the identified modal properties. To do so, the influences of the type of measured excitation and of type of unmeasured noise on the modal properties will be investigated.

Section 3 will present the detailed measurement campaign that was held on the Tilff cable-stayed footbridge. First, the setup and protocol will be described, then the identification algorithm will be applied on the signals recorded during the detailed measurement campaign in order to obtain the identified modal parameters. The measurements will be realised with and without pedestrians in order to assess their influence on the identified modal properties for a real-life case.

1   State of the art

In this section, the different methods of dynamic identification will be presented and compared. The two main types of methods are the Experimental Modal Analysis and the Operational Modal Analysis and are chosen depending whether the excitation is measured or not, respectively. Indeed, in EMA, the forces applied on the system are known and can be applied by a shaker, impact hammer, ... Whereas in OMA, the forces used for the identification are not measured or known such as pedestrians walking on the footbridge, wind, ...

Operational Modal Analysis with eXogenous forces consists in a combination of the two previous methods, meaning that both measured and unmeasured forces are taken into account in the system. These methods are illustrated in Figure 1 and will be explained in more details in Section 1.1 for EMA, Section 1.2 for OMA and Section 1.3 for OMAX.
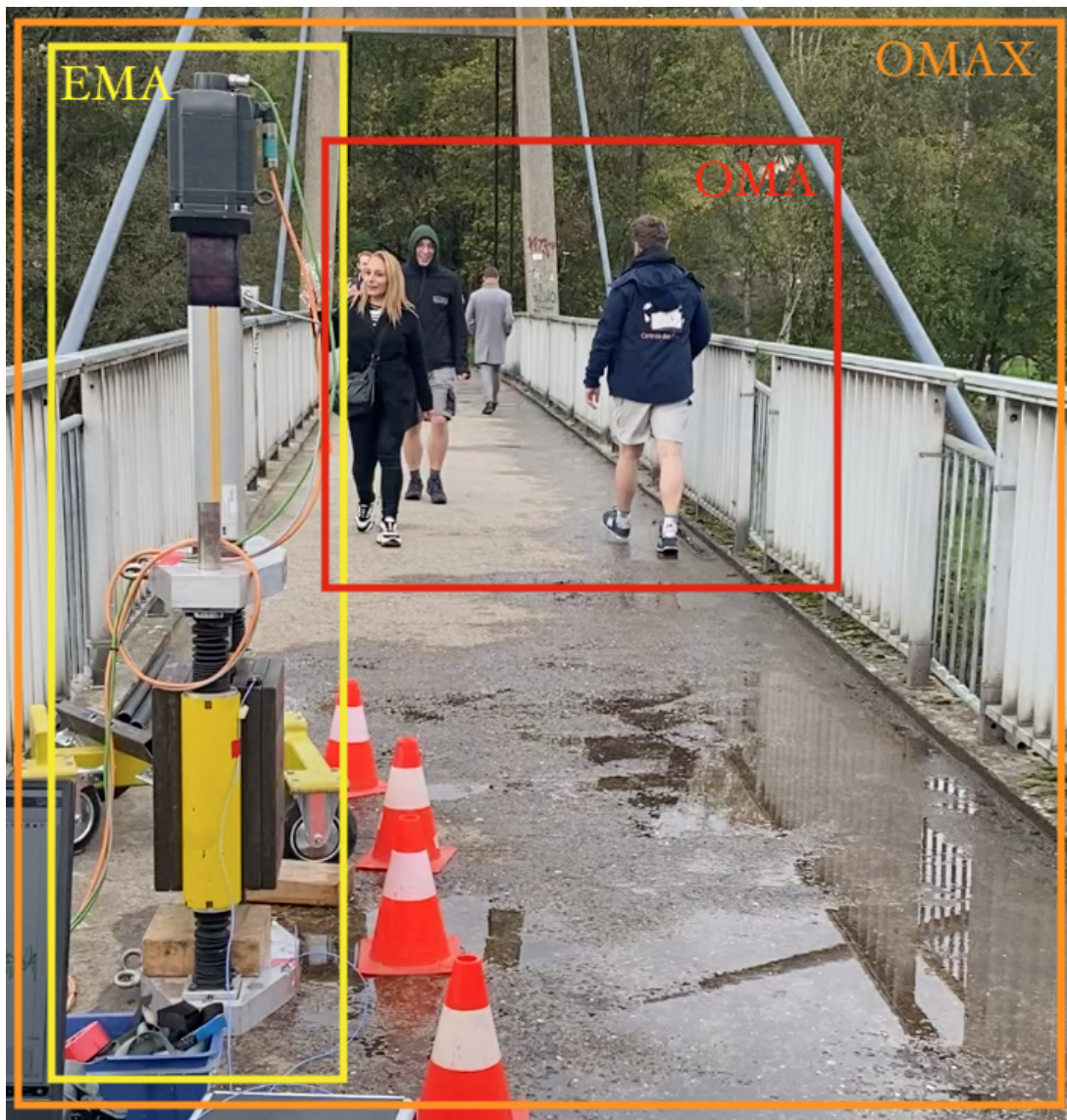

Figure 1: Illustration of the OMAX method being a combination of EMA (uses only artificial forces) and OMA (uses only ambient forces). In this figure, those forces are represented by a shaker and pedestrians respectively.

1.1   Experimental Modal Analysis

As explained previously, EMA determines the modal properties of structures by applying a known force on it, with the use of a shaker for example. Figure 2 shows the main steps of the dynamic identification methodology currently used by V2i [1].
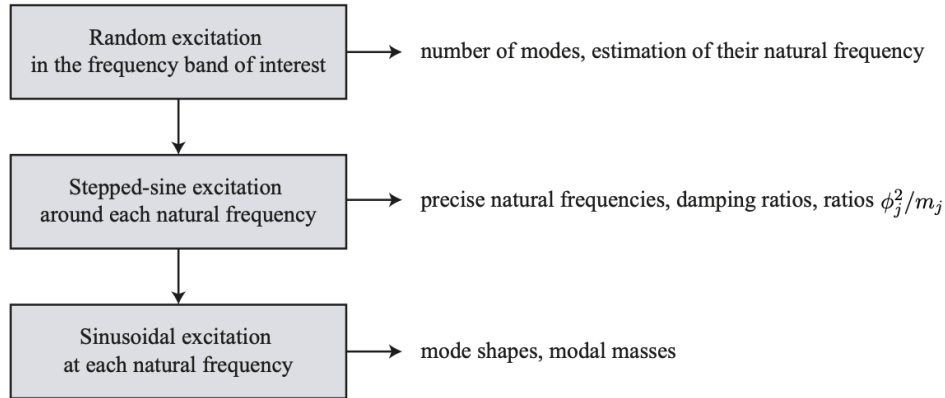

Figure 2: General methodology used by V2i to extract the modal properties of a footbridge using EMA approach [2]. The ratios ϕ_j^2/m_j represent the modal amplitude at the location of the shaker over the generalised masses. A modal mass is the mass that is activated in a certain vibration mode.

This is indeed EMA as the different excitations are applied thanks to a shaker developed by V2i and University of Liège (this one will be presented in more details in Section 3.1.1 but its characteristics can also be found in [2]). This methodology has already been tested and successfully worked in several applications where the access to the site could be limited or restricted for pedestrians, as it is mentioned in [2]. However, a study on *La Belle Liégeoise* footbridge (that can be found in the same article) questioned the validity of the approach when the traffic could not be limited. In this measurement campaign, the attention was drawn on the vertical modes situated between 1.6 and 2.7 Hz, in the central part of the footbridge, which are the frequencies that are the most likely to be excited by the pedestrians [3]. This campaign was quite challenging due to the high level of the ambient forces (traffic). Indeed, only the modes outside the frequency range affected by the traffic could be identified accurately. A solution could be to use higher levels of shaker, so that the percentage of noise is reduced. However, this would result in a heavier and unpractical device. Indeed, in order to obtain all the modes accurately, sometimes the shaker needs to be moved to another position on the footbridge.

1.2   Operational Modal Analysis

OMA studies the structures under ambient vibrations or normal operating conditions. Those types of vibration are generally not quantifiable. It could be pedestrians, wind, water, ... So that only the response of the structure is measured. The excitation is thus assumed to be a Gaussian white noise: a random excitation having equal intensity at different frequencies. The problem with this method is that all the modal properties of the system cannot be identified. Indeed, since the excitation cannot be imposed, some modes are more excited than others by the ambient forces. Moreover, the mode shapes cannot be scaled in an absolute sense, for example to unity modal mass [4, 5], unless the measurement is repeated with a significant added mass or by removing significantly some mass

of the system [6]. This is particularly complicated for such heavy structures as footbridges.

OMA is mainly used for structural health monitoring of structures. Indeed, a change in modal properties can be observed when the structure is damaged. If cracks appear in a footbridge, they will affect the modal properties such as a change in damping ratio for example, due to the friction [7]. It should be noted that the modal characteristics can also change in function of the temperature [8]. More information can also be found in [9] concerning vibration-based structural health monitoring. However, this is beyond the scope of this work where only pedestrians loads will be considered, to keep it simple.

1.3   Operational Modal Analysis with eXogenous forces

In this work, the modal analysis of a footbridge using the OMAX method will be performed. As already mentioned, it is a combination of experimental modal analysis and operational modal analysis. So that both unmeasured ambient forces and measured artificial forces are taken into account. However, the ambient forces are considered a real part of the excitation. In other words, it is a combined operational-experimental approach used to identify the modal characteristics of the footbridges.

An algorithm called Combined Subspace Identification (CSI) has been implemented in [10] in order to take both contributions (ambient and artificial forces) into account. It consists in a generalisation of the Stochastic Subspace Identification (SSI) and Deterministic Subspace Identification (DSI). Indeed, those methods are a particular case of the CSI. The details of those two methods and many applications of the CSI algorithm can be found in [10].

The details of the CSI algorithm will be given in Section 1.3.1 but is briefly introduced here after. The response of the structure can be computed using a time integration algorithm by imposing some measured and unmeasured forces on it. Thanks to the imposed forces and the response of the structure, the CSI algorithm can be used to determine the modal properties of the structure. The process is illustrated in Figure 3.
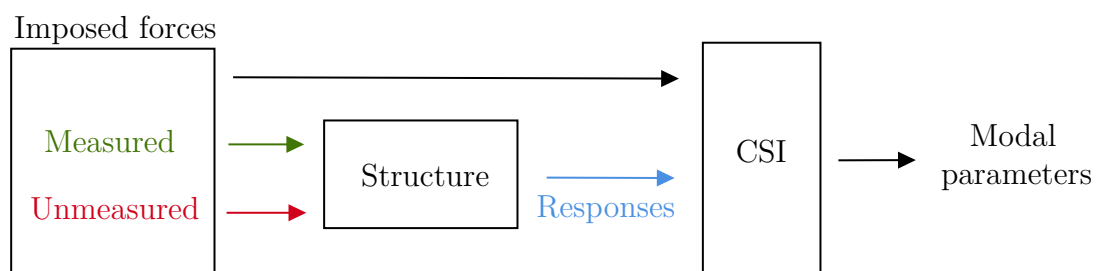
Figure 3: Methodology to determine the modal properties of a structure using the CSI algorithm.

1.3.1   Combined Subspace Identification algorithm

The CSI algorithm has been implemented in a function called *subid.m*, given in the annex files of [10]. It allows to solve the combined identification problem posed in [10]. The problem can be stated as in Figure 4.

Combined identification problem

Given s measurements of the input $u_k \in \mathbb{R}^m$ and the output $y_k \in \mathbb{R}^l$ generated by the unknown combined system of order n:

$$
\begin{aligned}
x_{k+1} &= Ax_k + Bu_k + w_k \\
y_k &= Cx_k + Du_k + v_k,
\end{aligned}
\tag{1}
$$

with A, B, C, D the dynamical system matrices, x_k the state vector of the system at sample time instant and w_k and v_k zero mean, white vector sequences with covariance matrix:

$$
\mathbf{E}[\begin{pmatrix} w_p \\ v_p \end{pmatrix} \begin{pmatrix} w_p^T & v_p^T \end{pmatrix}] = \begin{pmatrix} Q & S \\ S^T & R \end{pmatrix} \delta_{pq},
\tag{2}
$$

determine the unknowns matrices A, B, C, D, Q, S and R and the order of the identified system n.

Figure 4: Combined identification problem adapted from [10].

This problem can be solved thanks to the robust combined algorithm presented in p. 131 of [10]. A summary of this algorithm is given in Figure 5.
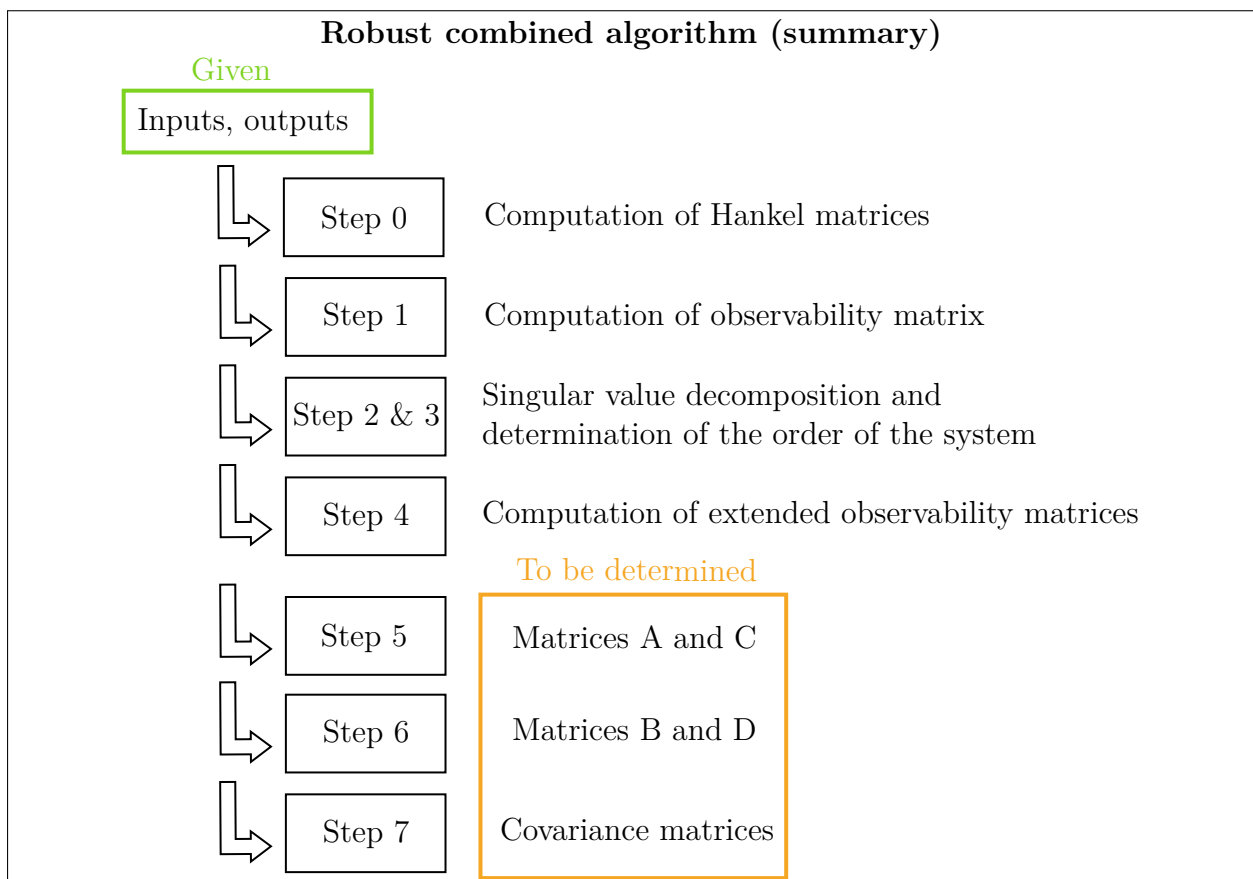
Figure 5: Summary of the main steps of the robust combined algorithm adapted from [10].

The different steps will be described in order to give a general idea of the computation of the modal properties with the CSI algorithm. Some details about the notation will not

be given explicitly, if more theoretical information is needed, one should check the page of [10] that is referenced in the text.

1.3.1.1 Step 0: Construction of the block Hankel matrices

- Block Hankel matrices are built from the outputs (or responses) y and inputs u of the system. A block Hankel matrix is a matrix constructed thanks to the given input-output data where each ascending skew-diagonal from left to right is constant. For example, input block Hankel matrix is defined as:

$$U_{0|2i-1} \overset{\text{def}}{=} \begin{pmatrix} u_0 & u_1 & u_2 & \cdots & u_{j-1} \\ u_1 & u_2 & u_3 & \cdots & u_j \\ \cdots & \cdots & \cdots & \cdots & \cdots \\ u_{i-1} & u_i & u_{i+1} & \cdots & u_{i+j-2} \\ \hline u_i & u_{i+1} & u_{i+2} & \cdots & u_{i+j-1} \\ u_{i+1} & u_{i+2} & u_{i+3} & \cdots & u_{i+j} \\ \cdots & \cdots & \cdots & \cdots & \cdots \\ u_{2i-1} & u_{2i} & u_{2i+1} & \cdots & u_{2i+j-2} \end{pmatrix} \quad \begin{matrix} \text{"past"} \\ \\ \text{"future"} \end{matrix}$$

Figure 6: Input block Hankel matrix as defined in [10].

More information about the notations and the assumptions of those matrices can be found in [10]. However, what is important to mention for the following of this thesis is that the number of blocks rows i is a user-defined index. It should be large enough *"i.e. at least larger than the maximum order of the system one wants to identify"* [10]. Indeed, the maximum order of the system that can be estimated will be equal to i times the number of outputs [10]. Theoretically, and for statistical purposes, $i \to \infty$. However, the computational time is proportional to i^2 so that a trade-off must be realised.

- A matrix composed of the input Hankel matrix followed by the output Hankel matrix is created.

- The orthogonal-triangular decomposition of this matrix is performed thanks to the *qr.m* matlab function and its triangular upper part is obtained by applying the function *triu.m*. This matrix is called R in the code, for historical reasons, but is different from the R matrix in Equation (2). Finally, one should remove the unnecessary zeros from R, so that R is a square matrix of size $2(m+l)i$ because when summing all the columns of p. 164 of [10] one has:

$$mi + m + m(i-1) + li + l + l(i-1) = 2(m+l)i. \tag{3}$$

With m, the number of rows of the input data u and l, the number of rows of the output data y.

1.3.1.2 Step 1: Computation of the observability matrix

- R matrix can be partitioned into several smaller matrices. Figure 7 shows the structure of matrix R.
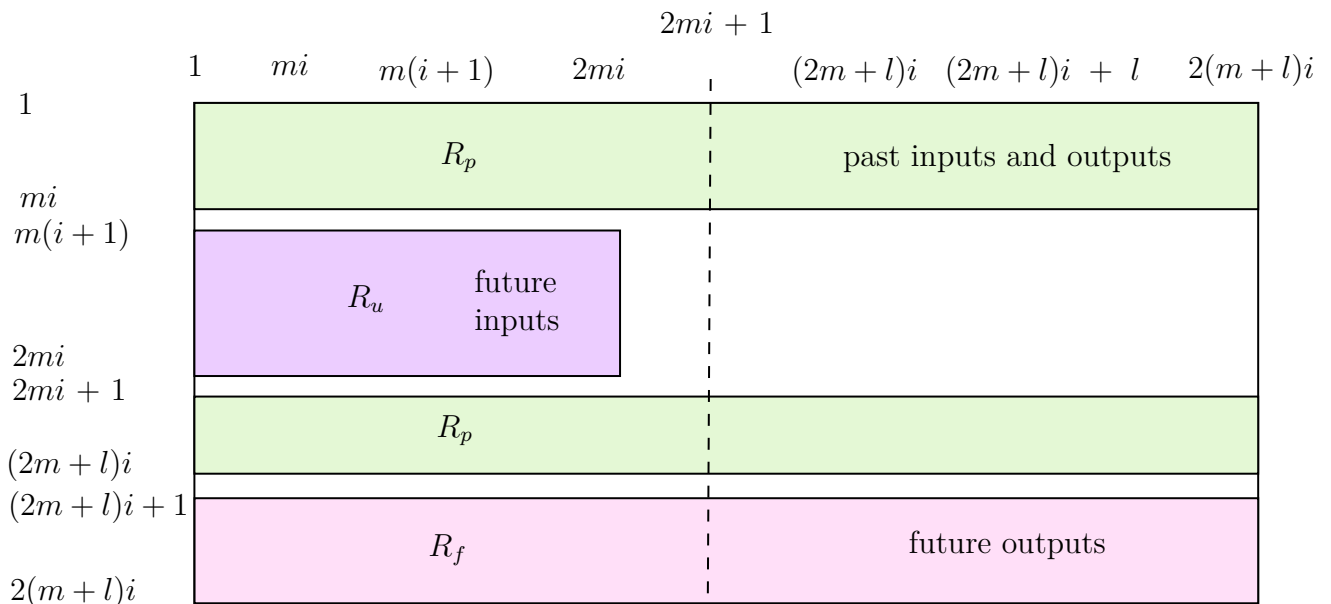
Figure 7: Structure of matrix R.

- The matrices of perpendicular future outputs R_{fp} and of perpendicular past inputs and outputs R_{pp} can also be obtained from the previously defined matrices. These matrices consist in projections of future or past outputs (R_f or R_p) onto the future inputs (R_u), and will be used to compute the observability matrix. More information about oblique projection can be found in [10].

- This observability matrix O_i is computed as defined in Equation (6.11), p. 166 of [10] so that:

$$O_i = R_{fp} * R_{pp}^\dagger * R_p, \tag{4}$$

where † denotes the Moore-Penrose pseudo-inverse (that can be computed with function *pinv* of Matlab). The observability gives a measure of how well internal states of a system can be inferred from knowledge of its external outputs.

1.3.1.3   Step 2: Singular value decomposition of the observability matrix

- Matrix WO_iW is computed by projecting the observability matrix O_i onto the future inputs R_u. The extra projection tends to give better numerical conditioning according to [10].

- The singular value decomposition (svd) of WO_iW is computed such that:

$$WO_iW = USV^T, \tag{5}$$

where U are the left singular vectors, S is a rectangular matrix with non-negative real numbers on its diagonal (the singular values), V are the right singular vectors and ^{T} denotes the transposed vector. This decomposition can be realised by applying the function *svd.m* and the singular values are obtained by taking the diagonal of matrix S.

1.3.1.4   Step 3: Determination of the order of the system

- The order of the system n can be given by the user or, if it is not, a plot is displayed in order to select the right order by inspecting the singular values in S.

- Thanks to the order of the system the singular value decomposition is partitioned in order to determine matrices U_1 and S_1.

1.3.1.5   Step 4: Computation of the extended observability matrices

- Γ_i and Γ_{i-1} are determined such as:

$$\Gamma_i = U_1 S_1^{1/2} \tag{6}$$
$$\Gamma_{i-1} = \underline{\Gamma_i}, \tag{7}$$

where Γ_i is the extended observability matrix and $\underline{\Gamma_i}$ is obtained by removing the last l rows of Γ_i.

- Their Moore-Penrose pseudo-inverse is computed and will be useful for the next step.

1.3.1.6   Step 5: Computation of matrices A and C

- The following set of linear equations can be solved to obtain A and C:

$$\underbrace{\begin{pmatrix} X_{i+1}^d \\ Y_{i/i} \end{pmatrix}}_{\text{LHS}} = \begin{pmatrix} A & B \\ C & D \end{pmatrix} \underbrace{\begin{pmatrix} X_i^d \\ U_{i/i} \end{pmatrix}}_{\text{RHS}}. \tag{8}$$

X_i^d and X_{i+1}^d should be determined such as:

$$X_i^d = \Gamma_i^\dagger O_i \quad \text{and} \quad X_{i+1}^d = \Gamma_{i-1}^\dagger O_{i-1}. \tag{9}$$

The explanation of the notation $\cdot_{i/i}$ can be found in p. 164 of [10]. The solution of this equation is given by dividing the left hand side (LHS) by the right hand side (RHS) in order to solve the system in a least square sense. The residuals of that equation (ρ_v and ρ_w) can also be computed and will be useful to compute the covariance matrix.

- The Γ's can be recomputed from matrices A and C because the first ones were only estimations (see p. 123, alteration 1 of [10]). As stated in p. 129 of [10], C is defined as the first l rows of Γ_i and $A = \Gamma_i^\dagger \Gamma_i^0$ where:

$$\Gamma_i^0 = \begin{pmatrix} \overline{\Gamma_i} \\ 0 \end{pmatrix}, \tag{10}$$

with $\overline{\Gamma_i}$ is the extended observability matrix without the first l rows and the zeros are introduced to ensure stability.

- The pseudo-inverses of the Γ's can then be recomputed, as well as the right and left hand sides from the set of linear equations (8).

1.3.1.7   Step 6: Computation of matrices B and D

- Matrices B and D can be determined by solving the following equation in a least square sense (Equation (4.61) p. 127 of [10]):

$$\text{vec}\begin{pmatrix} D \\ B \end{pmatrix} = \left[\sum_{k=1}^{i} Q_k^T \otimes N_k \right]^{\dagger} \text{vec } P. \tag{11}$$

With:

- $\otimes$ the Kronecker product.
- P and Q computed as in p. 125 of [10]:

$$P \triangleq \underbrace{\begin{pmatrix} \dfrac{\Gamma_{i-1}^{\dagger} Z_{i+1}}{Y_{i/i}} \end{pmatrix}}_{\equiv \text{LHS}} - \underbrace{\begin{pmatrix} A \\ C \end{pmatrix} \Gamma_i^{\dagger} Z_i}_{\equiv \text{RHS}}, \tag{12}$$

$$Q \triangleq U_f \equiv R_u. \tag{13}$$

- N_i matrices computed as in p. 126 of [10]:

$$N_i \triangleq \begin{pmatrix} M_{i-1} - L_{1/i} & 0 & \dots & 0 & 0 \\ -L_{2/i} & 0 & \dots & 0 & 0 \end{pmatrix} \begin{pmatrix} I_l & 0 \\ 0 & \Gamma_{i-1} \end{pmatrix}, \tag{14}$$

where I_l is a identity matrix and $L = (L_1; L_2)$
and M are computed as in p. 119 of [10]:

$$L \triangleq \begin{pmatrix} A \\ C \end{pmatrix} \Gamma_i^{\dagger} \quad \text{and} \quad M \triangleq \Gamma_{i-1}^{\dagger}. \tag{15}$$

1.3.1.8   Step 7: Determination of the covariance matrix

- Q, S and R can be determined from the residuals of Equation 8: ρ_w and ρ_v. Indeed:

$$\begin{pmatrix} Q & S \\ S^T & R \end{pmatrix} = E_j \left[\begin{pmatrix} \rho_w \\ \rho_v \end{pmatrix} \begin{pmatrix} \rho_w^T & \rho_v^T \end{pmatrix} \right]. \tag{16}$$

The covariance is then computed by multiplying the residuals vector computed in step 5 by its transposed form. In order to obtain Q, R and S, the covariance matrix have to be partitioned accordingly.

So that all the unknowns from Figure 4, have been determined.

1.3.2   Comparison with the previous methods

Compared to the two previous methods (EMA and OMA), the advantages of the OMAX method are:

- Since noise is taken into account, the level of the shaker does not have to be way higher than the artificial forces in order to cover the noise. **Smaller shakers** can then be used, which is more convenient as the setup could need to be modified in order to identify several modes [4, 11];

- Since the modes are excited by the artificial forces, it is possible to obtain the modal masses and thus **mass-normalised mode shapes**. This is not possible with a classic method only relying on ambient excitation (OMA) [4, 12, 5];

- Ambient forces are usually confined to a narrow frequency band, so that only a small number of modes can be identified [4, 11]. A **larger frequency range** can then be covered using a shaker;

- OMAX method allows to **determine the frequencies, damping ratios and modes shapes all at once** while the current method used by V2i requires to perform three different steps as shown in Figure 2, allowing to obtain the same results in less steps. This will be proven in Section 3.2.1 where, thanks to a detailed measurement campaign realised on the Tilff cable-stayed footbridge, both method will be compared;

- Finally, from a practical point of view, using OMAX for the identification of the modal properties of a footbridge does **not require to close the footbridge** to the pedestrian traffic, which is a significant advantage for the experimental testing of existing in-use footbridges.

However, the main disadvantage of OMAX is that the noise is considered to be a white noise [12], which may not be the case for ambient forces. Indeed, the forces induced by pedestrians are a sum of sinusoidal component, for example [3]. So that, the main goal of thesis is to show what is the effect of adding an increasing level of noise on the identified modal properties, even when this noise is not a white noise sequence. To do so, a numerical model will be developed in order to test the CSI algorithm with different types of loading and different types of noise. The observations will then be checked thanks to an experimental measurement campaign.

2 Numerical part

In this section, the creation of a simplified model of Tilff cable-stayed footbridge and the methodology used to identify its modal parameters thanks to the CSI algorithm will be exposed. This was achieved by developing Matlab codes, which will be detailed in this section and are available on MatheO [13]. A preliminary measurement campaign was held in order to roughly determine the first modal properties of the real structure, which will be helpful to create the model, and will also be presented.

The general outline of the Matlab codes is presented in Figure 8. The CSI algorithm comes from [10] and the basis of the other functions come from the V2i staff. The codes have obviously been adapted to the cases that will be studied in this paper.

| Step 0 | Creation of a **simplified model** on BeamZ |

| Step 1 | Computation of the **reference** modal characteristics |
| | (eigenfrequencies, damping ratios, mode shapes) |

| Step 2 | Step 3 | Step 4 |

Definition of the ambient and artificial **excitations**
(and their relative level)

Computation of the **response** of the structure
(time integration method)

Dynamic identification using the **CSI** method
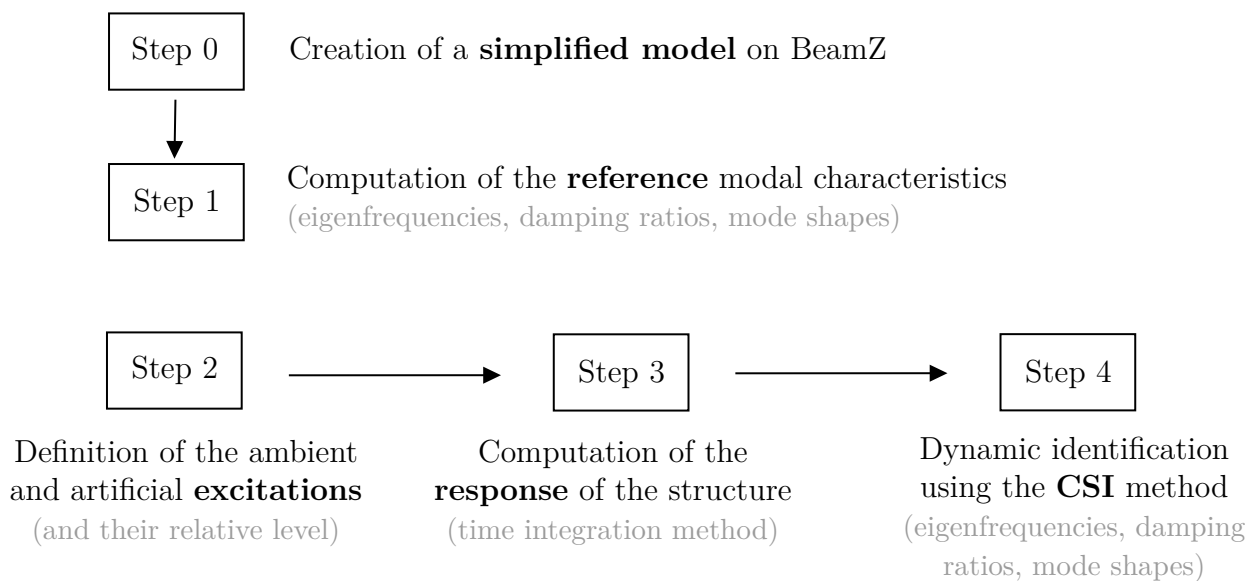(eigenfrequencies, damping ratios, mode shapes)

Figure 8: Steps developed in the Matlab codes.

Thanks to the information obtained with the preliminary measurement campaign, a simplified model will be created and its modal matrices, characterising its behaviour, will be extracted (Step 0, Section 2.2.1). This will allow to compute the reference modal characteristics of the system (Step 1, Section 2.2.2). Then, the scheme illustrated in Figure 3 will be implemented by first defining the ambient and artificial excitations (Step 2, Section 2.2.3). The response of the structure to these excitations can be computed thanks to a time integration method (Step 3, Section 2.2.4). Finally, some parameters of the CSI algorithm will be discussed (Step 4, Section 2.2.5).

The reference modal properties were computed in order to make sure that the identified modal properties with 0% noise are consistent. However, the main goal of the analysis of the results part will be to study the effect of an increasing noise level on the identified modal properties. This will be studied in two cases: variation of the type of excitation (Section 2.3) and variation of the type of noise (Section 2.4.2).

2.1 Preliminary measurement campaign

In order to prove that the algorithm is robust, it will first be tested on a simplified model of the Tilff cable-stayed footbridge. A preliminary measurement campaign was held on the 2nd of September on the real site in order to roughly extract the modal properties of the footbridge. This 74-m long footbridge built around 1970 allows pedestrians to cross the river (*L'Ourthe*) and is situated near Liège, Belgium. It is a cable-stayed footbridge composed of a concrete pylon. The deck consists in a concrete slab surrounded by a metal casing, the whole only resting on the pylon (not built in). A picture of this footbridge can be observed in Figure 9.

Figure 9: Tilff cable-stayed footbridge.

Since the traffic is considered to be insufficient, installing a tuned mass damper (a device allowing to damp out the vibrations, calibrated on one or several modes) on this footbridge would be too expensive. So that it can easily be excited by knee-bending on its first frequencies. This technique (that can be observed in [14]) consists in a group of people bending the knees at a desired frequency thanks to a metronome and will be used without the help of a shaker for this preliminary measurement campaign. The excitation have been applied at several locations on the footbridge by trial and error, in order to observe at best the tested modes. A more detailed measurement campaign will be realised later and discussed in Section 3.

Three accelerometers were used in order to measure the vibrations. The first two were placed at mid-span on both sides of the footbridge (next to the anchoring of the medium stay cables) and the last was placed at quarter span (next to the anchoring of the longer stay cable). A schematic top view of the footbridge can be observed in Figure 10 and a close up of the cables is shown in Figure 11.
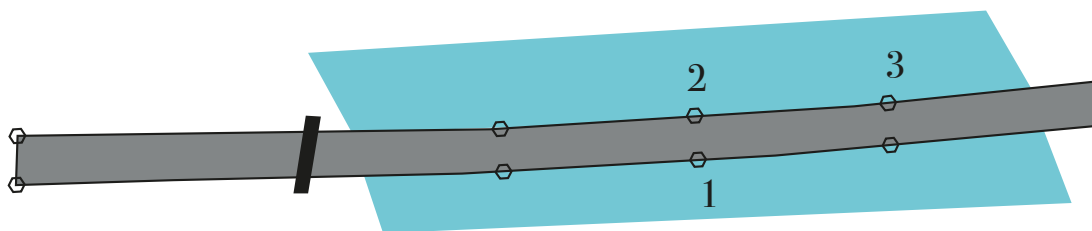

Figure 10: Schematic top view of the Tilff cable-stayed footbridge (about to scale). The hexagons represent the locations of the anchoring of the cables on the deck, the dark shape represents the pylon and the blue shape represents the river. The numbers correspond to the position of the accelerometers.

Figure 11: Illustration of the cables.

Several types of excitation were applied. These loadings are summarised in Table 1 and were mainly applied between the medium and long cable anchorings and beyond those of the longest cables for the deck excitation. Figure 12 shows the evolution of the acceleration of the footbridge for the different loadings. The results are only shown for accelerometer 1, to avoid redundancy.

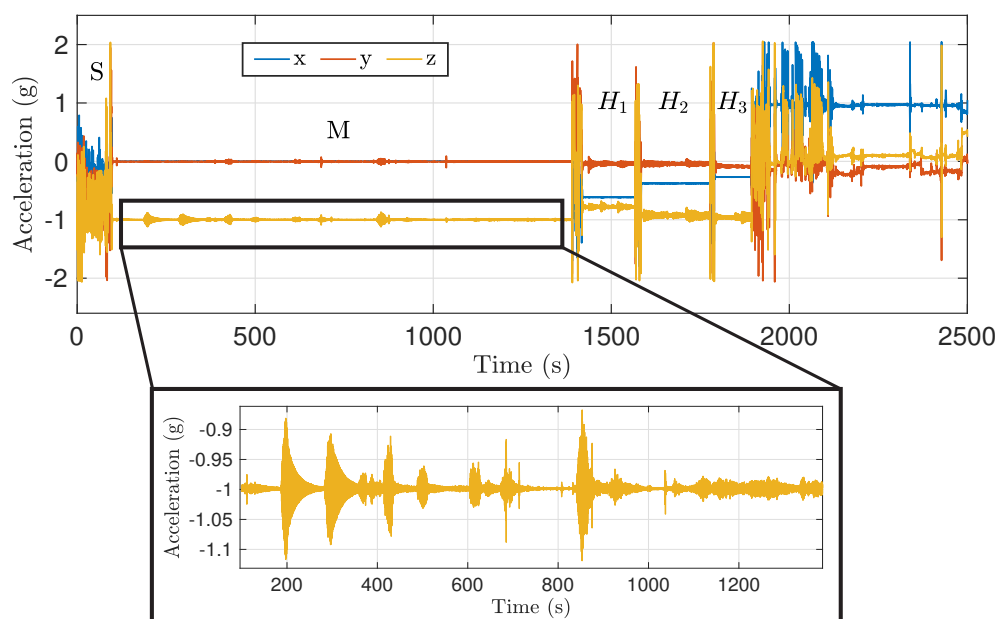| Label	Start (s)	End (s)	Description
S	0	100	Synchronisation of the accelerometers
M	100	1370	Main tests (on the deck)
H_1	1420	1560	Shortest stay cable excitation
H_2	1589	1770	Medium stay cable excitation
H_3	1796	1891	Longest stay cable excitation

Table 1: Loadings and time schedule.

Figure 12: Time response of accelerometer 1 and zoom on the z-axis time plot.

As it can be seen in Table 1 and Figure 12, the first step was the synchronisation of the accelerometers. This operation is repeated in between the different types of loading. Then the main tests (on the deck) started. Some preliminary measurements allowed to roughly determine the first eigenfrequencies of the footbridge so that, thanks to a metronome, these ones could be excited by a group of five people doing the knee-bending technique. The tested frequencies were 1.59, 2.25, 2.83 and 3.64 Hz. It was not possible to do knee-bendings above these frequencies, the rate being too high for humans to be excited in that way. Thanks to the recorded temporal signals, the plot of the power spectral density (PSD) of the structure can be obtained and is observed in Figure 13. This type of graph allows to show the frequency content of the signal.
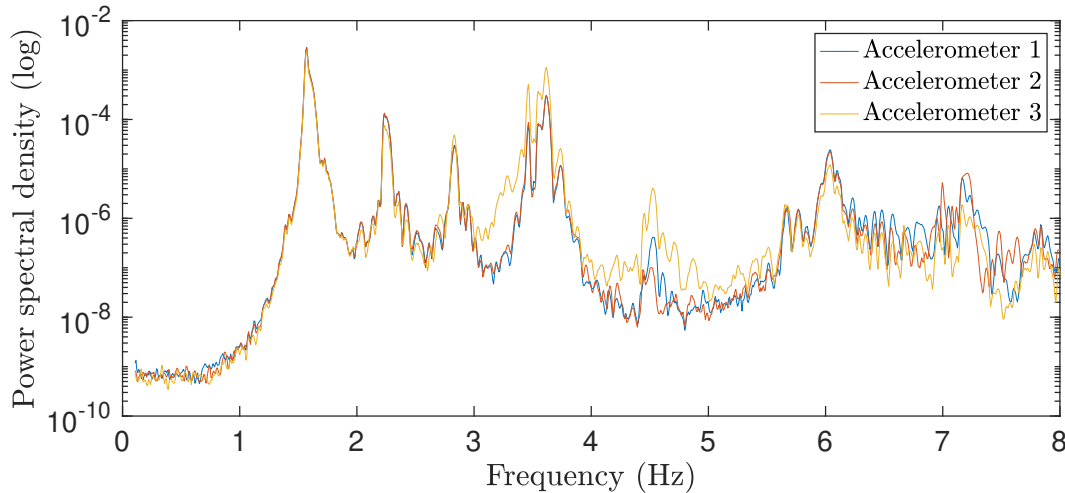

Figure 13: Power spectral density of the structure for the main tests of preliminary measurement campaign.

The first three eigenfrequencies (corresponding to the first three peaks) can easily be determined since the footbridge was excited at those frequencies. They respectively correspond to the first frequency of the deck and the frequencies of the long and medium stay cables. This was determined by looking at the response of the footbridge to the knee-bending excitations and will be verified by computing the PSD of the periods H_1, H_2 and H_3. However, the frequencies above 3 Hz can hardly be identified since they are only excited by the weak ambient forces. This justifies the need for the use of a shaker hence a combined identification method. Indeed, it will be possible to obtain a clearer spectrum, by imposing a random signal in a limited range of frequency. This will be shown in Section 3.2.1.1.

After the main tests, accelerometers 2 and 3 were shut down. The first one was successively moved from the left shortest stay cable to the left longest one in order to determine the frequency content of the stay cables by shaking them by hand (the left is taken by looking at the pylon from the longer span of the footbridge). This can be done by looking at the power spectral densities computed for the periods H_1, H_2 and H_3. Figure 14 shows the power spectral densities for each cable, allowing to determine an estimation of their fundamental frequencies and their harmonics.
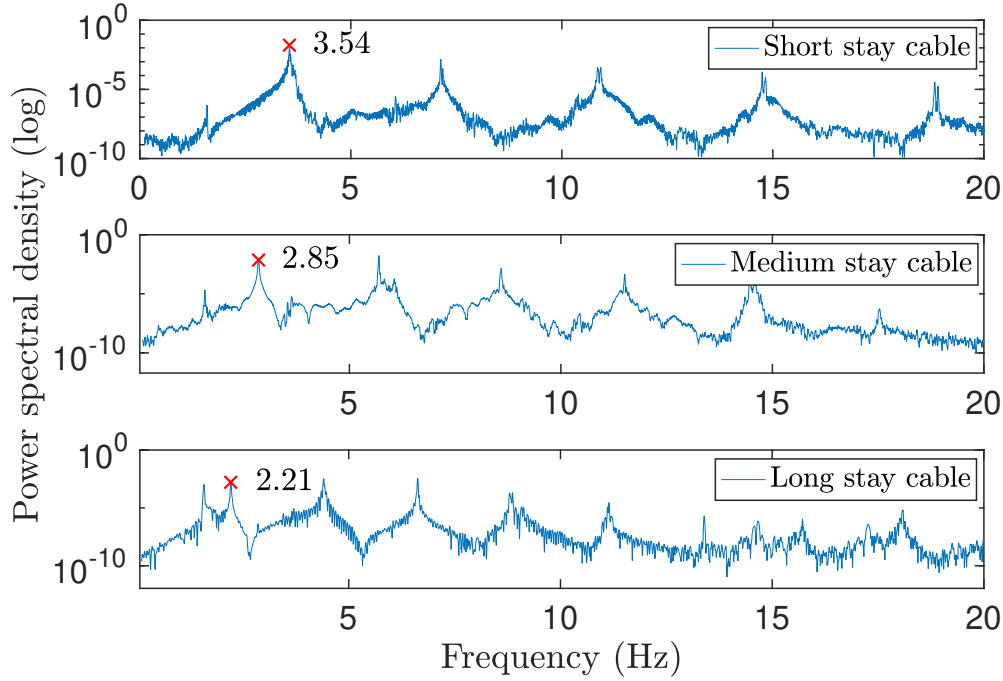
Figure 14: Power spectral densities of the different cables. They have been computed respectively over periods H_1, H_2 and H_3.

The fundamental frequencies of the long and medium stay cables indeed correspond to the second and third peaks observed in Figure 13. Concerning the fourth peak of that same figure, it cannot clearly be distinguished. Indeed, it should correspond to a mode of the short stay cable or an interaction between the second mode of the deck and the short stay cable. However, as previously mentioned, a more detailed test campaign will give a clearer view of the frequency spectrum of the structure thanks to the shaker.

For the following of the thesis, it is planned to focus only on the deck modes. Indeed, the considered ambient forces will be caused by pedestrians walking on the footbridge, but this will be further explained in Section 2.2.3. It thus remains to determine the damping ratios associated to the first two frequencies of the deck. To do so, the peak-picking or half power point method can be applied to the square root of the power spectral density of Figure 13. The method is illustrated in Figure 15.
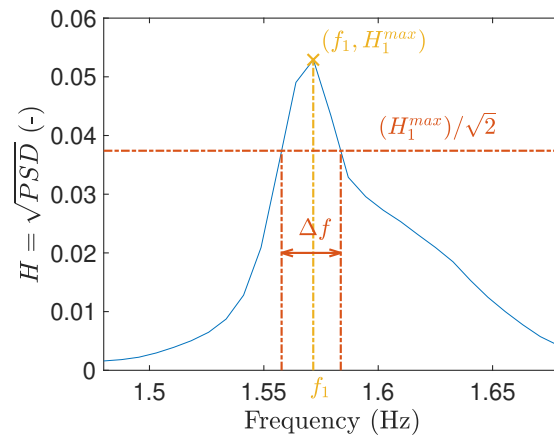

Figure 15: Peak-picking method on first vibration mode.

As already mentioned, the method will be applied to the square root of the PSD which will be called H (or it is in reality called Amplitude Spectral Density). In the figure above, a zoom has been made on the first peak of H, but the same method can be applied to the other peaks. First, the peak is located at (f_1, H_1^{max}), where f_1 is the first frequency of the deck and H_1^{max} is its corresponding value on the y-axis. The half power points are computed so that their height is at $H_1^{max}/\sqrt{2}$. The distance between these two points on the x-axis is Δf, from which one can define the quality factor Q. Finally, the damping ratio ζ_1 can be estimated thanks to those two parameters, so that:

$$Q \cong \frac{f_1}{\Delta f} \quad \text{and} \quad \zeta_1 \cong \frac{1}{2Q} = \frac{\Delta f}{2f_1}. \tag{17}$$

It should be noted that this method is only theoretically valid for a single degree of freedom system so that the damping can be overestimated if the method is applied for structures having close modes [15]. Furthermore, this method strongly depends on the frequency resolution of the measurements, which have been shown to not be optimal for a simple excitation doing knee-bendings (see Figure 13, above 3 Hz). Lastly, due to the interpolations that had to be done to find the two half power points, this can lead to some additional errors. However, the goal here is not to identify precisely the modal characteristics of the footbridge but to obtain an estimation in order to create a simplified numerical model.

Finally, the modal properties of the first two modes of the deck are summarised in Table 2. The frequencies are obtained by looking at the location of the peaks in Figure 13 on the x-axis and the damping ratios are computed as previously explained.

Frequencies (Hz)	Damping ratios (%)
1.57	0.83
3.61	0.57

Table 2: Rough estimation of the first two modal properties of the deck.

A more detailed measurement campaign will be held in Section 3 in order to determine the first two modal properties more accurately. However, even if those parameters are only an approximation, this preliminary campaign was only to define some parameters to develop the model of Section 2.2, which is not a perfect representation of the real structure as it will be explained.

2.2 Development of a simplified model

In this section, the different steps of Figure 8 will be detailed. First, a simplified model will be created on BeamZ software and its modal properties will be determined, which will be taken as a reference. Then, both ambient and artificial excitations that will be applied on the model will be defined. The response of the system to those excitations will be computed thanks to a time integration method, that will also be presented in this section. This is followed by a discussion about the parameters of the CSI algorithm.

2.2.1 Step 0: Creation of the BeamZ model

Now that the first modal properties of the real structure were estimated (see Table 2), a **simplified** model of the Tilff cable-stayed footbridge can be created. The model is created on the BeamZ software [16], which is a set of Matlab routines developed by Vincent Denoël (ULiège). It allows to draw some beam models, to compute their behaviour to different types of loads and to obtain the mass M and the stiffness K matrices of the system. The simplified model is represented in Figure 16 and the characteristics of the different geometries are summarised in Table 3.
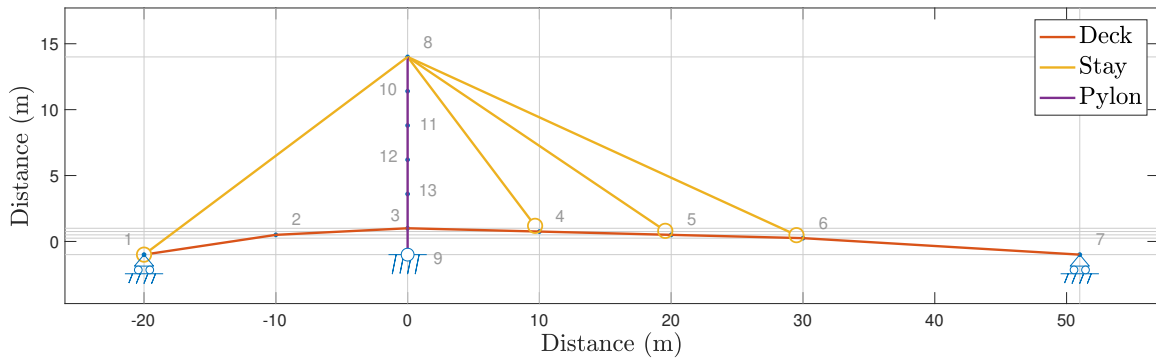

Figure 16: Simplified model of the Tilff cable-stayed footbridge. The different colors represent the different geometries.

Geometry	Material	Cross-section (m^2)	Inertia (m^4)
Deck	Steel	0.25	0.013
Stay (cable)	Steel	0.002	6×10^{-7}
Pylon	Concrete	0.6	0.035

Table 3: Characteristics of the different geometries adapted in order to obtain frequencies close to those obtained with the preliminary measurement campaign.

An important comment to be done is that this is only a simplified numerical model that does not represent exactly the reality. Indeed, the dimensions in distance were respected to a certain extent, but the geometries were chosen so that the first two eigenfrequencies of the model roughly correspond to those of the real structure. Moreover, the frequencies of the cables will not be captured by the BeamZ model since they are represented by a single element that is hinged on the deck. However, the aim of this model is only to evaluate the method described in Figure 3 for the deck part, not to predict the behaviour of the real structure.

The model uses Hermite polynomials of degree three ($X^3 - 3X$) to represent the elements. Moreover, it should be noted that this model is only 2D so that each node has three degrees of freedom (DOFs). Figure 17 shows the degrees of freedom of a 2D node.
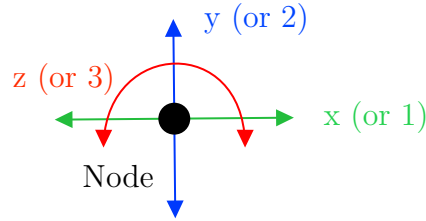

Figure 17: Degrees of freedom of a 2D node.

The model has 13 nodes, 16 elements, but only 35 DOFs since the vertical degree of freedom is blocked on nodes 1, 7 and 9 as well as the horizontal one for node 9. Indeed:

$$13 \text{ nodes} * 3 \text{ DOFs} = 39 \tag{18}$$

$$39 - 4 \text{ blocked DOFs} = 35 \text{ DOFs}. \tag{19}$$

The fact that the model is 2D is not a problem since torsion modes were not observed in the frequency range of interest during the preliminary measurement campaign. Indeed, due to the symmetry of the cables, they will block the torsion modes. Moreover, underneath the concrete slab, a closed metal casing is included so that it reduces the torsion compared to if there were only two beams sustaining the concrete slab. Indeed, due to the high torsional stiffness of the metal casing, the torsion modes will be found at higher frequencies.

Figure 18 summarises the purpose, inputs and outputs of step 0.
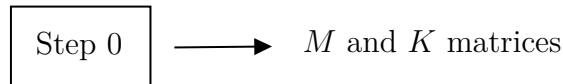
Figure 18: Inputs and outputs of step 0.

2.2.2   Step 1: Computation of the modal properties of the model

The system at rest is defined by the governing equation of motion, which is given by:

$$\mathbf{M\ddot{x}} + \mathbf{Kx} = 0. \tag{20}$$

So that solving this eigenvalue problem (thanks to the *eig* function of Matlab) leads to the modes shapes $\mathbf{\Phi}$ and eigenfrequencies f of the system. The first two frequencies of the system are summarised in Table 4.

Mode	1	2
Frequencies (Hz)	1.59	3.23

Table 4: First two eigenfrequencies of the simplified numerical model.

As a reminder, the parameters of the model (see Table 3) were set up so that the first two frequencies of the model would roughly correspond to those of Table 2, so that it is not surprising to find values close to those ones. Concerning the modes shapes associated to that frequencies, they can be observed in Figure 19.
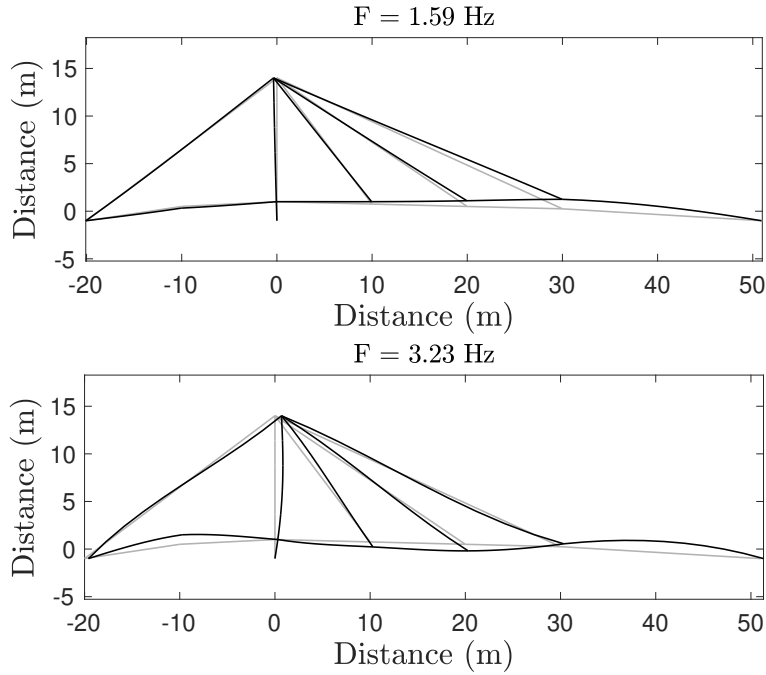

Figure 19: First two modes of the simplified numerical model. The gray lines represent the non-deformed structure and the black ones represent the deformed structure.

Those reference modes will only be used to be compared with the estimated ones and to justify the position of the shaker that will be chosen for the simulations (see Section 2.2.3). Indeed, they **cannot** be compared with those of the real structure since the inertia and cross-sections of the different parts are not respected (see Table 3).

Damping can also be introduced in the system thanks to the term $\mathbf{C\dot{x}}$ where $\mathbf{C}$ is the damping matrix. The system becomes:

$$\mathbf{M\ddot{x}} + \mathbf{C\dot{x}} + \mathbf{Kx} = 0. \tag{21}$$

Damping can be modelled thanks to the Rayleigh damping method or proportional damping assumption that states that the damping is given by the weighted sum of mass and stiffness matrices. So that:

$$\mathbf{C} = a * \mathbf{M} + b * \mathbf{K}. \tag{22}$$

The first two damping ratios (ζ_1 and ζ_2) are chosen to be equal to those of Table 2. By definition:

$$\omega_1 = 2\pi f_1 = \sqrt{\frac{k_1}{m_1}} \tag{23}$$

$$\zeta_1 = \frac{c}{c_{critic}} = \frac{c}{2m_1\omega_1} = \frac{1}{2m_1\omega_1}(am_1 + bk_1) = \frac{1}{2}\left(\frac{a}{\omega_1} + b\omega_1\right), \tag{24}$$

where ω is the angular velocity and c_{critic} is the critical damping ratio. The same can be expressed for the second modal characteristics (f_2, ζ_2) so that one has two equations with two unknowns, a and b. By solving this system, one has:

$$a = \frac{2\omega_1\omega_2}{(\omega_1^2 - \omega_2^2)}(\omega_1 * \zeta_2 - \omega_2 * \zeta_1) \quad \text{and} \quad b = \frac{2\omega_1\omega_2}{(\omega_1^2 - \omega_2^2)}(\zeta_1/\omega_2 - \zeta_2/\omega_1). \tag{25}$$

So that matrix $\mathbf{C}$ can now be computed with Equation (22). Thanks to the modes shapes obtained when solving the eigenvalue problem, one can find the generalised version of the matrices such as:

$$\mathbf{M}^* = \Phi^T\mathbf{M}\Phi, \quad \mathbf{K}^* = \Phi^T\mathbf{K}\Phi \quad \text{and} \quad \mathbf{C}^* = \Phi^T\mathbf{C}\Phi. \tag{26}$$

Finally, the following damping ratios are computed as:

$$\zeta_i = \frac{\frac{1}{2}\mathbf{C}^*}{2\pi f_i \mathbf{M}^*}, \tag{27}$$

which is derived from Equation (24).

Figure 20 summarises the purpose, inputs and outputs of step 1.

M and K matrices $\longrightarrow$ Step 1 $\longrightarrow$ Reference modal characteristics f, ζ, Φ
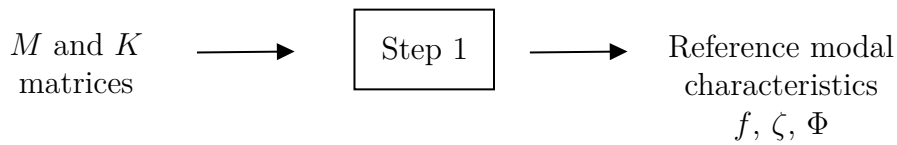
Figure 20: Inputs and outputs of step 1.

2.2.3   Step 2: Definition of the ambient and artificial excitations

The step 2 of the methodology consists in defining the inputs u of the system: the ambient F_{amb} and artificial F_{art} excitations. The ambient forces aim to represent the unmeasured forces such as wind or pedestrians crossing the footbridge. The artificial forces represent the specified excitation that can be exerted by the shaker, for example. First, the results will be analysed when the noise is a limited band Gaussian white noise (Section 2.3). Then, the noise will be generated by pedestrians, which will be developed in Section 2.4.1.

Since the analysis will be made on the first two frequencies of the system and since OMAX method makes the assumption that the noise is a Gaussian white sequence, the noise will be defined as in Table 5 for the first part of the tests.

Case	Ambient forces	
	Type	Frequency range
Low (L)	Random signal	1 to 3 Hz
High (H)		2 to 4 Hz

Table 5: Definition of the cases that will be tested for a white noise.

Due to the random nature of the signals, the simulations must be repeated several times for the same case in order to limit the dependency to the sampling. A number of 100 iterations is chosen arbitrarily. An illustration of the shape of power spectral density of the noises defined in Table 5 can also be observed in Figure 21.

(a) Simulated.

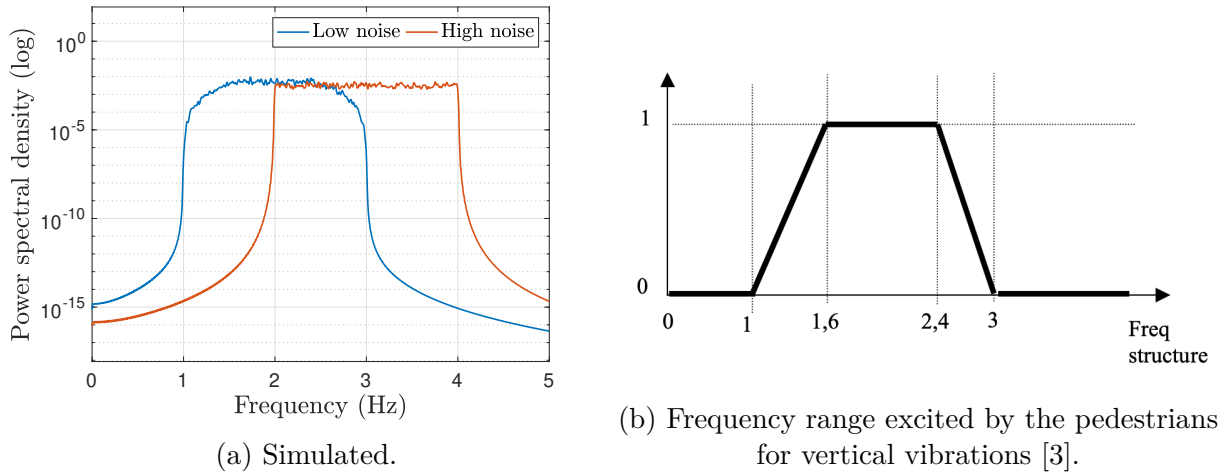(b) Frequency range excited by the pedestrians for vertical vibrations [3].

Figure 21: Illustration of the shape of the (white) noises.

The PSD of low noise has a rounded shape compared to the one of the high noise because the goal was to simulate the frequency range excited by the pedestrians. Indeed, as it can be seen in Figure 21b, the loading that needs to be taken into account is described by a reduction coefficient. This one translates the fact that the closer in frequency to the range [1.6 - 2.4] Hz, the higher the risk to put the footbridge into resonance [3]. That is why this shape is only used for this frequency range and not the other ones that will be tested.

The noise should be applied as if there were uncorrelated distributed forces on all the elements. In order to make the results independent of the mesh, a random pressure on the elements will be applied instead of a random nodal force. Doing so, the results will have less sensitivity to the length of the elements. However, the fact the loading is not necessarily coherent is not taken into account, but this is beyond the scope of this thesis. If needed, more information about those effects can be found in [17]. An illustration of this method can be observed in Figure 22 and is explained here after.
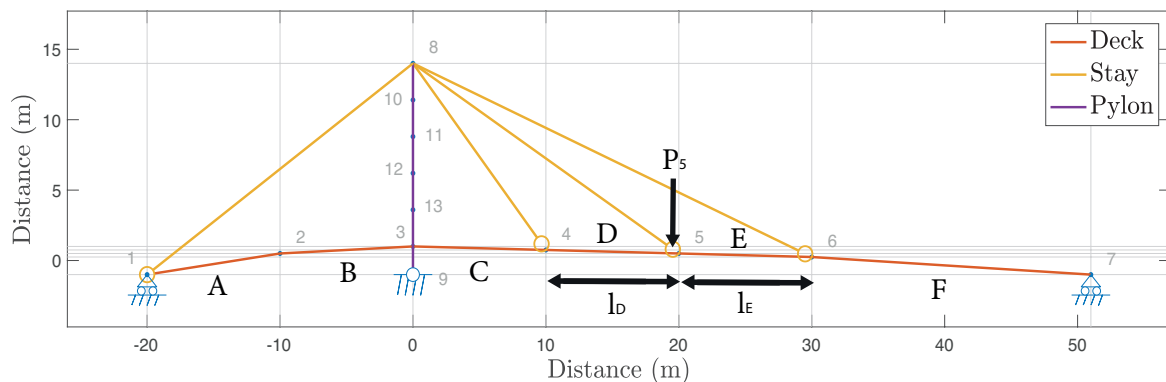

Figure 22: Illustration of the method used in order to make the results independent of the length of the elements.

For example, the force that will be applied at node 5 is given by:

$$P_5 = P_D \frac{l_D}{2} + P_E \frac{l_E}{2}. \tag{28}$$

Where P_i ($i = 2, ..., 6$) are the nodal forces, l_X are the length of the elements and P_X are the random pressures applied on element X. This ones are limited band randomly generated signals (one for each element) as defined in Table 5. For all the nodes, one has:

$$
\begin{pmatrix} P_2 \\ P_3 \\ P_4 \\ P_5 \\ P_6 \end{pmatrix} = \frac{1}{2} \begin{pmatrix} l_A & l_B & 0 & 0 & 0 & 0 \\ 0 & l_B & l_C & 0 & 0 & 0 \\ 0 & 0 & l_C & l_D & 0 & 0 \\ 0 & 0 & 0 & l_D & l_E & 0 \\ 0 & 0 & 0 & 0 & l_E & l_F \end{pmatrix} \begin{pmatrix} P_A \\ P_B \\ P_C \\ P_D \\ P_E \\ P_F \end{pmatrix}. \tag{29}
$$

The level of the ambient forces will progressively be increased to see its effect on the modal parameters. Indeed, in the first part of the analyses the noise will be defined as the ratio between the root mean square (rms) value of the ambient forces F_{amb} and the one of the artificial forces F_{art} such as:

$$\% \text{ of noise} = \frac{rms(F_{amb})}{rms(F_{art})}. \tag{30}$$

The value of $rms(F_{art})$ is set to 1 so that the level of noise correspond to $rms(F_{amb})$. The levels of noise that will be tested are: $[0, 0.5, 1, 2, 4, 6, 8]$ %, which values are chosen arbitrarily. In order to illustrate this definition, Figure 23 shows the difference in amplitude of the artificial force (in blue) compared to the amplitude of the ambient forces (in orange and yellow). They respectively correspond to ambient forces with a rms of 1% and 8%.
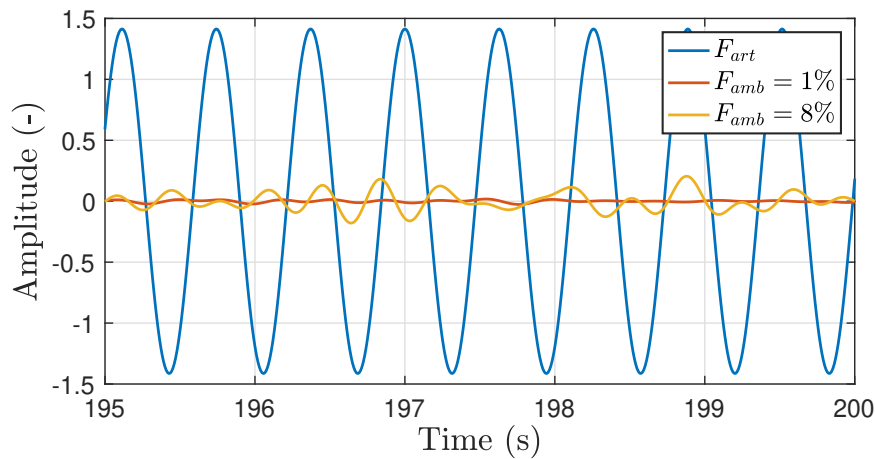
Figure 23: Illustration of the artificial and ambient forces for 1 and 8% noise level.

As the noise is considered to be applied by pedestrians and as only the modes of the deck are of interest, the ambient forces will only be applied on the deck. Indeed, they will be applied on nodes 2 to 6 of Figure 16 on the vertical degree of freedom, because nodes 1 and 7 cannot move due to the configuration. This configuration of the applied ambient forces is only valid for the model that will be analysed in Section 2.3. Indeed,

the noise will be defined in another way (see Section 2.4.1) for the analysis of Section 2.4.2.

The artificial excitation is considered to be provided by a shaker, it is then chosen to apply it at node 5 on the vertical degree of freedom. Indeed, the shaker should not be located on the node of one of the mode one wants to identify. In theory, the shaker should be located where the amplitude of the mode is maximum in order to excite it optimally. However, in order to excite several modes, a compromising location should be chosen. So that, by looking at Figure 19, node 5 seems to be a good position for the two modes. It is easy to change the location of the shaker for the simulations but in real life, this device can be quite heavy so that if this manipulation can be avoided, it is more convenient. Concerning the type of artificial force that will be applied by the shaker, this will be discussed in Section 2.3. Finally, the vertical responses of the footbridge to the excitations will be measured at nodes 2 to 6. All these positions are summarised in Figure 24.
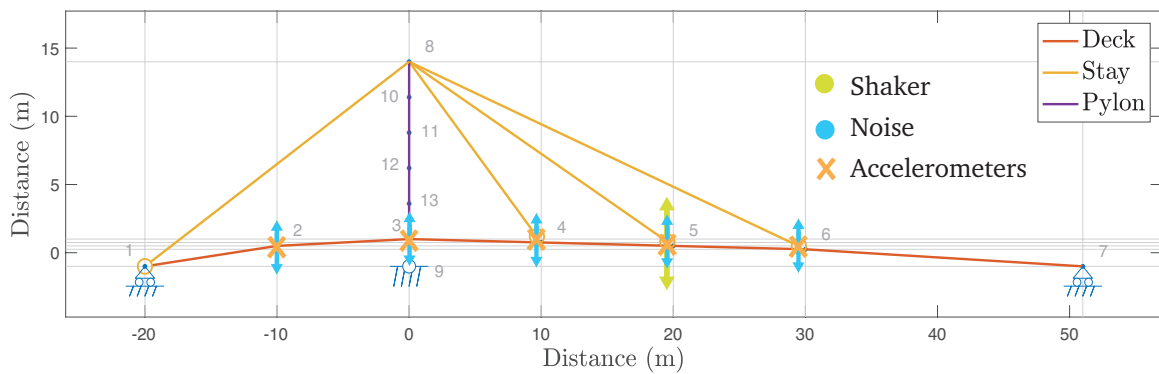
Figure 24: Position of the artificial force (shaker), of the ambient forces (noise) and of the measured responses (accelerometers).

Figure 25 summarises the purpose, inputs and outputs of step 2.
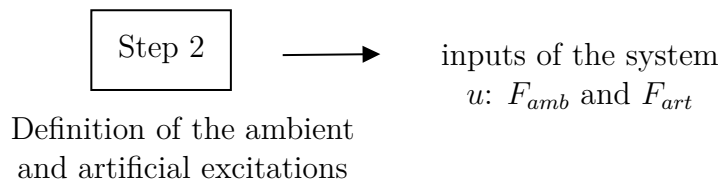
Figure 25: Inputs and outputs of step 2.

2.2.4   Step 3: Computation of the response of the structure

To compute the response of the structure to the imposed excitation at the desired locations, Newmark implicit time integration method will be used. It is a prediction-correction scheme. In contrast, explicit methods only use the current state to compute the following one. They are easier to implement in practice and are quicker but the time step should be small enough in order to obtain good results. However, even if it is a little more costly to implement, the implicit method have a higher stability when the right parameters are set [18]. The algorithm of Newmark method is presented in Figure 26.

Figure 26: Newmark time integration [19].

The matrices $\mathbf{M}$, $\mathbf{C}$ and $\mathbf{K}$ are known as well as the initial conditions on displacement ($\mathbf{q}_0 = 0$) and velocity ($\dot{\mathbf{q}}_0 = 0$). The acceleration at initial time $\ddot{\mathbf{q}}_0$ can then be computed.

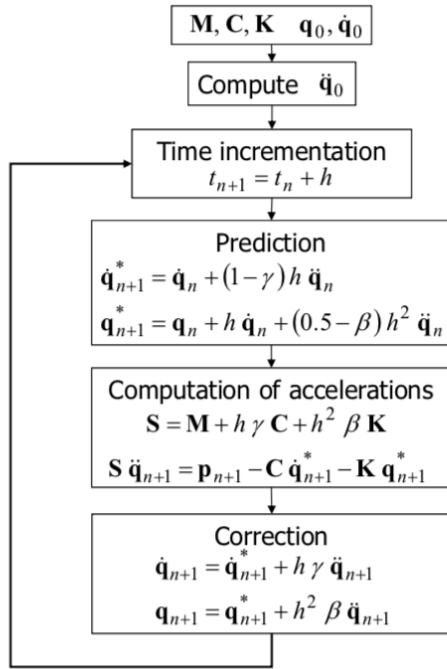Then, the time is incremented by a time step h. The prediction of the displacement $\mathbf{q}_{n+1}$ and the velocity $\dot{\mathbf{q}}_{n+1}$ at time t_{n+1} are computed.

Thanks to the iteration matrix $\mathbf{S}$, the acceleration $\ddot{\mathbf{q}}_{n+1}$ at time t_{n+1} can also be computed.

Finally, a correction for displacement and velocity at time $n + 1$ is made before re-iterating.

An important comment has to be done regarding the parameters used in this method. In fact, to ensure the stability of the scheme, β, γ and the time step h have to be chosen carefully. The condition of stability of this scheme are summarised in the (β, γ) plane in Figure 27.
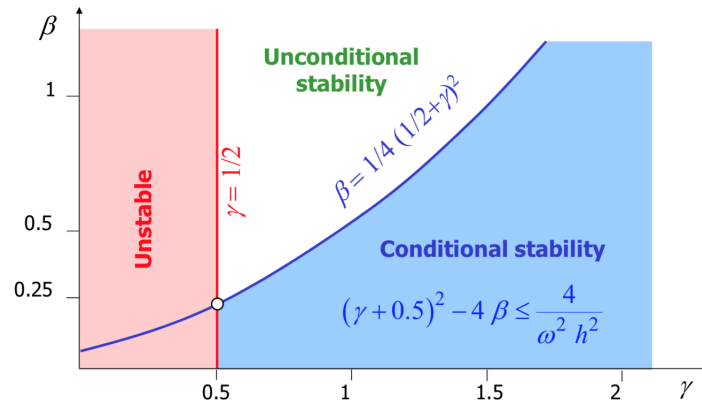
Figure 27: Stability of the Newmark method in function of its parameters [19].

The first remark is that γ must be greater or equal to 0.5 otherwise the algorithm would not be stable at all. The algorithm can also be conditionally stable only if the time step h respects the equation presented in the blue part of Figure 27. In this work, $\gamma = 1/2$ and $\beta = 1/4$ are chosen in order to make the time step independent of γ and β and to offer the maximum accuracy while being stable. This is known as the average constant acceleration Newmark method. In this case, the periodicity error obtained by the comparison between the exact dynamic response of a one degree of freedom oscillator under initial conditions and the numerical solution is given by [19]:

$$\frac{\Delta T}{T} = \frac{\omega^2 h^2}{12}. \tag{31}$$

The periodicity error translates the frequency offset of the peak in the PSD graph due to the choice of a finite time step. This is illustrated in Figure 28.

Figure 28: Illustration of periodicity error.

Indeed, the time step has to be chosen in order to minimise the periodicity error as well as the computation time. IT is not possible to realise both at the same time so that a trade off between accuracy and speed should be done. Generally, a rule of thumb is that:
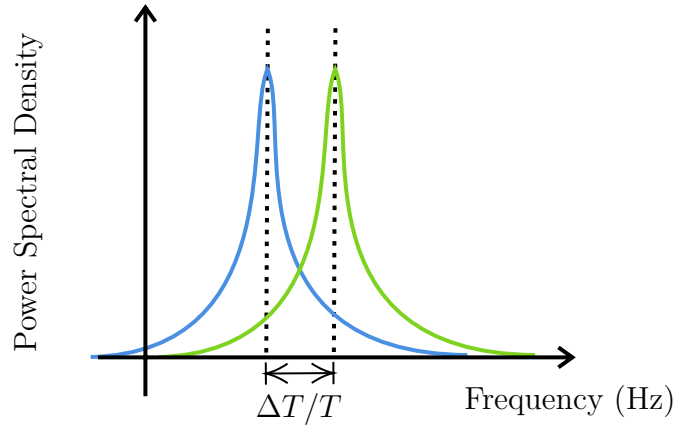
$$h < \frac{T_n}{20},\tag{32}$$

where $T_n = 1/f_n$ is the period of the highest frequency one wants to identify. In this case, the highest frequency is 4 Hz (for the case when the noise is in the high range, see Table 5). So that the time step should be less than 0.0125 seconds. A time step of 0.01 seconds has then been chosen for the simulations. This leads to less than 1% of periodicity error for both first frequencies (1.59 and 3.23 Hz), which is acceptable.

Figure 29 summarises the purpose, inputs and outputs of step 3.
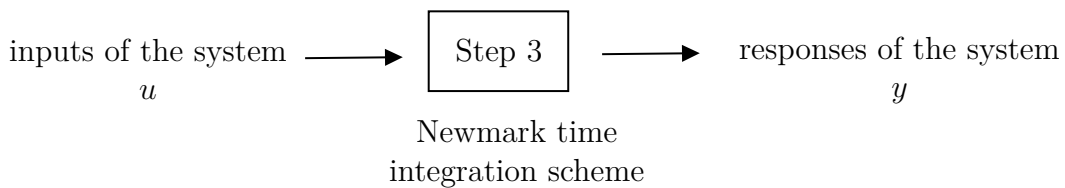
Figure 29: Inputs and outputs of step 3.

2.2.5 Step 4: Identification of the modal properties thanks to the CSI

This step is the one that will apply the combined subspace identification algorithm explained in Section 1.3.1. The *subid.m* function takes as inputs:

- The excitation u defined in step 2 (Section 2.2.3) composed of the ambient and artificial forces;
- The responses of the system y computed in the previous step (Section 2.2.4). These responses are computed at fives locations as it was illustrated in Figure 24;
- The system model order n;

- A parameter i, which is the number of block rows used in the Hankel matrices. As it was already mentioned in Section 1.3.1.1, parameter i should at least be larger than the maximum order of the identified system one wants to identify. However, it should not be chosen too large because the computational time is proportional to i^2 [10]. It is advised in [10] to choose i as follows,

$$i = 2 \cdot \frac{\text{Maximal order}}{\text{Number of responses}} = 2 \cdot \frac{35}{5} = 14. \tag{33}$$

The outputs of this function are the different matrices described in Figure 4, from which the modal properties of the system can be extracted thanks to the following equations [9]:

$$f_i = \frac{\lambda_i}{2\pi} \quad \text{and} \quad \zeta_i = \frac{-Re(\lambda_i)}{|\lambda_i|} \qquad \text{with} \qquad \lambda_i = \frac{\ln(D_i)}{h}. \tag{34}$$

Where D_i are the values of the diagonal of the matrix obtained with the *eig.m* function applied on matrix A, $|\cdot|$ denotes the complex modulus and Re is the real part operator.

The identification process is repeated for several system orders and a stabilisation diagram can be built in order to choose the adequate one. **By convention**, the frequency at order n is considered to be stabilised if it has less than 1% error with the value of the frequency computed at order $n-1$. The same is done for the damping but the limit is at 5% error, still by convention [20]. This diagram helps separate the real poles from the numerical ones. Indeed, a real pole will stabilise as the order increases, while this is not the case for the spurious ones. Figure 30 shows an example of this type of diagram for a random excitation between 1 and 4 Hz without noise.
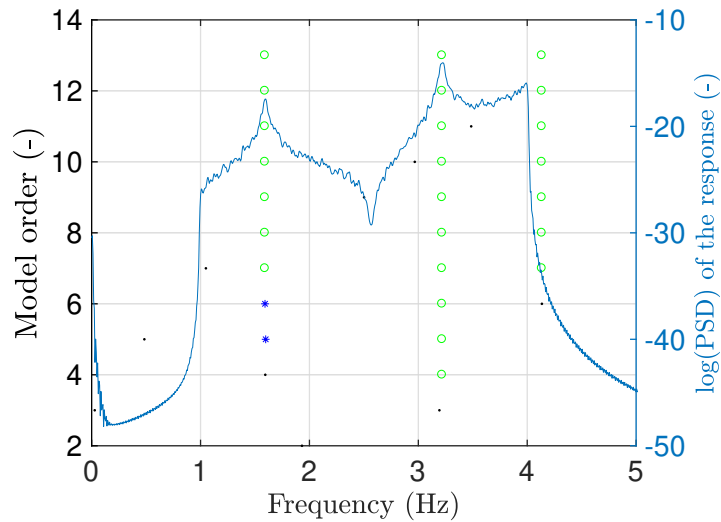
Figure 30: Example of a stabilisation diagram. The green circles represent a pole that stabilised in both frequency and damping ratio while the blue stars mean that the pole only stabilised in frequency. A black dot means that the detected pole neither stabilised in frequency nor in damping ratio.

This stabilisation diagram shows that in the range 1-4 Hz, the system has 3 eigenfrequencies at 1.59, 3.23 and 4.16 Hz. Indeed, to be considered stable a pole should remain green (stable in frequency and damping) for several consecutive orders. In this work, this value is set to 4 consecutive green circles because due to the high number of data to be

checked, it had to be performed automatically. So that when 4 consecutive green dots are found, the code performs a mean with the 4 values found for the frequency and damping. However in reality, when it is possible to check the results manually, the frequency and the damping ratio evolutions can be plotted in function of the order separately and one should choose the order where both quantities stabilised. Finally, thanks to the order chosen, one can obtain the frequencies, damping ratios and modes shapes at that order.

Figure 31 summarises the purpose, inputs and outputs of step 4.

Excitation, u
Responses, y
System order, n $\longrightarrow$ Step 4 $\longrightarrow$ Identified modal
Number of block   characteristics
Hankel matrices, i OMAX $f, \zeta, \mathbf{\Phi}$
            (*subid.m* function)
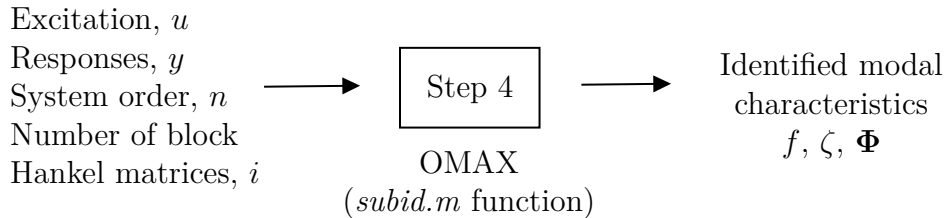
Figure 31: Inputs and outputs of step 4.

2.2.6 Summary

In this section, the methodology implemented on the Matlab codes was presented. First, a simplified model of Tilff cable-stayed footbridge was created in BeamZ and its reference modal characteristics were computed. Then, the definitions of the excitation and noise were given. The response of the structure to those loads could be computed thanks to a Newmark time integration method. Finally, by using the knowledge of the excitation and the response of the system, the CSI algorithm can be applied to obtain the identified modal characteristics of the model.

However, the definition of the artificial excitation was not explicitly given in step 2 (Section 2.2.3). Indeed, several parameters such as the excitation signal, bandwidth or simulation time must be varied in order to assess their influence on the modal parameters, as the level of noise increases. That is the aim of Section 2.3.

2.3 Influence of the type of excitation

In this section, the influence of the type of excitation on the modal properties of the system will be studied when the level of noise is increased. Figure 32 summarises the content of this section with the different variations that will be studied.

Section 2.3.1

Noise **outside** frequency range of interest

⟹ Should obtain consistent results with the identification method of Section 1.1

Type of signal: random
Simulation time: 15 min
Bandwidth: 0.2 Hz centered on frequency of interest

Section 2.3.2

Noise **inside** frequency range of interest

⟹ Study the effect of increasing noise level on modal properties

Section 2.3.2.3

a) Variation of the *bandwidth* of excitation: i) **0.02** and ii) **0.6** Hz

b) Variation of the *type of signal*: **sweep**

Variation of the speed of sweep (*simulation time*): **7** min

→ Only for f_1, the results for f_2 can be found in Appendix A.2.

Type of noise: random between 1-3 Hz or 2-4 Hz depending on the studied frequency, as defined in Table 5.

Figure 32: Structure of the analysis of the results section when noise is a random signal. This will allow to determine what is the influence of the varying parameters on the modal properties when the level of noise is increased.

The first tests will be done using a random excitation of 0.2 Hz bandwidth centered on the frequency of interest, i.e. one of the first two frequencies of the deck (1.59 Hz or 3.23 Hz), for a 15 min simulation. These choices have been done knowing that:

- The *random excitation* is **generated a single time** and is filtered accordingly, in order to always have the same excitation profile, no matter the test performed.

- The *simulation time* should be **large enough to remove the transient effects** and the tests realised by V2i on footbridges generally last 15 min by excitation type.

- The *bandwidth* of the excitation could have been chosen larger since the first two frequencies are far from each other. However, for a real structure as on *La Belle Liégeoise* footbridge in Liège, the number of modes in a very narrow range can be high. In order to ease the identification (less or no filtering of the data), **one should excite the lower number of mode possible** so that the bandwidth should be chosen small enough. This will be proven in Section 3.2.1.4 where the signals will

need to be filtered. However, the bandwidth should be **large enough to capture the resonance peak** and thus the right damping ratio (this will also be proven, in Section 2.3.2.3 a) i)).

In addition to the excitation previously defined, noise will be added **outside** and **inside** the frequency range of interest to see its **effect on the identified modal parameters**. For this part of the analyses, the noise is defined as a limited band random signal (see Table 5 and Section 2.2.3) regenerated at each iteration. The influence of the noise type will be studied in Section 2.4. Since the noise is regenerated at each iteration, the simulations must be **repeated several times** in order to limit dependency to the sampling. The simulations were then repeated 100 times for each case and a boxplot of the stabilised data can be obtained for each level of noise. *"A boxplot allows to represent easily a set of data where the central mark is the median and the edges of the box are the 25th and 75th percentiles. The whiskers extend to the most extreme data points the algorithm considers to not be outliers, and the outliers are plotted individually as red crosses"* [21].

The following analyses will only be done for a noise in the frequency range of interest, since the case when noise is outside the frequency range of interest should give consistent results with the identification method currently used by V2i (Section 1.1 and [2]): the modal parameters should be close to the reference value when the noise is outside the frequency range of interest. A study on the bandwidth of the excitation will be performed in order to determine its influence (Section 2.3.2.3 a)). Finally, a sine sweep will be simulated instead of a random for the measured excitation and a parametric study on the speed of the sweep will also be realised (Section 2.3.2.3 b)).

2.3.1   Noise is outside the frequency range of interest

In this section, the effect of noise on the modal properties of the system will be studied, when this noise is outside the frequency range of the interest. In this case, the excitation will always be a random signal of 0.2 Hz bandwidth centered on the frequency of interest, applied for 15 min.

2.3.1.1   Frequencies and damping ratios

Before analysing the results, some comments about the graphs have to be done:

- The median values for the frequency at 0% noise (which correspond to the identified value without noise) are slightly offset from their reference value (computed in Section 2.2.2, Table 4) due to the **choice of the time step**. That is why two types of limits are defined: those for reference value (in blue) and those for the identified value at 0% noise (in grey). Indeed, the periodicity error was less than 1% (as discussed in Section 2.2.4) but the distance between the grey and blue lines should decrease to zero as the time step decreases. However, this would result in a quite long simulation time so that a trade-off between accuracy and speed had to be done. The reference lines are not shown for the damping graphs since the periodicity error only applies for the frequency (the peak is only offset, not deformed, see Figure 28).

- For the following figures, only the lines for the identified values will be shown, for sake of readability. Indeed, the goal will be to study the effect of the noise on the identified value, compared to the one identified at 0% noise.

- The lines showing the limits for 1% error on frequency and 5% on the damping are also represented just to make the comparison easier between the different cases.
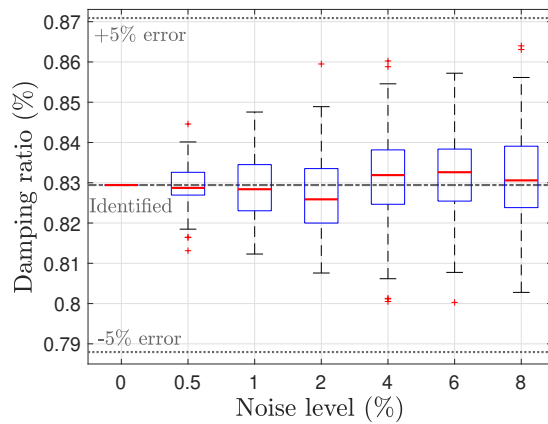
Figures 33 and 34 (shown at the beginning of next page) respectively show the behaviour of the first and second modal properties of the system when the noise is outside the frequency range of the excitation.
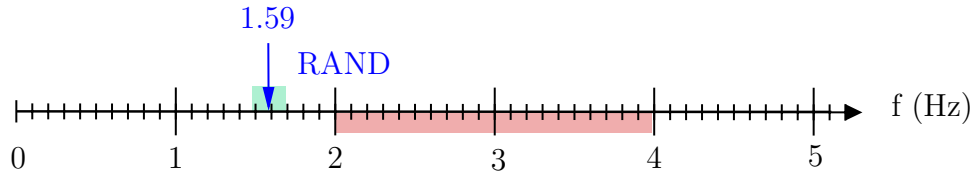
(a) Illustration of the case tested. The green box shows the range of the known excitation and the red one, the range of the unknown noise.
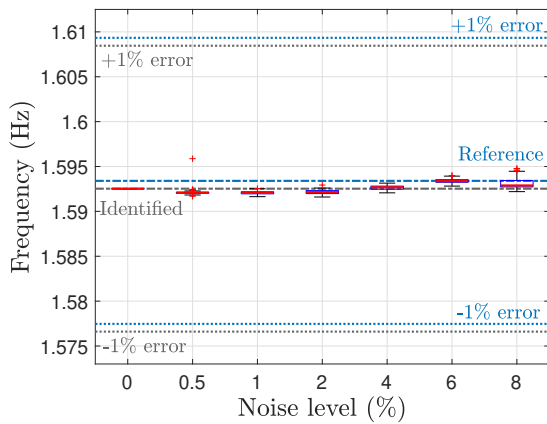
(b) Frequency.

(c) Damping ratio.

Figure 33: Results for the identified modal parameters of the system computed with the CSI algorithm for a high unmeasured noise outside the frequency range of interest and a known random signal of 0.2 Hz bandwidth around frequency 1 (1.59 Hz).

In either cases (Figures 33b and 34b), the identified value at 0% level of noise is close to the reference value (less than 1% error) showing that the CSI algorithm allows to correctly identify the modal properties of a given system when there is no noise. Concerning the evolution of the identified value with an increasing level of noise, the variation in frequency is negligible no matter the level of noise for both cases.

Concerning the evolution of the identified value for damping ratios, the same conclusion can be drawn, at least for mode 2 (Figure 34c). The observations are also verified for mode 3, which is shown in Appendix A.1. Indeed, for the damping of mode 2, the whiskers of the boxplots are close to the median value. However, the variability is higher in the case of mode 1 (Figure 33c), even if the median values follow the same tendency (close to the identified value).

(a) Illustration of the case tested. The green box shows the range of the known excitation and the red one, the range of the unknown noise.

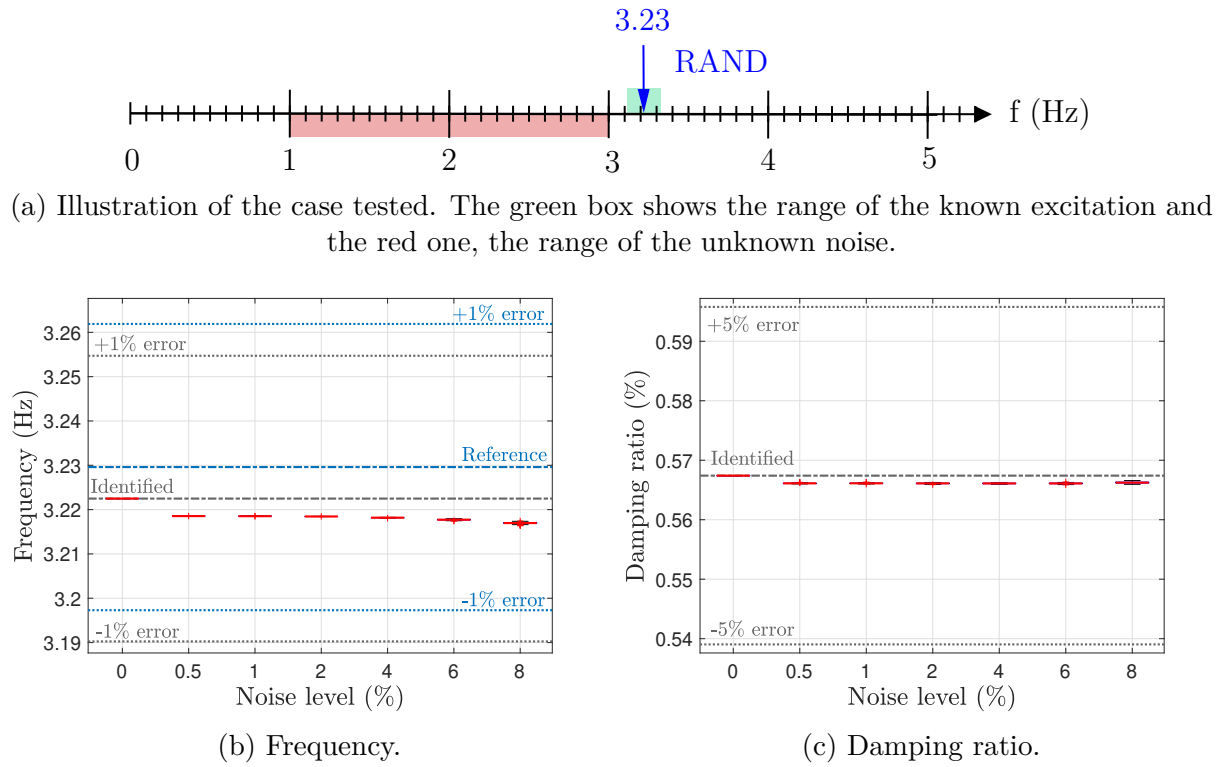

(b) Frequency.

(c) Damping ratio.

Figure 34: Results for the identified modal parameters of the system computed with the CSI algorithm for a low unmeasured noise outside the frequency range of interest and a known random signal of 0.2 Hz bandwidth around frequency 2 (3.23 Hz).

The difference between the two cases is that the noise is not defined in the same way. Indeed, the PSD of the noise from 1 to 3 Hz has a rounded shape while the one from 2 to 4 Hz has a more rectangular shape, as it was explained in Section 2.2.3 (see Figure 21). The rounded shape allows the noise to progressively increase/decrease whereas the rectangle shape cause a more sudden rise/drop of noise. So that the rectangular shape as a stronger influence on the frequencies close to its edges compared to the rounded one. Moreover, the noise is not on the same side for the two frequencies. In order to compare the two cases, noise should be at the left of the first frequency. So that by defining the outside noise from 0.49 to 1.49 Hz instead of 2 to 4 Hz for mode 1, one should obtain clearer results, with less variability. These values have been computed in order to roughly have the same configuration than for mode 2. Indeed:

$$\frac{1}{3.23} * 1.59 = 0.49 \quad \text{and} \quad \frac{3}{3.23} * 1.59 \simeq 1.49. \tag{35}$$

The results obtained with this new definition for the outside noise of mode 1 are shown in Figure 35.

(a) Illustration of the case tested. The green box shows the range of the known excitation and the red one, the range of the unknown noise.

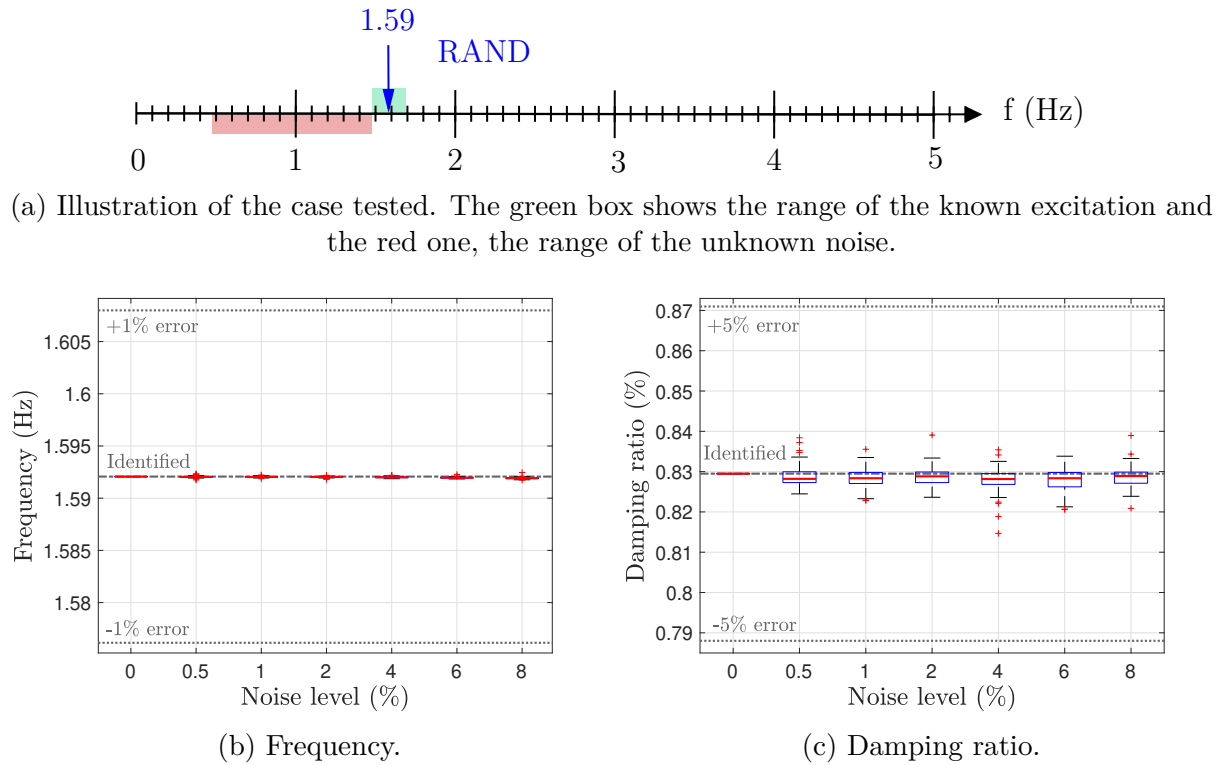

(b) Frequency.

(c) Damping ratio.

Figure 35: Results for the identified modal parameters of the system computed with the CSI algorithm for a low unmeasured noise outside the frequency range of interest and a known random signal of 0.2 Hz bandwidth around frequency 1 (1.59 Hz).

Comparing Figures 33c and 35c, one can see that the whiskers converged to the median value by putting the noise at the left of the excitation. The remaining variability is certainly due to the shape of the noise (that is still rectangular, as it was explained in Section 2.2.3). So that, what can be retained from the first part of this section is that when the noise is outside the frequency range of interest, the frequencies and damping ratios are close to their identified values at 0% noise, no matter the level of noise. This is even more correct if the noise is in a lower frequency range than the excitation.

2.3.1.2   Mode shapes

The mode shapes obtained with the function *subid.m* are in complex form. In order to determine if they are real or complex, one should measure their modal complexity thanks to Argand diagrams. This diagram plots the imaginary part of the mode shape in function of its real part. A real mode is represented on the Argand diagram by coefficients having a very close phase shift. Indeed, a mode is real only if it represents an in-phase vibration (standing wave), so that the node of vibration stays at the same location. However, a complex mode shape represents an out-of-phase vibration (travelling wave) so that the node of vibration does not stay at the same location [22]. After checking if the modes were indeed real ones, they can be normalised before being plotted. Figure 36 shows an example of Argand diagram for one estimation of the first mode as well as its normalised version.
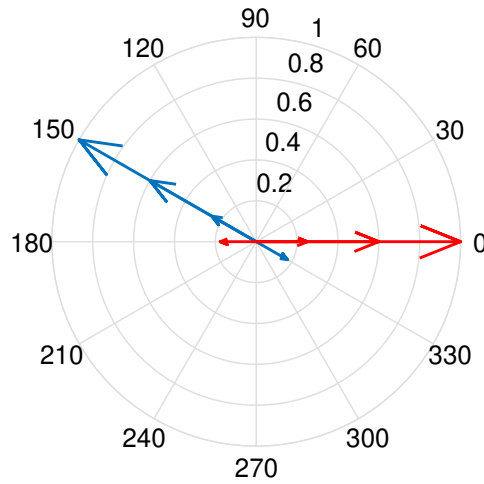
Figure 36: Argand diagrams for one estimation of mode shape 1, raw (blue) and normalised (red) versions. This type of diagram plots the imaginary part of the mode shape in function of its real part.

The arrows being all aligned show that the computed mode is indeed a real one. Since the tests were performed 100 times for each level of noise, one can obtain the median value of the vertical displacement for each measured node. The fact that only the vertical displacement is measured comes from the configuration shown in Figure 24. Finally, the median values of the first two mode shapes for an increasing level of noise can be observed in Figure 37 and compared with the reference ones obtained in Section 2.2.2, Figure 19.
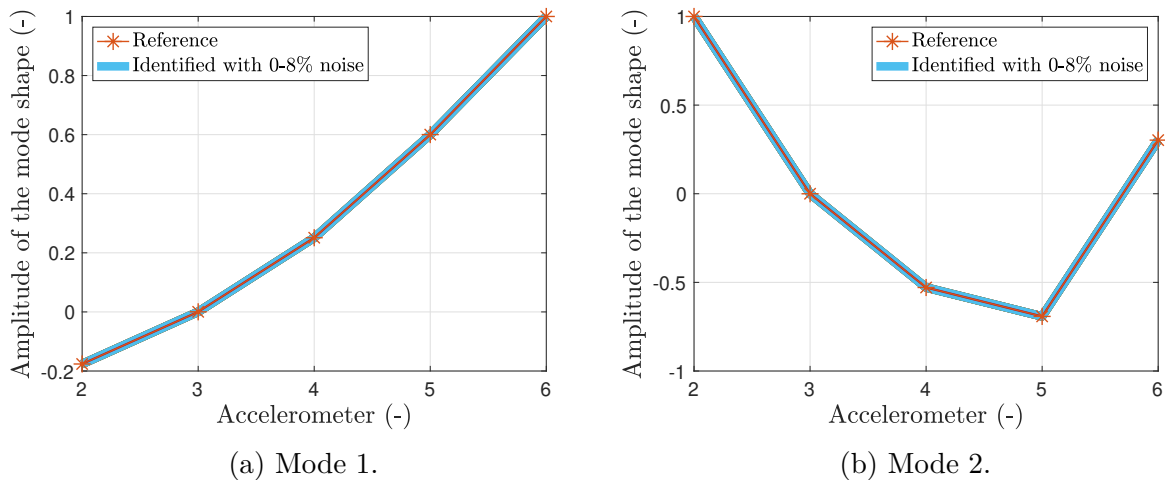

(a) Mode 1.

(b) Mode 2.

Figure 37: Comparison between the reference and the identified mode shapes of the system computed with the CSI algorithm for an increasing noise level outside the frequency range of interest.

It should be noted that due to the configuration shown in Figure 24, the modes are only accurate for the points in which the acceleration is measured, only on the vertical degree of freedom. That is why this type of representation has been chosen to present the results for the mode shapes. One can see that, as the frequency and the damping ratio, the median values of the identified vertical displacement at each node are consistent with the reference values. The different lines for the identified mode shapes with noise cannot be distinguished, that is why a single caption is present for all the curves (0 to 8% of

noise). The lines showing the 25th and 75th percentiles are not shown because they are indistinguishable for the median lines.

For both modes, the displacement of accelerometer 3 is equal to 0. This is due to the fact that the response was measured at the location of the pylon (see Figure 24) so that the displacement at this location is minimal. The location of highest displacement is not at the location of shaker (position 5), so that a better position for the shaker could have been chosen to optimally excite those modes. However, as it was already mentioned in Section 2.2.3, a compromise on the location of the shaker had to be done in order to excite both modes at the same time.

As it can be seen, when noise is outside the frequency range of interest, the identified modal properties are close to the identified value at 0%, no matter the level of noise. This was also the case for the identification method currently used by V2i (see Section 1.1 and [2]) so that, the most interesting case to study is to apply the CSI algorithm when noise is inside the frequency range of interest.

2.3.2   Noise is inside the frequency range of interest

In this section, the effect of noise on the modal properties of the system will be studied when this noise is inside the frequency range of the interest. As explained before, this case will be investigated more deeply than the previous one. This can be done by varying the bandwidth of the excitation or the type of signal to check if they have an influence on the identification of the modal properties.

2.3.2.1   Frequencies and damping ratios

Figures 38 and 39 (shown in the next page) show the results for the modal properties of the system when the noise is inside the range of the excitation. This one is still a random signal of 0.2 Hz bandwidth centered on the frequency of interest and is still applied for 15 min.

On those figures, it can be observed that when the noise is in the range of the frequency of interest, it has an higher influence on the damping ratio while it still has a poor influence on the frequency, compared to the case when noise is outside (Section 2.3.1). The higher the level of noise in the system, the more the median of the damping moves away from its identified value (computed at 0% level of noise) and the higher the variability in the results. Indeed, the minimum and maximum values starts to diverge more and more from the median value as the level of noise increases. The observations are also verified for mode 3, which is shown in Appendix A.1. This behaviour can be explained by looking at the power spectral density of the response of the footbridge in function of the percentage of noise. This is shown in Figure 40 (shown at the beginning of the next page) for mode 2 but the same applies for mode 1.

(a) Illustration of the case tested. The green box shows the range of the known excitation and the red one, the range of the unknown noise.

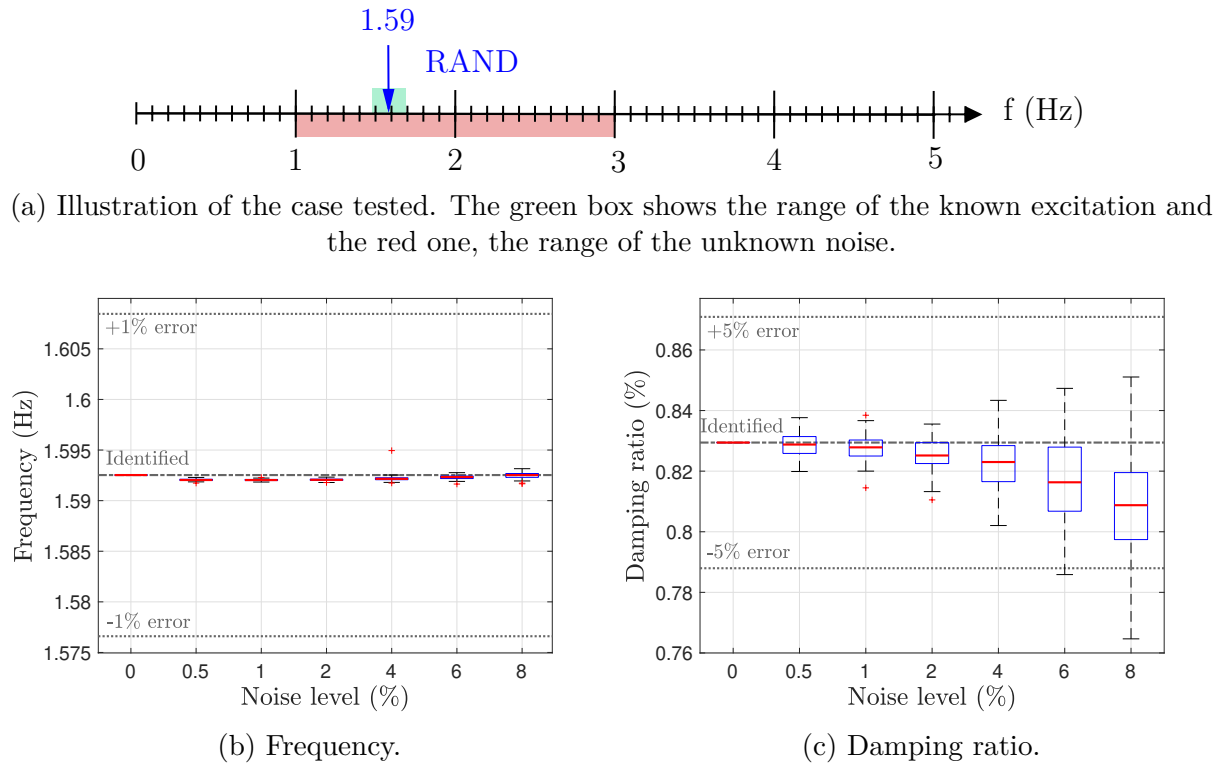

(b) Frequency.

(c) Damping ratio.

Figure 38: Results for the identified modal parameters of the system computed with the CSI algorithm for a low unmeasured noise inside frequency range of interest and a known random signal of 0.2 Hz bandwidth around frequency 1 (1.59 Hz).

(a) Illustration of the case tested. The green box shows the range of the known excitation and the red one, the range of the unknown noise.

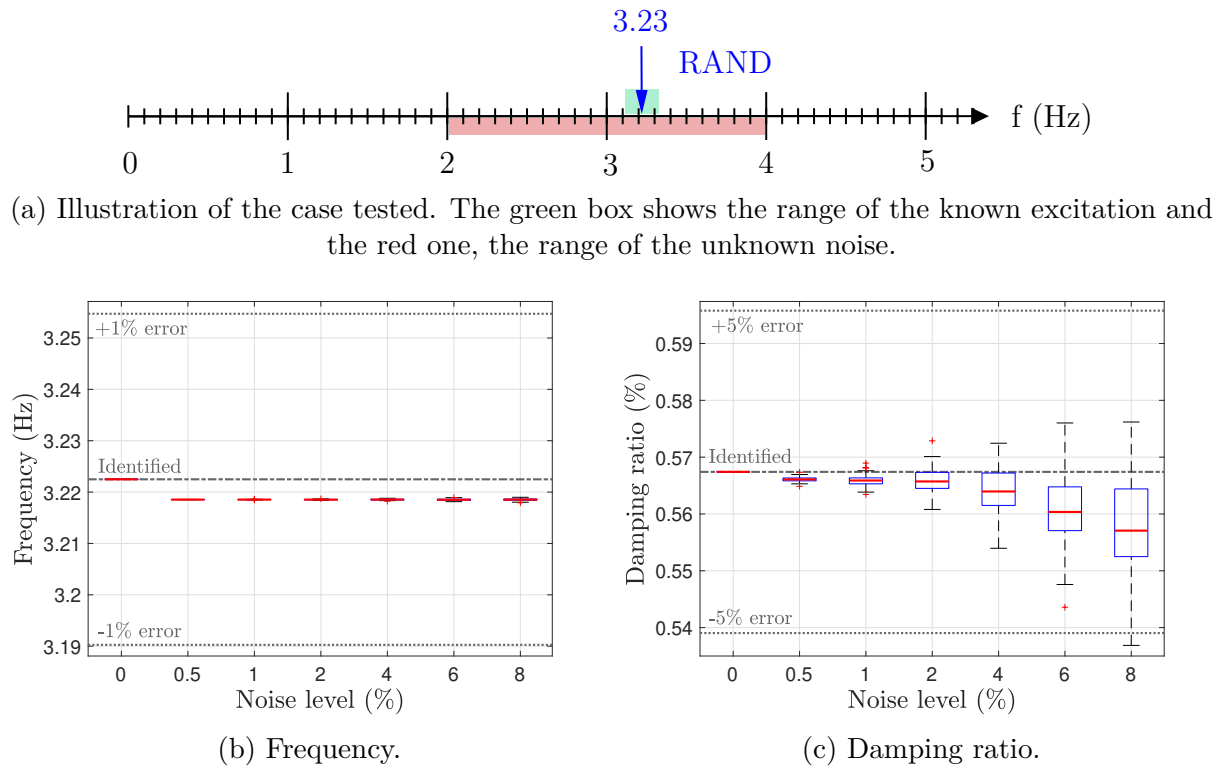(b) Frequency.

(c) Damping ratio.

Figure 39: Results for identified the modal parameters of the system computed with the CSI algorithm for a high unmeasured noise inside frequency range of interest and a known random signal of 0.2 Hz bandwidth around frequency 2 (3.23 Hz).
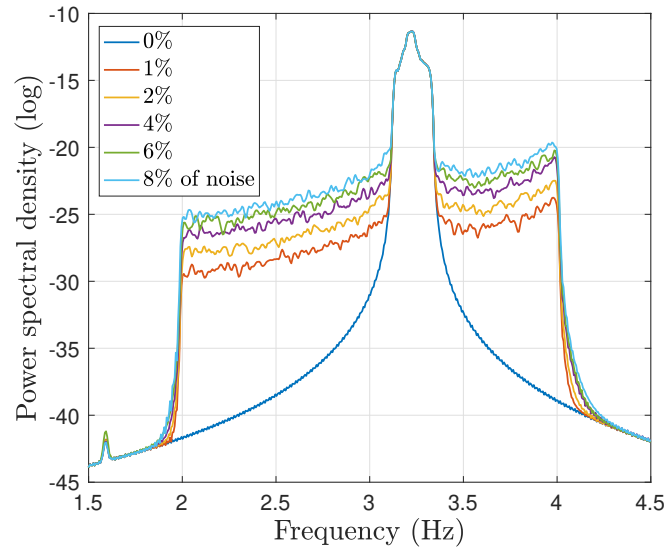
Figure 40: Power spectral density of the response of the footbridge in function of the level of noise for mode 2.

The horizontal axis of Figure 40 shows the same than Figure 39a excepted that now the amplitude component is also represented, on the vertical axis. One can see that as soon as noise is added in the system, the basis of the rise and drop of the peak is no longer distinguishable. As the level of noise increases, more and more portion of the rise and drop is covered. This could be why the damping ratio is more and more affected. Indeed, as it was seen in Equation (17), the damping ratio can be defined as the width of the peak over the resonance frequency, so that a larger peak for the same frequency translates into a higher damping ratio. As the level of noise increases, the width of the peak that can be identified becomes smaller so that this results into a smaller damping ratio, explaining the progressive degradation of the damping ratios towards lower values. However, the peak apex is well represented no matter the level of noise, so that the frequency can be correctly identified.

2.3.2.2   Mode shapes

Concerning the mode shapes obtained with the CSI algorithm when the noise is inside the frequency range of interest, they are not shown as they are the same than those obtained in Figure 37. This proves that **frequencies and modes shapes of this model are not really sensitive to noise compared to the damping ratios**, for the levels of noise tested. That is why the frequencies and modes shapes will not be represented in the following cases, because the conclusion does not change from the others cases: the frequency remains close to the identified value at 0% no matter the level of noise, as well as the shape of the mode.

### 2.3.2.3   Variation of the bandwidth and the type of the excitation

Now that the effect of the noise on the modal properties have been determined, some other parameters can be varied, as it was stated in Figure 32:

a) **Variation of the bandwidth of the excitation**

   In this section, the effect of taking a decreased (0.02 Hz) or an increased (0.6 Hz) bandwidth will be investigated.

i) **Decreased bandwidth: 0.02 Hz**
   Figure 41b shows the effect of taking a decreased bandwidth on the stabilisation diagram.
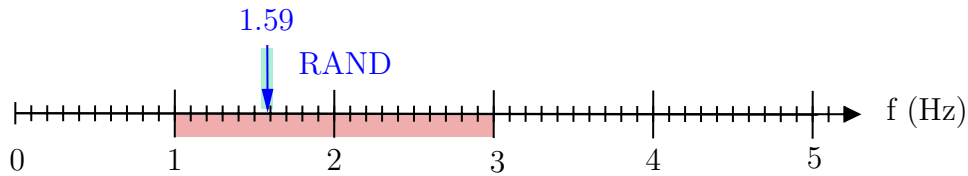
(a) Illustration of the case tested. The green box shows the range of the known excitation and the red one, the range of the unknown noise.
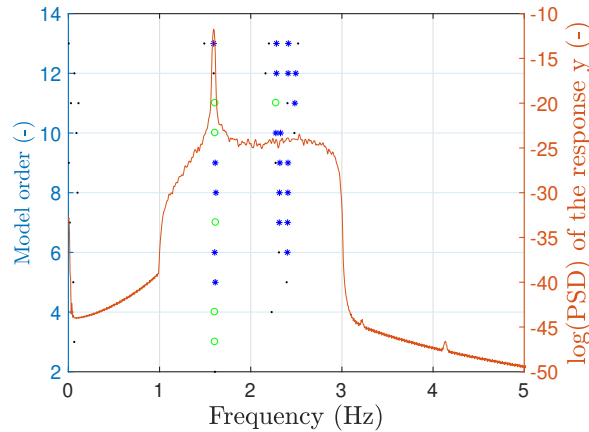
(b) Stabilisation diagram for a 8% level of noise.

Figure 41: Effect of taking a decreased bandwidth (0.02 Hz) on the stabilisation diagram of frequency 1 for a known random signal.

Taking a narrower interval is not a good solution as the **stabilisation diagram does not stabilise in damping for several consecutive orders** as it was defined in Section 2.2.5. Indeed, by exciting in a confined range like this one, there would not be enough points all around the rise and drop of the peak in the PSD graph, so that it will be difficult to compute the damping ratio. Indeed, the damping ratio can be associated to the width of the peak, as it was already explained. The illustration of taking a too narrow excitation band is presented in Figure 42.
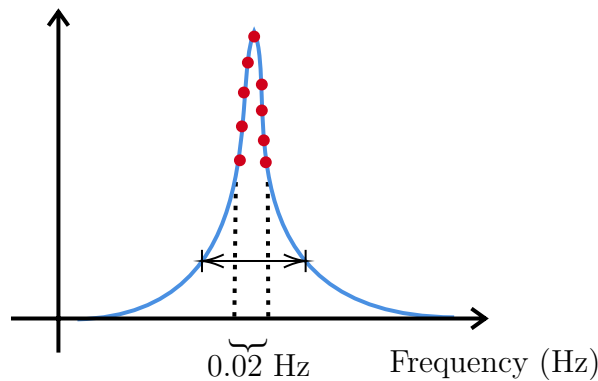

Figure 42: Illustration of taking a too narrow bandwidth on the estimation of the damping ratio. The red dots are the locations of the identified values with the random excitation.

So that the width of the peak cannot be correctly represented and so is the damping ratio. That is why a sine excitation would not be useful either to determine the damping ratio since it only excites at a given frequency. Anyway, a narrow band like this one is never used in practice. If two modes are really close in frequency and are in the range of the excitation chosen, the method is to put the shaker on the node of the undesired mode so that it is not measured.

ii) **Increased bandwidth: 0.6 Hz**
Both frequencies have different damping ratios with $\zeta_1 = 0.83\% > \zeta_2 = 0.55\%$. As it was already mentioned several times, the higher the damping ratio is, the wider the peak will be in frequency spectrum. So that a larger bandwidth of excitation should be taken for mode 1 than mode 2, in order to estimate the damping correctly. Figure 43b shows the results obtained for the damping ratio of frequency number one for a random excitation with an increased bandwidth (0.6 Hz).
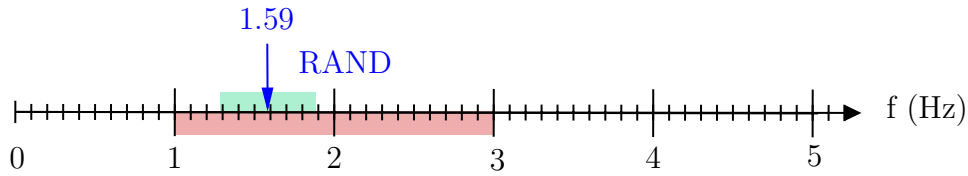
(a) Illustration of the cases tested. The green box shows the range of the known excitation and the red one, the range of the unknown noise.
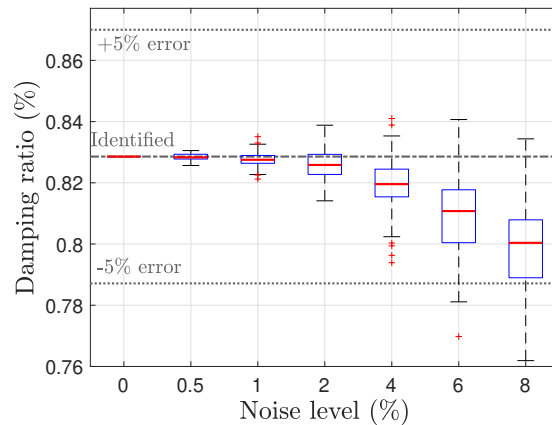
(b) Results for the damping for an increased bandwidth.

Figure 43: Effect of taking an increased bandwidth (0.6 Hz) on the damping ratio of frequency 1 for a known random signal.

One can see that taking a larger interval poorly influences the results (by comparing with Figure 38c), in this case. Indeed, the variability represented by the whiskers and percentile lines is smaller than the case with a 0.2 Hz bandwidth excitation but only for a very small percentage of noise ($< 1\%$). Indeed, as the level of noise increases, this difference is less and less pronounced. So that the interval was already large enough to determine the damping ratio with the 0.2 Hz bandwidth excitation. A small difference in the median values can be observed. Indeed, by looking at the 8% noise boxplot for Figure 38c and 43b for example, the median for the increased bandwidth is lower than

the case for the 0.2 Hz bandwidth. However, this difference is of the order of 1%. This difference could be due to the random nature of the noise signals so that the two cases are not exactly the same (the results depend on the noise signal that have been generated randomly). However, the most important thing to remember from this test is that the **bandwidth was already large enough to evaluate the damping ratio**. The tests were also performed for the second frequency of the system and the results (leading to the same conclusions) can be found in Appendix A.2.

b) **Variation of the type of the excitation**

One can also change the type of excitation to see if it has an influence on the results. Instead of using a random signal for the excitation, a sine sweep signal is now simulated for 15 minutes. A sine sweep consists in imposing a single frequency at any given time. However, the frequency varies in time from low frequency to high frequency, in this case. So that for mode 1 (1.59 Hz), the starting frequency is chosen to be 1.49 and will progressively be increased up to 1.69 Hz until the end of the simulation.

The simulation time can also be adapted in order to study the influence of speed of the sweep. The same test is thus realised, but for a 7 min simulation time. The results for the damping ratios are presented in Figure 44.
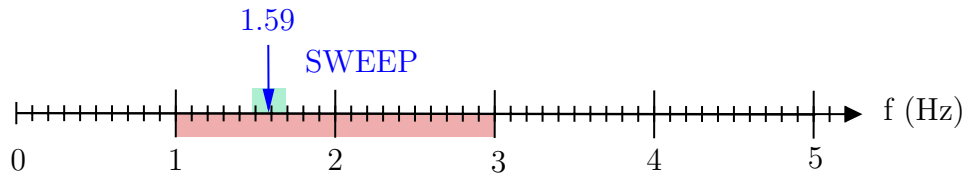
(a) Illustration of the case tested. The green box shows the range of the known excitation and the red one, the range of the unknown noise.
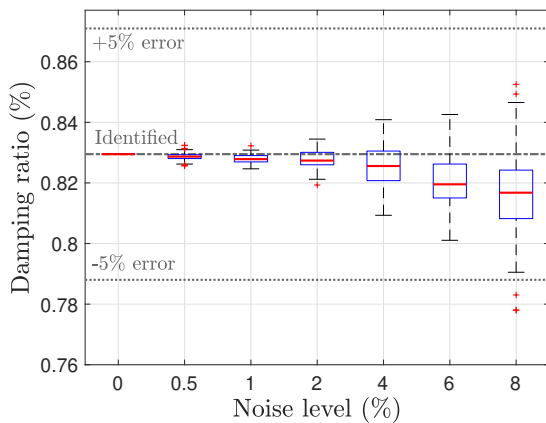
(b) For a 15 min simulation.
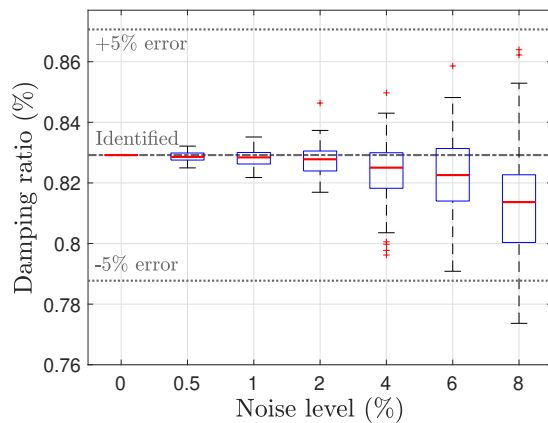
(c) For a 7 min simulation.

Figure 44: Change in type of excitation signal - sine sweep between 1.49 and 1.69 Hz.

Using a sweep signal for the same simulation time (Figure 44b) shows the same effect than extending the bandwidth: the variability represented by the whiskers and percentile lines is smaller than the case with a random excitation of 0.2 Hz bandwidth (Figure 38c) but only for a small percentage of noise. Moreover, a difference in the median values can be observed but this one is of less than 1%. So

that **imposing a sweep signal leads to approximately the same results than imposing a random excitation**. **Decreasing the simulation time** leads to an **increased variability** on the values when comparing the results in Figures 44b and 44c. This is due to the fact that if the speed of the sweep is too high, the system has less time to stabilise, even if it will not reach steady state with this type of excitation. The tests were also performed for the second frequency of the system and the results (leading to the same conclusions) can be found in Appendix A.2.

2.3.3   Summary

In this section, the influence of the noise on the identified modal properties as well as the influence of the type of excitation was investigated. The simulations were repeated 100 times so that boxplots have been used to represent the results obtained for a defined level of noise. The first tests were performed with a random excitation of 0.2 Hz bandwidth centered on the frequency of interest for a 15 min simulation:

- When the noise was **outside** the frequency range of interest, all modal parameters (frequencies, damping ratios and modes) were close the identified value at 0% noise. So that they were independent of the level of noise in the system and the variability of the results was very low. This was even more true when the noise was in lower frequency range than the frequency range of the excitation.

- When the noise was **inside** the frequency range of interest, the same conclusion could be drawn concerning the frequencies and mode shapes. However, concerning the damping ratios, a progressive degradation of the results towards lower values (compared to the identified value at 0% noise) was observed as the level of noise increased up to 8%. So that the most sensitive values to the noise are the damping ratios, in this case.

  Then the bandwidth of the excitation, the type of signal and the simulation time were modified in order to asses their respective influence:

  - Taking a *too narrow interval* leads to no results as the stabilisation diagram did not show stable poles for several consecutive orders. Indeed, if the bandwidth is not large enough, it is not possible to correctly represent the rise and drop of the resonance peak in the PSD and thus the damping ratio cannot be estimated correctly.

  - Taking a *larger interval*, in this case, did not have a big influence on the results for the damping ratio meaning that the frequency range of the excitation was already large enough in order to estimate it.

  - Applying a *sweep signal* as excitation led to the same conclusion: it does not have a big influence on the results compared to the random excitation. However, decreasing the simulation time for the sweep shows a larger variation in the results (the min and max values move away from the median values), showing that the simulation should be realised for a long enough time in order to obtain more precise results.

Now that the influence of the type of excitation have been assessed, one can investigate what is the influence of the type of noise on the system. Indeed, the noise will now be represented by several pedestrians walking back and forth on the footbridge. This case will be investigated in Section 2.4

2.4 Influence of the type of noise

As said before, it could be interesting to simulate some pedestrians as they can be the source of noise going from about 1 to 3 Hz [3]. The aim of this section is thus to model the noise as several pedestrians crossing the footbridge back and forth, each at their own pacing rate, instead of limited band random signals (as it was realised in Section 2.2.3). This will be realised in Section 2.4.1. However, the loading contribution of a pedestrian can be described by a sinusoidal force [3]. As a recall, the OMAX method makes the assumption that the noise is a Gaussian white noise. So that the effect of not having a white noise anymore will be studied in Section 2.4.2. The tests will be performed for an increasing number of pedestrians crossing the footbridge so that the level of noise is progressively increased.

2.4.1 Force induced by the pedestrians

The force induced by a pedestrian on a footbridge can be vertical, normal or tangential. In this case since the model is only 2D and since only the vertical modes of the deck are of interest, only the vertical load will be taken into account. Since modal forces will be used, the system should now be written in modal form, so that:

$$\mathbf{M}^*\ddot{\mathbf{q}} + \mathbf{C}^*\dot{\mathbf{q}} + \mathbf{K}^*\mathbf{q} = \mathbf{F}_p + \mathbf{P}^*_{shaker}. \tag{36}$$

Where the generalised force imposed by the shaker is computed as $\mathbf{P}^*_{shaker} = \mathbf{\Phi}^T P_{shaker}(t)$ and $\mathbf{F}_p$ is the vertical force imposed by the pedestrians. Its definition is given by Equation 37 [3] and thanks to the properties of the Dirac delta one has:

$$\mathbf{F}_p = \int_0^L F_p^v(t)\delta(x_p - v_p t)\mathbf{\Phi}(x_p)dx = F_p^v(t)\mathbf{\Phi}(v_p t), \tag{37}$$

with v_p being the forward speed of the pedestrian assumed to be constant and x_p its position on the footbridge. The vertical pedestrian load can be described by the following Fourier Series [3]:

$$F_p^v(t) = W + \alpha_{1,v}W\sin(2\pi f_s t) + W\sum_{i=2}^{n}\alpha_{i,v}\sin(2\pi i f_s t - \varphi_i). \tag{38}$$

In [3], it is advised to only keep the first two terms because the coefficients $\alpha_{i,v}$ for $i > 1$ become too small to be considered. The parameters and their common values are summarised in Table 6.

Parameter	Name	Value
W	Weight of pedestrian	Between 500-900 N
$\alpha_{i,v}$	Dynamical load factor	$\alpha_1 = 0.34 - 0.09 * log(n_p)$ (if $n_p < 10$) $\alpha_1 = 0.25$ (if $n_p > 10$) n_p = number of pedestrians on the footbridge
φ	Phase angle of ith harmonic relative to the first harmonic	$\varphi_2 = \varphi_3 = \pi/2$

Table 6: Values and names of the different parameters appearing in the pedestrian vertical load equation (38) [3].

Concerning the pacing rate f_s and the forward speed v_p, they are related. Table 7 shows their typical values for different types of walks.

	Pacing rate f_s (Hz)	Forward speed v_p (m/s)
Slow	1.7	1.1
Normal	2.0	1.5
Fast	2.3	2.2
Jog	2.5	3.3
Sprint	> 3.2	5.5

Table 7: Typical values for pacing rate f_s and forward speed v_p of a pedestrian [23].

Usually, slow to fast walks are the most observed ways to walk on footbridges, so that the values of v_p will be randomly generated in the interval [1.1 - 2.2] (m/s) and the value of f_s will be interpolated in the interval [1.7 - 2.3] (Hz), for each pedestrian. The weight of the pedestrian will also be randomly generated in the interval cited in Table 6. This will allow to obtain a random vertical force for each pedestrian.

Now that the vertical force of the pedestrian $F_p^v(t)$ have been determined one should compute the modal form $\mathbf{\Phi}(v_p t)$ of Equation 37. To do so, the modes of the footbridge should be interpolated at the position of the pedestrian. Its instant position x_p can be computed as follows:

$$x_p(i, k) = x_0(k) + v_p(k) * (t(i) - t_0(k)), \tag{39}$$

where $t(i)$ is the time instant, k is the kth pedestrian, x_0 is the initial position of the pedestrian and t_0 is the phase shift of the pedestrian. Since the goal is to simulate the pedestrian walking back and forth on the footbridge, the initial position is randomly chosen between the beginning (x_{start}) and the end (x_{end}) of the footbridge. t_0 is equal to 0 at the beginning of the walk and will be useful to simulate the back and forth movement of the pedestrian. The speed of the pedestrian is positive if going towards the right and negative if going towards the left. This is illustrated in Figure 45.
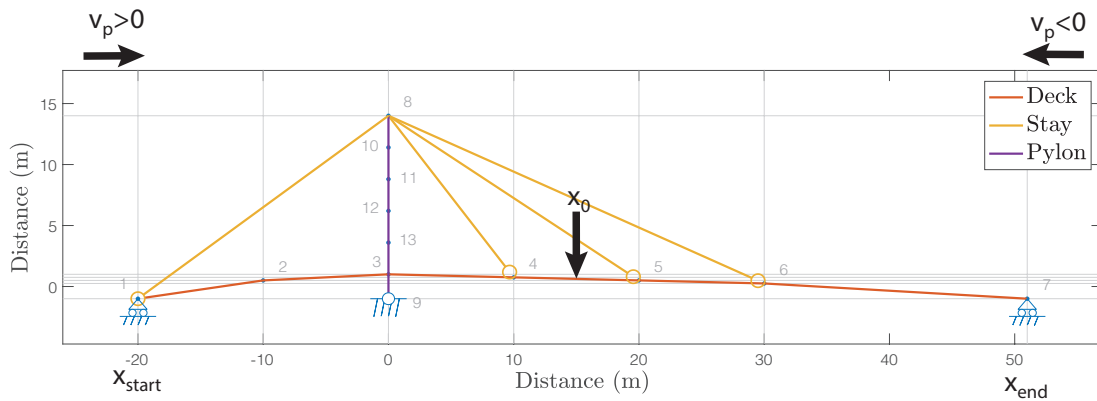

Figure 45: Illustration of the parameters in the position equation of the pedestrians (Equation 39).

Once the pedestrian reaches one of the ends of the footbridge (x_{start} or x_{end}), its speed v_p changes sign, its new initial position is equal to x_{start} or x_{end} and t_0 is equal to the time instant $t(i)$ at which it reached the extremity. So that during all the simulation time, the pedestrian is walking back and forth on the footbridge. The content of this section is coded in the function *loading_model_test.m* and is also available on MatheO [13].

Figure 46 shows one estimation of the imposed dynamic charge obtained for mode 1 for 1, 5 and 10 pedestrians and their respective power spectral densities.
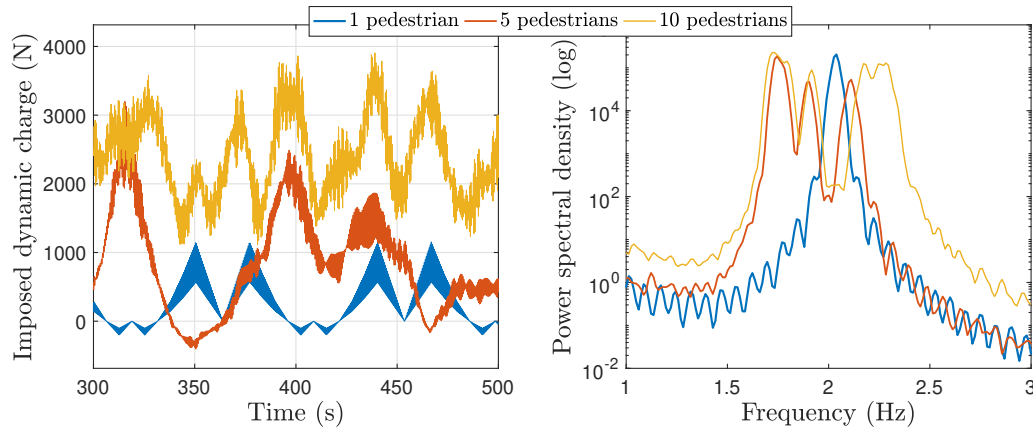

Figure 46: Imposed dynamic charges applied to the footbridge along time for different numbers of pedestrians and their associated power spectral densities. This example is shown for mode 1.

One can see that, the more pedestrians are walking on the footbridge at the same time, the higher the imposed dynamic charge is and the higher the response of the footbridge will be. Indeed, the imposed dynamic charge is computed by summing the $\mathbf{F}_p$ for the different pedestrians. Moreover, the more pedestrians are added, the wider the frequency content becomes. However, some dominant frequencies can be spotted, this is known as coloured noise. So that the white noise assumption is not met anymore. This means that the "*frequency components cannot be separated from the eigenfrequencies of the system and they will appear as poles of the state matrix A* [20]". This will be shown in the analysis of the results (Section 2.4.2). The case with one pedestrian is very particular as its random characteristics (speed, weight...) can differ consequently from one pedestrian to another. Moreover, its frequency content is very narrow as it will only have a peak at the pacing rate of the single pedestrian.

2.4.2 Analysis of the results

In order to see what is the influence of using a noise induced by pedestrians, a random signal will be applied by the shaker. The level of the shaker will be set to the highest value the shaker designed by V2i can provide (4500 N, see Table 9) and the number of pedestrians will progressively be increased. Table 8 shows the different steps that were performed in order to obtain the results for this case.

Step	Number of pedestrians	Force imposed by the shaker (N)	Objective
1	0	4500	Compute the rms value of the response for the shaker alone
2	1, 3, 5, 8, 10	0	Compute the rms value of the response for the pedestrians alone
3	0, 1, 3, 5, 8, 10	4500	Compute the modal properties

Table 8: Steps performed in order to obtain the results in the case where the noise is induced by pedestrians: the value of the force imposed by the shaker is settled and the number of pedestrians is increased.

The steps 1 and 2 of Table 8 allow to define the percentage of noise. Thanks to step 1, one can compute the root mean square value of the response of the footbridge (the one obtained after the Newmark computation) for the shaker alone $rms(y)_{shaker}$, with a force of 4500 N. The same is done for the pedestrians alone $rms(y)_{pedestrians}$, but is repeated 100 times in order to build boxplots since several parameters in the computation of the vertical force of the pedestrians (Equation (37)) are randomly generated. For this case, the noise is then defined as:

$$\% \text{ of noise} = \frac{rms(y)_{pedestrians}}{rms(y)_{shaker}}. \tag{40}$$

For each number of pedestrians, a percentage of noise can then be defined. Once the percentage of noise has been defined, one can run the algorithm for both parameters at the same time (step 3 of Table 8) and the results (identified modal properties of the system) can be analysed. The results will be analysed for two systems:

a) *MODEL 1*: System with fundamental frequency at **1.59** Hz (that is the model that have been used up to now);

b) *MODEL 2*: System with fundamental frequency at **2** Hz.

Indeed, as it was shown in Figure 21b and Table 7, 1.59 Hz is very close to the starting value of the interval defining the pacing rate of pedestrians ([1.6 or 1.7 - 2.3] Hz). So that the system having a fundamental frequency at 1.59 Hz is a limiting case. That is why the study will also be done for a system having a fundamental frequency of 2 Hz. This model was obtained by modifying the inertia and cross sections of the different geometries as it was done in Section 2.2.1 in order to obtain its fundamental frequency at the desired value.

For each system, the effect of having the **noise inside** or **outside the frequency range of interest** will be studied. So that the simulations have the same goal of Section 2.3 but now the noise is caused by the pedestrians and is thus no more white. The results will once again be compared to limits showing 1% error on the frequency and 5% error on the damping ratio with their respective values identified at 0% noise, in order to compare the different cases.

a) **MODEL 1: System with fundamental frequency at 1.59 Hz**

Noise is inside the frequency range of interest

First, thanks to the steps 1 and 2 of Table 8, one can define the percentage of noise for a random excitation around frequency one and a noise inside the frequency range

of the excitation. The results for the definition of the noise level are presented in Figure 47. The results for the modal properties obtained with the step 3 of Table 8 can be observed in Figure 48.

(a) Illustration of the case tested. The green box shows the range of the known excitation and the red one, the range of the unknown noise.

(b) Boxplots.

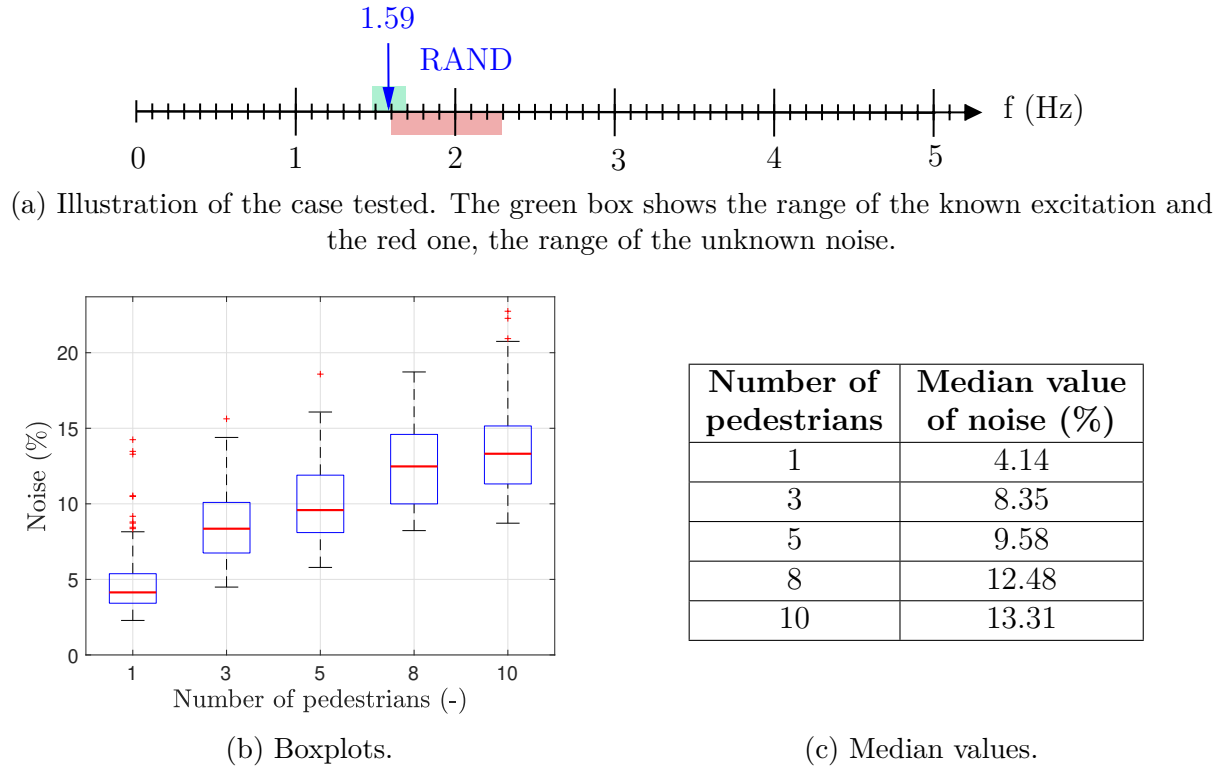| Number of pedestrians	Median value of noise (%)
1	4.14
3	8.35
5	9.58
8	12.48
10	13.31

(c) Median values.

Figure 47: Percentage of the noise in function of the number of pedestrians for a system with a fundamental frequency at 1.59 Hz for its first eigenfrequency.

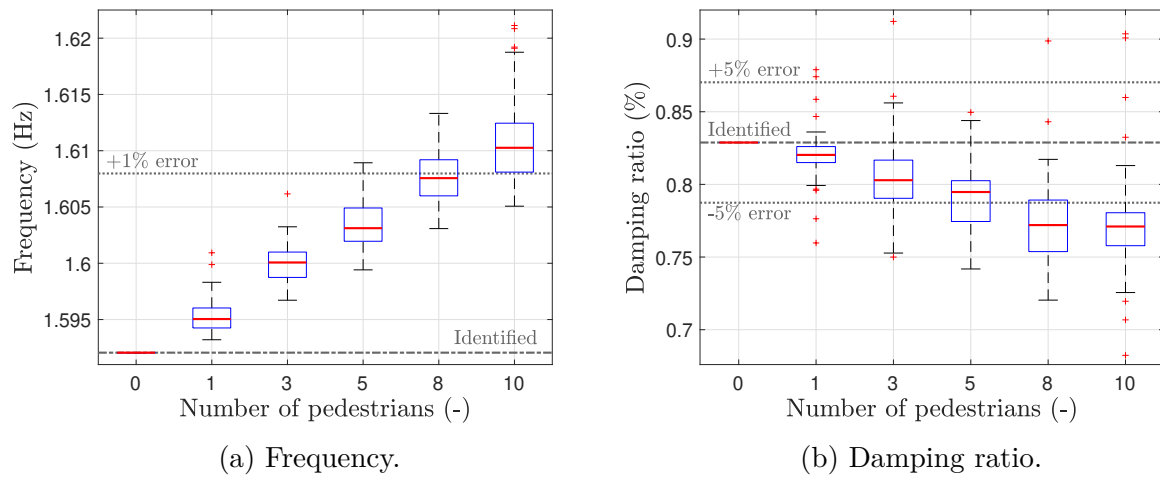(a) Frequency.

(b) Damping ratio.

Figure 48: Results obtained with the CSI algorithm for frequency number one (1.59 Hz) for a known random excitation of 0.2 Hz bandwidth and an unmeasured excitation caused by pedestrians walking back and forth on the footbridge.

One can see that increasing the number of pedestrians leads to an increasing level of noise (Figure 47). The first thing that can be observed concerning the modal properties is that the damping ratio (Figure 48b) roughly has the same behaviour than in Section 2.3.2. Indeed, the higher the noise, the more the median values are moving away from the identified value at 0% noise. However, the difference now is that it seems that the median value converges to an asymptote as the level of noise increases, there is a saturation effect. Indeed, adding more and more pedestrians will not necessarily mean that the damping ratio will decrease proportionally. In other words, as the number of pedestrians is increased, the influence of the added pedestrian is decreasing. Indeed, as it can be seen in Figure 46, the effect of adding more and more pedestrians is only translated in a wider frequency content, not in a consequently higher power spectral density. Concerning the limits, it can be concluded that beyond a certain number of pedestrians, one should be careful with the results obtained (more than 5% error on the damping). Here this value is 5 pedestrians, however this value depends on the system and on the studied frequency as it will be seen in the other cases. It also depends on the criterion that is chosen to tell if the results are acceptable or not. Here a 5% error was chosen in order to compare the different cases but one could chose to put the limit at 1% error for example.

Concerning the frequency (Figure 48a), the conclusion differs from the one that was drawn in Section 2.3.2. Indeed, the frequency now varies with the percentage of noise, which was not the case when the noise was a random white one. As explained in Section 2.4.1, this could be due to the fact that as the noise is not white anymore, the system considers noise as poles of the state matrix A so that the noise appears on the stabilisation diagram as a real pole. So that, as the level of noise increases, the value of the frequency converges towards the value of the noise. That is why in this case the frequency converges towards higher values (from 1.59 Hz to 1.6/1.7 Hz which is the beginning value of the noise range).

However, as it was already mentioned, this case is a limiting one as it can be seen in Figure 47a so that, before drawing conclusions about the system poles, one should observe what happens with a more general case as the one with a fundamental frequency at 2 Hz.

Noise is outside the frequency range of interest

Once again, the noise is first defined thanks to the first two steps of Table 8 and is presented in Figure 49. The results of step 3 of the same table (modal properties of the system) can be observed in Figure 50.

(a) Illustration of the case tested. The green box shows the range of the known excitation and the red one, the range of the unknown noise.

(b) Boxplots.

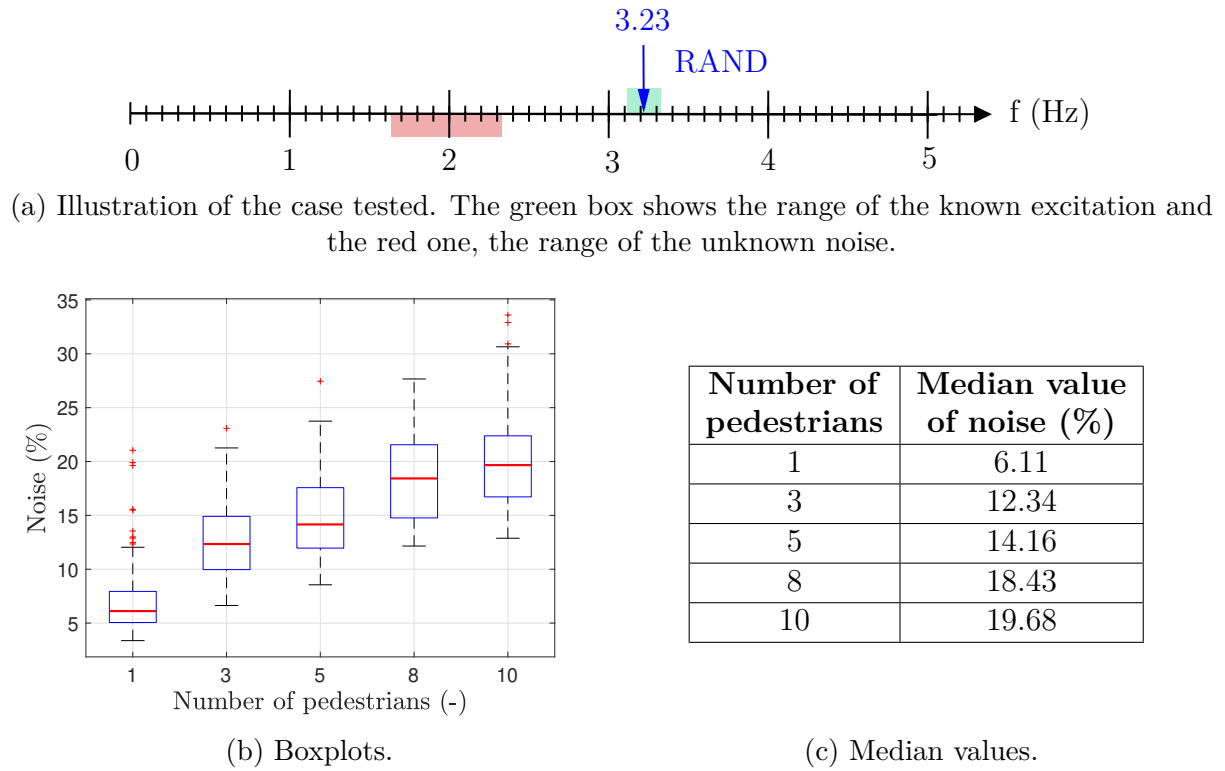| Number of pedestrians	Median value of noise (%)
1	6.11
3	12.34
5	14.16
8	18.43
10	19.68

(c) Median values.

Figure 49: Percentage of the noise in function of the number of pedestrians for a system with a fundamental frequency at 1.59 Hz for its second eigenfrequency.
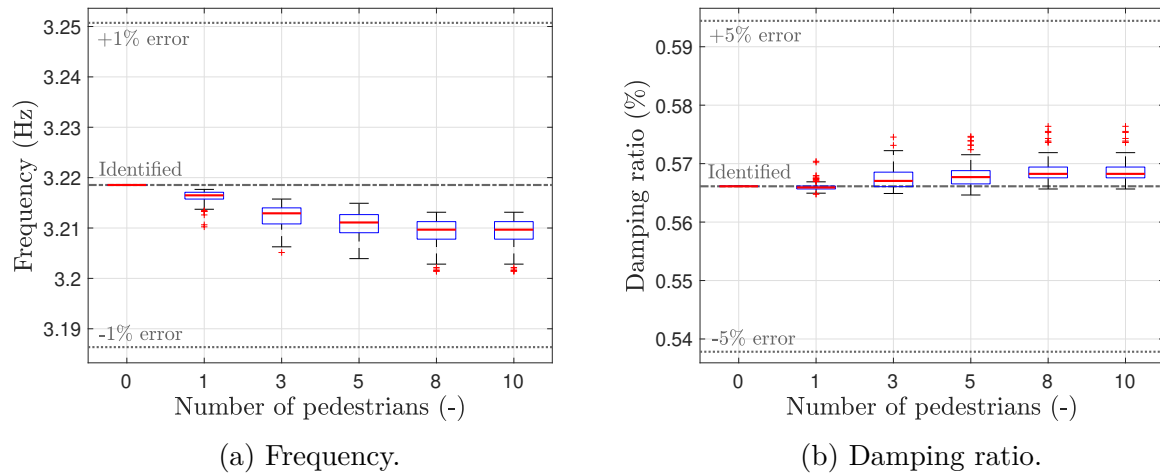

(a) Frequency.

(b) Damping ratio.

Figure 50: Results obtained with the CSI algorithm for frequency number two (3.23 Hz) for a known random excitation of 0.2 Hz bandwidth and an unmeasured excitation caused by pedestrians walking back and forth on the footbridge.

Once again, increasing the number of pedestrians leads to an increasing level of noise (Figure 49). By comparing the tables of Figure 47c and 49c, one can see that the percentage of noise is slightly higher in the case of the second eigenfrequency. This is due to the fact that the damping of this frequency is lower than the damping of the first one. So that, for the same level of shaker, the amplitude of the vibrations caused by the pedestrians will be higher and by definition (Equation 40) the percentage of noise will be higher. However, the $rms(y)_{shaker}$ will also slightly change so that the cases are not totally comparable.

The results obtained for the damping in this case (Figure 50b) are in agreement with the conclusions drawn in Section 2.3.1.1. Indeed, the percentage of noise barely has an influence on the results, the medians are close to the identified value at 0% noise. However, a small influence on the frequency seems to appear (Figure 50a), but as the level of noise increases, this median value seems to stabilise. As the converging value has less than 1% error with the identified value at 0% noise, this effect can be considered to be negligible. So that, no matter the level of noise, when it is outside the frequency range of interest, both modal properties are close to the identified value at 0% noise.

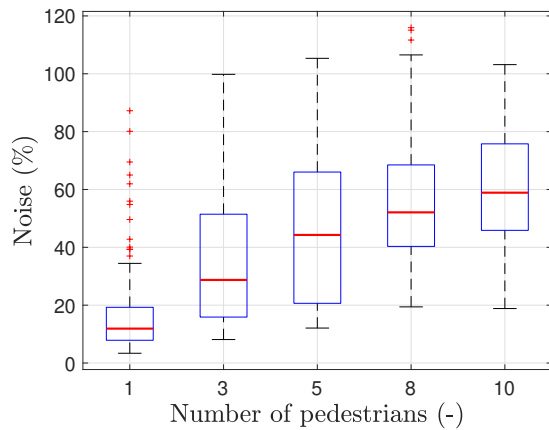b) **MODEL 2: System with fundamental frequency at 2 Hz**

As it was mentioned, the previous case (with a fundamental frequency of 1.59 Hz) was a particular one as the first frequency of the model was close to the beginning value of the noise induced by pedestrians. So that, the behaviour of another model with a fundamental frequency at 2 Hz can be also be studied.

Noise is inside frequency range of interest

Once again, the noise is first defined thanks to the first two steps of Table 8 and is presented in Figure 51. The results of step 3 of the same table can be observed in Figure 52.
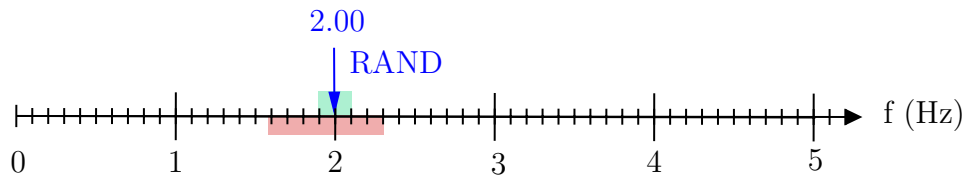
(a) Illustration of the case tested. The green box shows the range of the known excitation and the red one, the range of the unknown noise.

Number of pedestrians	Median value of noise (%)
1	11.89
3	28.72
5	44.27
8	52.09
10	58.88

(b) Boxplots.   (c) Median values.

Figure 51: Percentage of the noise in function of the number of pedestrians for a system with a fundamental frequency at 2 Hz for its first eigenfrequency.

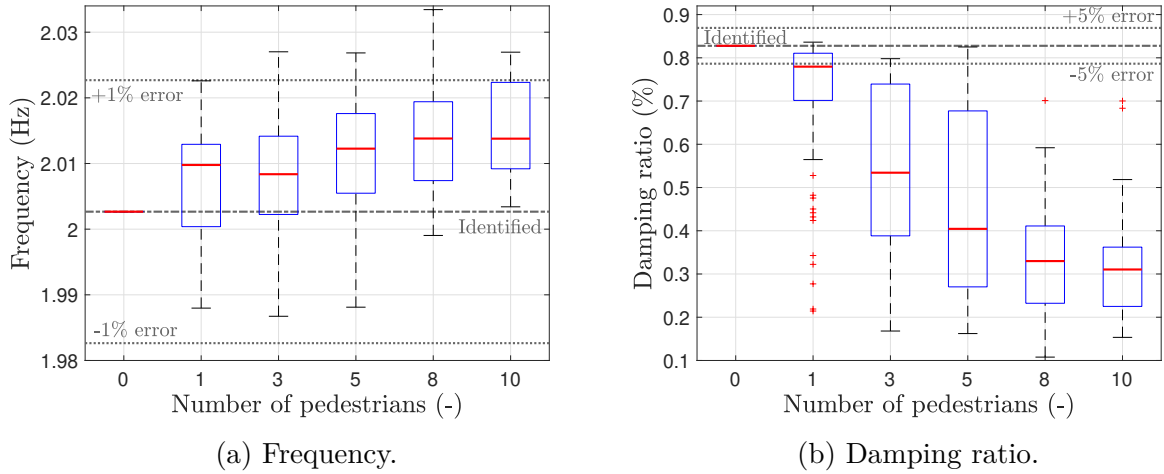(a) Frequency.   (b) Damping ratio.

Figure 52: Results obtained with the CSI algorithm for frequency number one (2 Hz) for a known random excitation of 0.2 Hz bandwidth and an unmeasured excitation caused by pedestrians walking back and forth on the footbridge.

One can see that increasing the number of pedestrians leads to an increasing level of noise (Figure 51), just as in the other cases. However, in this case the level of noise is more consequent when comparing Table 47c and Table 51c). This is due to the fact that the frequency of the model is now in the middle of the noise range as it can be seen in Figure 51a, resulting in a higher noise level. As the percentage of noise is higher for a given number of pedestrian when comparing both models (e.g. 9.58% noise for 5 people, model 1 and 44.27% noise for 5 people, model 2), it means that the limit for 5% error on the damping ratio will be crossed for less pedestrians than the previous system. This is indeed, what is observed here. The limit is crossed between 1 and 3 pedestrians (Figure 52b) while it was between 5 and 8 pedestrians for the previous model (see Figure 48b). So that an universal number of pedestrian for which the identified modal properties will overcome the limit cannot be defined, as it was explained. A solution to improve the results (obtain medians closer to the identified value) for a larger number of pedestrians would be to increase the force imposed by the shaker. Nevertheless, the same saturation behaviour for the damping ratio as in the system with a fundamental frequency at 1.59 Hz is observed.

Concerning the frequency (Figure 52a), the variability in the results is higher than in Figure 48a due to the fact that the excitation is now surrounded by the noise (see Figure 51a). However, the median value is quite stable considering the high percentage of noise, compared to Figure 48a. This could be explained by the fact that now the noise is approximately symmetric around the first frequency. However, compared with Section 2.3.2.1, the frequency should not be dependent of the noise level. That proves that using a coloured noise indeed has an influence on the poles of the state matrix A as it was stated in Section 2.4.1.

Noise is outside the frequency range of interest

Once again, the noise is first defined thanks to the first two steps of Table 8 and is presented in Figure 53. The results of step 3 of the same table can be observed in Figure 54.

(a) Illustration of the case tested. The green box shows the range of the known excitation and the red one, the range of the unknown noise.

Number of pedestrians	Median value of noise (%)
1	24.16
3	58.36
5	89.95
8	105.83
10	119.65

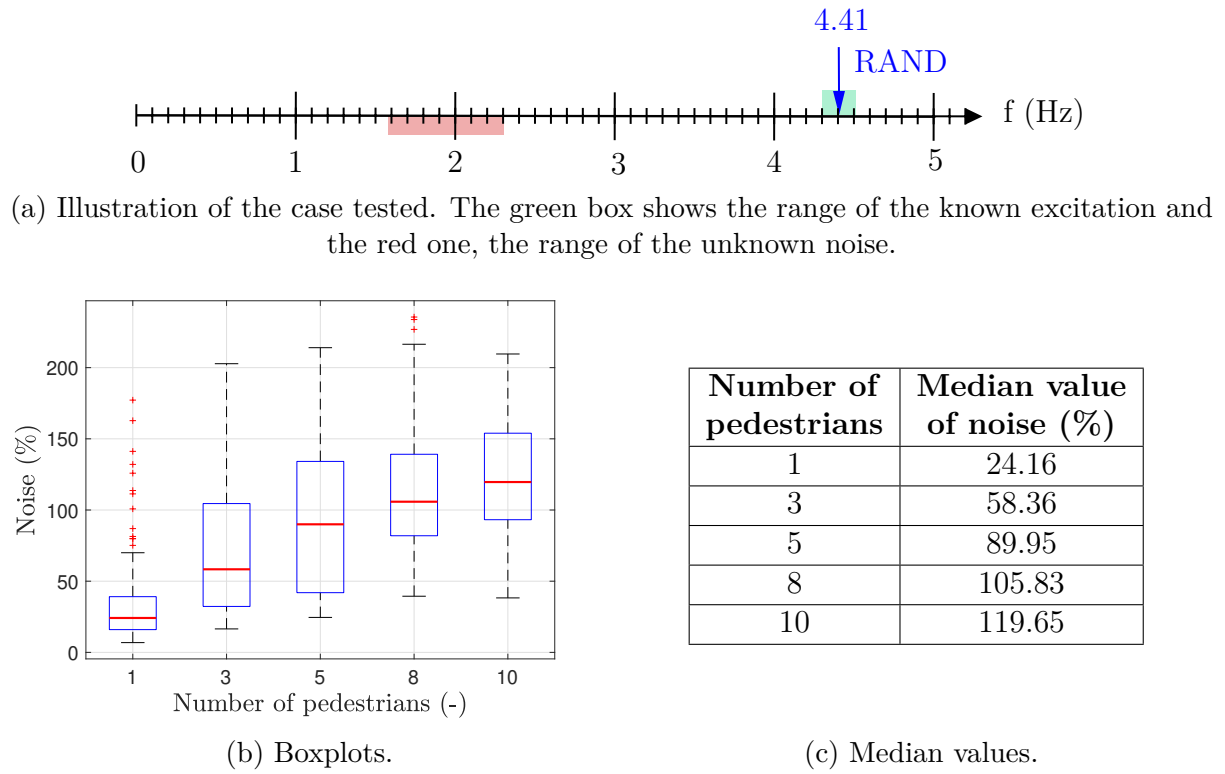(b) Boxplots.   (c) Median values.

Figure 53: Percentage of the noise in function of the number of pedestrians for a system with a fundamental frequency at 2 Hz for its second eigenfrequency.

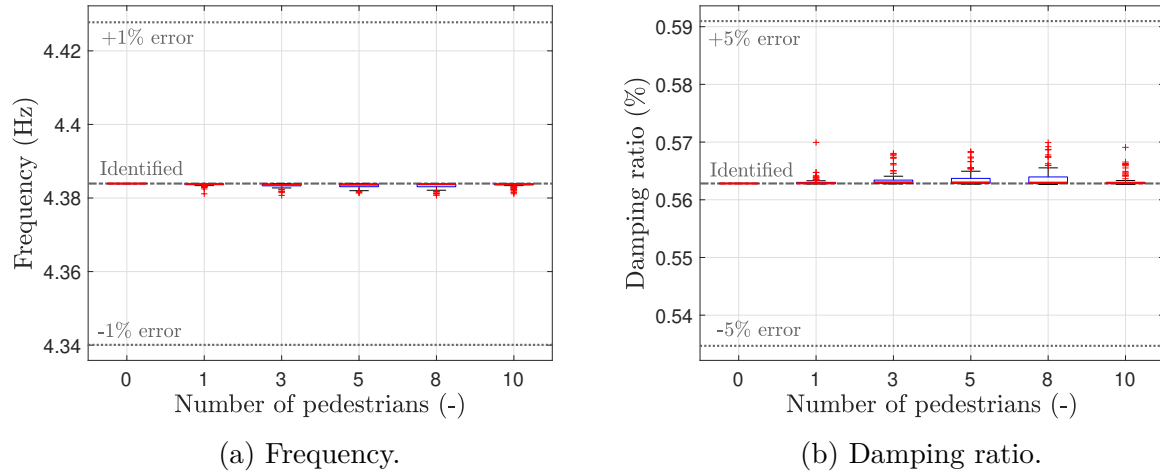(a) Frequency.   (b) Damping ratio.

Figure 54: Results obtained with the CSI algorithm for frequency number two (4.41 Hz) for a known random excitation of 0.2 Hz bandwidth and an unmeasured excitation caused by pedestrians walking back and forth on the footbridge.

One can see that for a number of pedestrians equal to or higher than 8, the percentage of error becomes higher than 100%. This means that, by definition (see Equation 40), the rms value of the displacement is higher in the case where the pedestrians are walking alone than in the case where the shaker is operating alone. However, as the noise is outside the frequency range interest, the same conclusion than in Section 2.3.1.1 can be drawn: no matter the level of noise, it barely influences the results. The difference with Figure 50 is that the frequency is further than

the noise range as it can be seen when comparing Figures 49a and 53a so that the influence of the noise is more present for model 1 than model 2.

2.4.3   Summary

In this section, the noise was modeled as several pedestrians crossing the footbridge walking back and forth. Increasing the number of pedestrians leads to an increased imposed dynamic charge but also to a wider frequency spectrum, as each pedestrian walks at its own pacing rate. However, some dominant frequency components stand out due to this pacing rate, which is supposed to be constant. The white noise assumption is thus not met anymore. The fact of not having a white noise anymore was then investigated.

Two systems were analysed:

- Model 1 with a fundamental frequency at 1.59 Hz which was a limiting case as the first frequency was close to the starting value for the noise caused by pedestrians (1.6/1.7 Hz);

- Model 2 with a fundamental frequency at 2 Hz.

What can be retained is that:

- When the noise was **outside** the frequency range of interest, the noise had little to no influence on the modal properties of the system. This was clearer for model 2 than model 1 because the noise was further from the frequency of interest in the case of model 2.

- When the noise was **inside** the frequency range of interest:

  – Concerning the **damping ratios**, the same behaviour was observed for both models: as the level of noise increased, a progressive degradation of the results towards lower values was observed, just as in Section 2.3.2.1. Excepted that instead of decreasing with an increasing level of noise, the results seemed to converge to an asymptote. This can be called a saturation effect, meaning that as more pedestrians are added, the effect of the added pedestrian decreases. However, a limit value beyond which the results overcome an acceptable percentage of error could not be determined as it depends on the system, the frequency and the limit value that one wants to set.

  – Concerning the **frequencies**, the conclusions differed from the one drawn in Section 2.3: Indeed, the frequency was now dependent of the level of noise. This was due to the fact that as the noise was not white anymore and showed dominant frequency components, the system considered the noise as poles of the state matrix A. Concerning the limiting case (model 1), the variability in the results was constant but the median values converged towards higher values (those of the noise). Concerning the other case (model 2), the variability was higher than model 1 but the median values remained quite constant, as the noise was centered on the frequency.

In order to validate the observations realised in the numerical part, the CSI algorithm can be tested with real life data, which will be investigated in Section 3.

3   Experimental part

In order to apply the CSI algorithm to a real life example, a more detailed measurement campaign has been realised on the Tilff cable-stayed footbridge. The first part of this section consists in describing the equipment as well as the setup. Then, the experimental protocol will be presented before analysing the results. The campaign was realised for two types of signals: with and without pedestrians. The CSI algorithm will be applied to the signals without pedestrians in order to compare the obtained modal properties with those obtained with the identification method currently used by V2i (see [2] and Section 1.1). Then, it will be applied to the signals with pedestrians in order to assess their influence on the modal parameters.

3.1   Equipment and setup

In this section, the excitation and acquisition devices will be presented. The excitation is imposed thanks to a shaker and the acquisition is made through accelerometers. Figure 55 shows the disposition of the different devices.
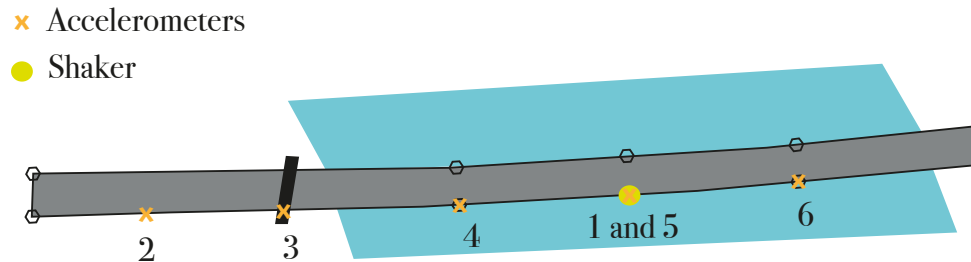

Figure 55: Schematic top view of the Tilff cable-stayed footbridge (about to scale) and setup of the 6 wireless accelerometers for the detailed measurement campaign. The hexagons represent the anchoring of the cables, the dark shape represents the pylon and the blue shape represents the river.

3.1.1   Excitation device

For this campaign, a portable shaker was used. This device has been developed by University of Liège and V2i and allows to impose different types of loading to the structure such as random or sine signals. It consists in a moving mass attached to a linear actuator. For this test, the shaker only excites the footbridge in its vertical axis. Only one set up was installed because the interest was to capture the vertical modes only. Indeed, as explained in Section 2.2.1, the torsion modes are in higher frequency ranges due to the metallic casing. Location 5 for the shaker is chosen because it seemed to be a good position to sufficiently excite the first two modes of the deck during the preliminary measurement campaign. As it was already mentioned, the shaker should be located where the displacement is maximal for the modes one wants to identify. However, as the mode shapes of this footbridge were not available beforehand, the optimal position could not be found.

Figure 56 shows a picture of this shaker and Table 9 shows its main characteristics.

Figure 56: Picture of the shaker. The moving mass consists in the dark gray plates and the yellow cylinders attached to the linear actuators.

Shaker characteristics	Values
Moving mass	50 kg for one pair of steel plates
Number of pairs of steel plates	3
Cylinders mass (yellow parts)	80 kg
Total (moving) mass	230 kg
Amplitude of motion (peak to peak)	20 cm (at 1 Hz) to 2 mm (at 10 Hz)
Maximal force it can provide when the moving mass is at maximum value (3 pairs of steel plates + 2 additional of 40 kg)	4500 N

Table 9: Characteristics of the shaker [2].

3.1.2 Acquisition devices

The acquisition was made thanks to two wired and six wireless accelerometers. This type of device allows to measure the acceleration of the structure.

Concerning the wired accelerometers, one was placed on the moving mass of the shaker to exactly measure the imposed force, and the other one at the location of the shaker on the deck to measure its response to the excitation. They are mainly used for monitoring purposes in this case. The wireless accelerometers were spread all along the footbridge to measure its response to the excitation, excepted accelerometer 1 that was placed on the moving mass of the shaker to measure the force imposed by the shaker. This configuration of the wireless accelerometers was chosen in order to cover at best all the length of the footbridge, to obtain an estimation of its mode shapes. The model that was used was the G-Link-200 8G whose technical sheet can be found on [24]. Thanks to the signals measured by the wireless accelerometers, the CSI algorithm can be applied as it uses the input loading (accelerometer 1) and the response of the structure (accelerometers 2 to 6).

3.2 Experimental protocol and analysis of the results

The principal objective of a dynamic identification campaign is to identify the modal properties of the structure (natural frequencies, the damping ratios, the modal masses and mode shapes). To do so, the protocol was divided into two parts: one without pedestrians and another one with pedestrians, in order to take their influence into account. The footbridge was not closed during the campaign, so that other pedestrians not involved in the campaign also contributed to the measurements. Figure 57 shows the main steps of the two parts as well as their respective objectives.
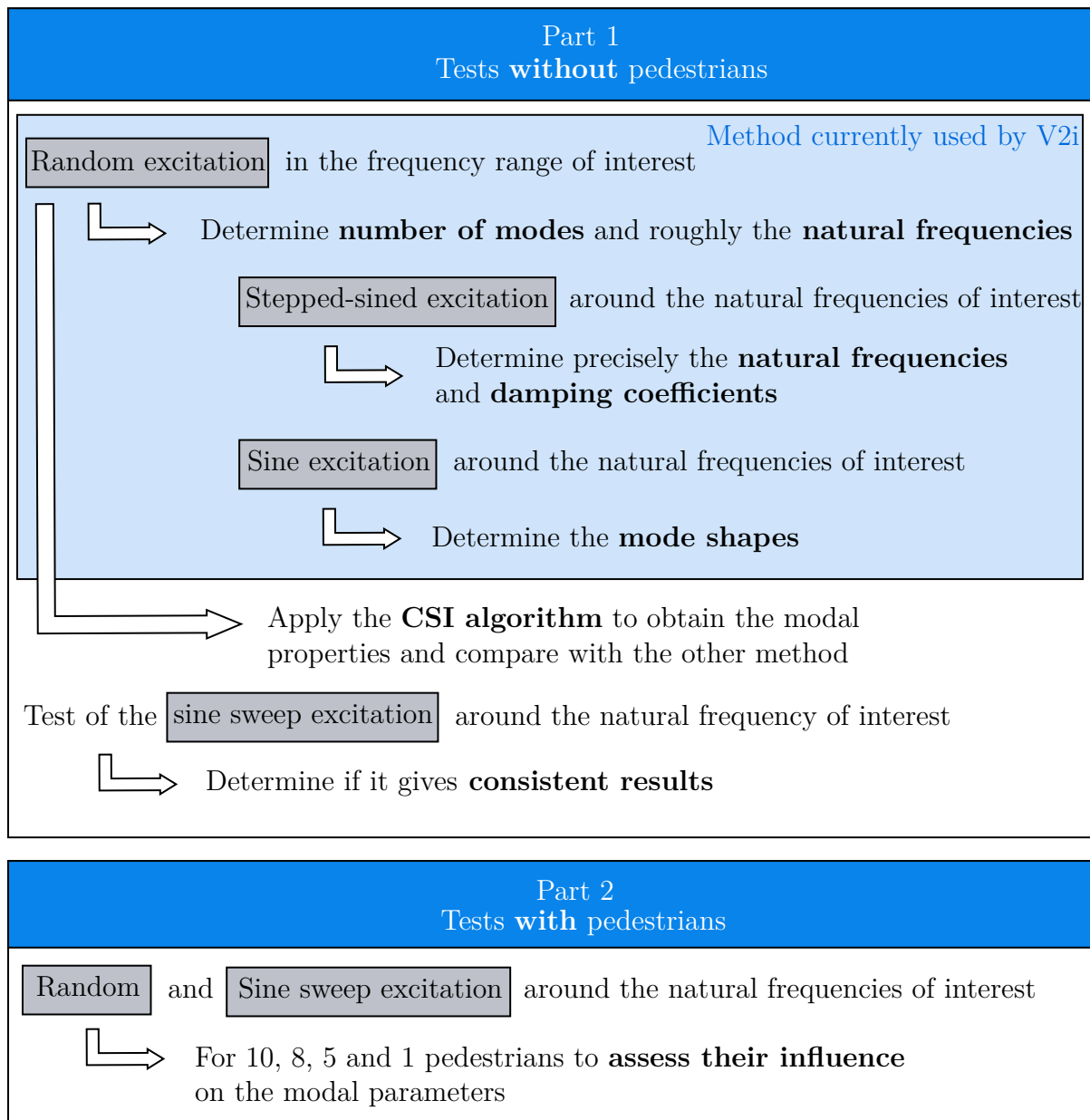

Figure 57: Main steps of the measurement campaign.

3.2.1 Part 1: tests without pedestrians

In this section, the modal properties of the footbridge obtained thanks to the identification process currently used by V2i will be compared to those obtained with the CSI algorithm. A sweep signal will also be tested in order to determine if it gives consistent results, as it

was seen in Section 2.3.2.3 that applying a random or sweep signal did not consequently changed the results.

3.2.1.1   Random excitation

The first part of the tests consisted in imposing a limited band random excitation (1 to 7 Hz) to the structure thanks to the shaker, for 15 minutes. The number of modes of the structure can be determined by computing the PSD of the signal measured on the footbridge. This will also allow to obtain a first estimate of their natural frequencies. Figure 58 shows the PSD of the signal for the different accelerometers.
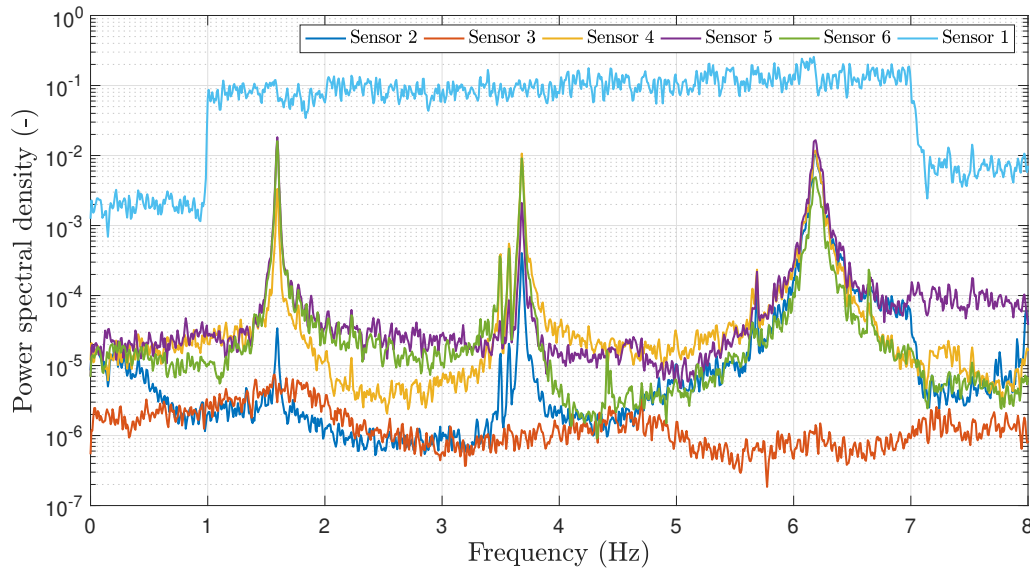

Figure 58: PSD of the signal captured by the accelerometers for a random excitation between 1 and 7 Hz.

Thanks to this figure several things can be observed:

- The random excitation in the range [1 - 7] Hz can be observed thanks to the light blue curve. Indeed, sensor 1 was placed on the moving mass of the shaker in order to measure the imposed force, as explained earlier.

- The orange curve does not show the peaks at the eigenfrequencies because sensor 3 was placed at the location of the pylon, which is attached to the foundation of the footbridge so that the displacement is minimal at that location.

- Sensor 2 recorded a lesser amplitude of displacement compared to the others sensors for mode 1. This means that mode 1 shows a small displacement at location 2 compared to the other locations. This will be observed in the plots of the mode shapes (see Figure 60a). So that, thanks to the amplitude of the power spectral density, one can already have an idea of the relative displacement in *absolute value* of the sensors.

- One can clearly see that the main frequencies are around 1.59, 3.68 and 6.18 Hz. Some less consequent peaks can be observed around 3.49 and 3.57 Hz. They correspond to the fundamental frequency of the short stay cables, by analysing the

frequency content of the cables in Figure 14. This will be validated in the next section were more refined tests will be performed around the natural frequencies. Two other less consequent peaks can be observed at 5.64 and 5.68 Hz. These could be the second harmonic of the medium stay cable as 2*2.85 = 5.7 Hz.

- Contrary to Figure 13, the peaks around 2 Hz corresponding to the fundamental frequencies of the long and medium stay cables are not observed anymore. This may be due to the fact that the location of the shaker was not optimally chosen to capture them. Indeed, for the preliminary measurement campaign, the excitation by knee-bending was made at several locations on the footbridge. However, as said earlier, the goal is to focus on the frequencies of the deck only, so that this is not a problem.

In conclusion, three modes of the deck can be observed the range [1 - 7] Hz, but only the first two will be studied in the following analyses. One can also apply the peak-picking method to the square root of the PSD to have a more precise estimation of the first two damping ratios compared to the preliminary measurement campaign. Table 10 summarises the first two modal characteristics of the Tilff cable-stayed footbridge.

Frequencies (Hz)	Damping ratios (%)
1.59	0.64
3.68	0.29

Table 10: Estimation of the first two modal properties of the deck.

Compared to the results of the preliminary measurement campaign (see Table 2), the frequencies are quite close. However, a consequent difference in the damping ratios can be observed. This could be due to the fact that:

1) The preliminary measurement campaign was not realised in the best conditions (knee-bending was the only excitation) so that the quality of signals was not optimal;
2) The peak-picking method strongly depends on the frequency resolution of the measurements. So that, if it is not optimal, the estimations of the damping ratios will not be optimal either (added to the numerous limitations of this method listed in Section 2.1);
3) In the preliminary measurement campaign, the modes were excited one by one, whereas in the detailed measurement campaign a wide band random signal excited the first three modes at the same time.

However, the random signal was mainly applied to have an idea of the values for the frequencies of the footbridge. The stepped-sine excitation will allow to determine the frequencies and the damping ratios more precisely.

3.2.1.2   Stepped-sine excitation

Now that the frequencies have been roughly estimated, a stepped-sine signal centered on the first two frequencies will allow to determine their exact values, their damping ratios as well as which mode they correspond to. A stepped-sine signal consists in imposing a sine signal by steps of frequency chosen small enough. The duration of the tests should also be long enough to remove the transient effects. Figures 59a and 59b show the frequency response function of the signal centered on 1.59 and 3.68 Hz, respectively.
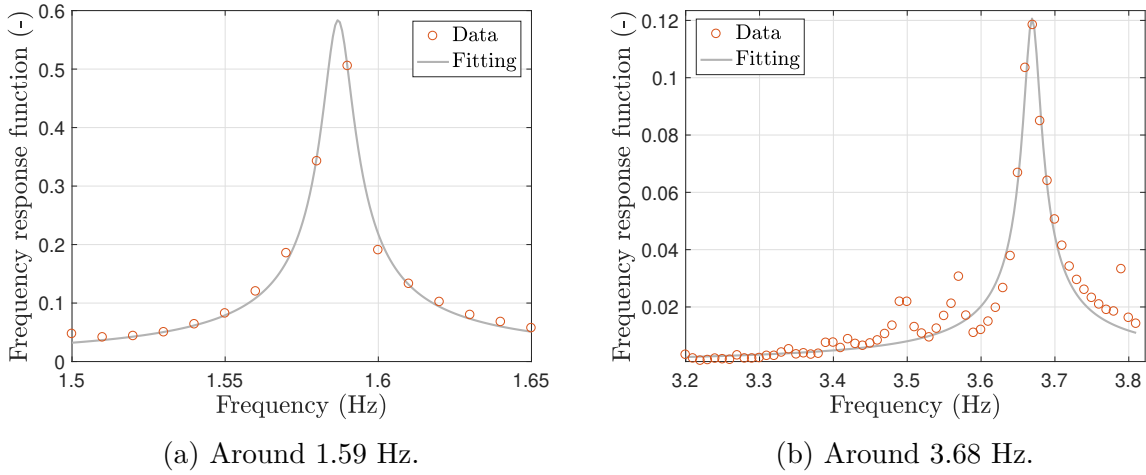
(a) Around 1.59 Hz.

(b) Around 3.68 Hz.

Figure 59: Fitting of the data for the stepped-sine signals.

One can clearly see the peaks appearing. More data have been recorded for mode 2 than mode 1 because a more refined time step has been chosen for the second one, in order to be sure to capture the modes of the cables situated between 3.4 and 3.6 Hz. Finally, a fitting of the data is realised thanks to the method cited in Section 1 and explained in [2]. Table11 shows the natural frequencies of the structure as well as the corresponding damping ratios. These ones were also determined thanks to the method previously mentioned.

Frequency (Hz)	Damping ratio (%)	Mode
1.59	0.33	Deck
3.49	/	Right short cable
3.56	/	Left short cable
3.67	0.33	Deck

Table 11: Modal properties of the structure obtained thanks to the stepped-sined excitation with the method described in [2]. The right and left sides are determined by looking at the pylon from the longer span of the deck.

Compared with the estimations done in the previous section (see Table 10), the results for the frequencies are close (close to 0% error). However, a higher percentage of error is observed for the damping ratios (more than 1% error). As already mentioned, the peak-picking method is not the most precise one and the parameters will be estimated with the CSI algorithm to have a more precise approximation.

The nature of the modes have been determined by looking at the response of the footbridge on site, to the different excitations. Indeed, as the stepped-sine imposes one frequency at a time, it is easy to look at the response of the footbridge when the desired value is reached. One can see that the two short cables have different natural frequencies. This is due to the fact that their tensions are not equal due to their manufacturing process. Indeed, the cables are made of steel surrounded by a sheath, itself filled with concrete. It is then possible that the amount of concrete is not equal in both cables or that cracks are present in the concrete, resulting in two different natural frequencies. However, as in the model, it is chosen to not study those frequencies.

3.2.1.3 Sined excitation

In this step, a sine signal at the frequencies of interest will be applied in order to determine the mode shapes of the real structure. The first two are presented in Figure 60.

(a) Mode 1 obtained with sine signal at 1.59 Hz.
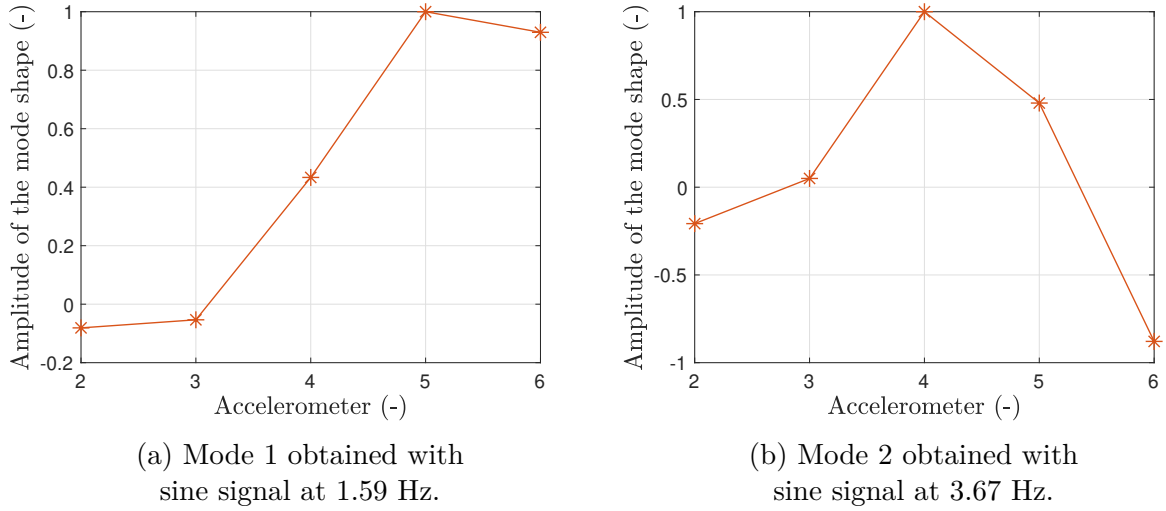
(b) Mode 2 obtained with sine signal at 3.67 Hz.

Figure 60: First two mode shapes of the Tilff cable-stayed footbridge obtained thanks to the sine excitation with the method described in [2].

Just as in the simulations, due to the configuration shown in Figure 55, the modes are only accurate for the points in which the acceleration is measured, only on the vertical degree of freedom. That is why this type of representation has been chosen to present the results for the mode shapes. One should be careful that the distance between the accelerometers has not be taken into account in these types of plots. However, as it can be seen in Figure 55, the configuration was chosen to roughly have the same distance between the accelerometers. As it was already mentioned, the modes computed for the simulations **cannot** be compared with the experimental ones due to the fact that the inertia and cross-section of the model have not been respected (see Section 2.2.1).

One can see that for both modes, the displacement at accelerometer 3 is close to 0, due to the fact that accelerometer 3 was placed at the location of the pylon. The amplitude of the movement is the highest at accelerometer 5 for mode 1 and accelerometer 4 for mode 2. Indeed, the first one corresponds to the location of the shaker while the second one corresponds to the location of the anchoring of the short cable. This means that, the location of the shaker was not optimally chosen to identify mode 2 but the reason was explained in Section 3.1.1: the modes of the footbridge were not available beforehand so that the position had to be chosen at best by analysing the behaviour of the structure during the preliminary measurement campaign.

3.2.1.4 CSI on signal recorded with the wide band random excitation

What can be interesting is to apply the CSI algorithm to the random signal without pedestrians. Indeed, in the current method used by V2i, it is possible to accurately determine the properties of the system when no pedestrians disturb the measurements. However, in order to obtain all the modal properties, three steps should be realised (see Figure 57). One of the advantages of the CSI algorithm is that based on only one type of signal, all these results can be found in one step.

In order to apply the CSI algorithm to the signal recorded for a random excitation, the transient parts of the signal are removed. Then, the cropped signal is filtered around the desired frequency and the CSI algorithm is applied. In order to compare the results, the signal will be filtered from 1.5 Hz to 1.65 Hz for the first frequency to be consistent with the tests realised in the stepped-sine part. However, for the second mode, the signal will be filtered from 3.6 Hz to 3.8 Hz in order to filter out the frequencies of the cables. In the case of a random excitation, the method can be applied to the whole signal or to portions of the signal to realise a moving average and the median value of all the estimations can be computed. Figure 61 illustrates the process.
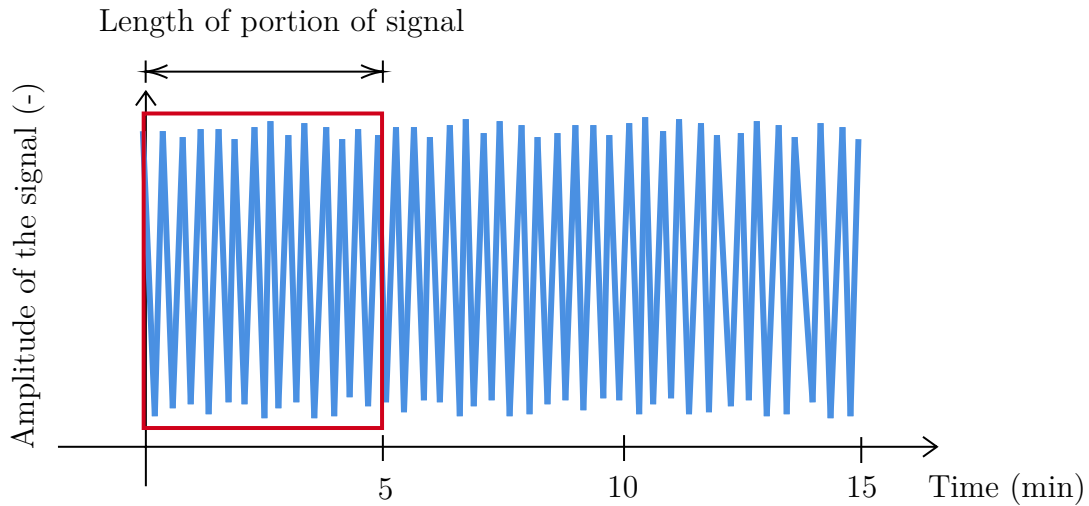
1) Apply CSI algorithm on this portion of signal
→ Obtain frequencies, damping ratios and mode shapes
→ Store in a variable;

2) Repeat the process with the following portion of signal
→ the box is moved from 3 **seconds** to the right at each iteration. This value is chosen in order to obtain enough estimations (around 100) on the whole signal;

3) Once the right limit of the box arrives to the end of the signal, the median of all the modal parameters obtained with the several estimations can be computed.

Figure 61: Illustration of the process performing a moving average.

Table 12 shows the modal properties of the structure obtained with the CSI algorithm thanks to the random signal without pedestrians for the whole signal and for the moving average technique.

	Whole signal		Moving average	
Mode	f (Hz)	$\zeta(\%)$	f (Hz)	$\zeta(\%)$
1	1.59	0.28	1.59	0.33
2	3.68	0.2	3.67	0.21

Table 12: Modal properties of the structure obtained with the CSI algorithm thanks to the random signal without pedestrians.

One can see that applying the CSI algorithm to the whole signal or by doing a moving average, the results are close but not exactly equal. The moving average values should be more accurate since the identification was applied to several portions of the signal allowing to obtain several estimations. It is indeed what is observed for mode number one when comparing with the results obtained in Table 11. However, the estimation of damping ratio of mode two is lower than its corresponding value in the same table. This could be explained by the fact that:

- The shaker was not optimally located to capture mode 2 as it was shown in Figure 60b. Indeed, the highest displacement for mode 2 is at the location of the anchoring of the shortest cable (location 4 in Figure 55);
- The possible interaction between the short stay cables and the deck makes it difficult to correctly identify the modal properties of the deck;
- The frequency range of the excitation is too wide so that it excites too much modes at the same time, making the analysis of the results complicated. Indeed, the signals must be filtered before applying the CSI algorithm, in order to obtain a stabilisation at low orders in the stabilisation diagram. Figure 62 shows an example of stabilisation diagram for the filtered and unfiltered signals for frequency number one.
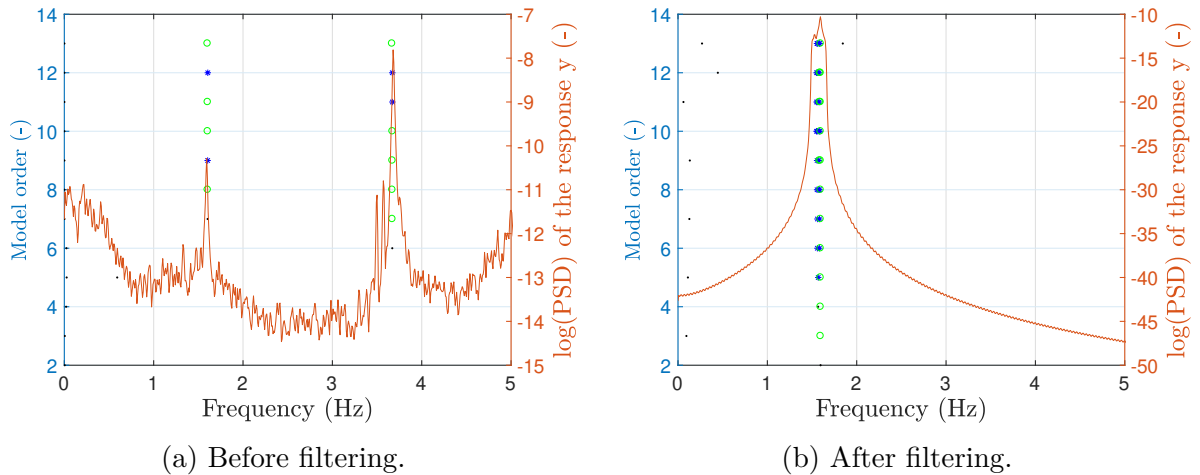

(a) Before filtering.

(b) After filtering.

Figure 62: Example of stabilisation diagram for the experimental data, obtained with a random signal from [1 - 7] Hz. In the second figure, the signal is filtered between [1.5 - 1.6] Hz in order to obtain stabilisation at lower orders for mode 1.

What should have been done to improve the results would have been to:

- Find the optimal position to capture mode 2 without the influence of the modes of the cables (however this was not possible to determine before the campaign as the mode shapes of the structure were not available).

- Perform a narrower random excitation around the frequencies of interest, one by one.

Comparing the results obtained in Table 12 with those in Table 10, it can be seen that the frequencies are close but the damping ratios are overestimated with the half-power point method, at least for mode 1 that is correctly evaluated.

Thanks to the CSI algorithm, one can also obtain the mode shapes of the structure. These ones can be observed in Figure 63.
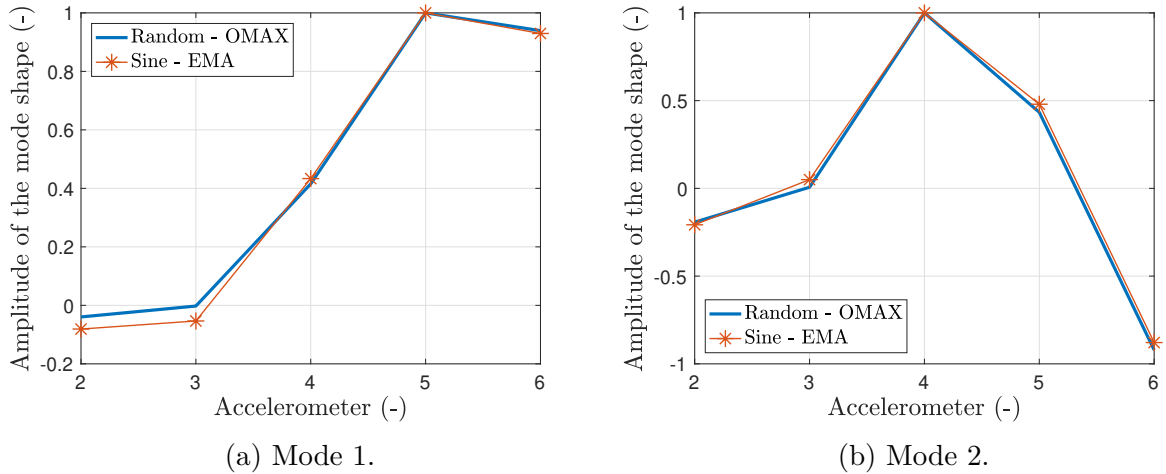

(a) Mode 1.   (b) Mode 2.

Figure 63: Comparison of the first two mode shapes of the Tilff cable-stayed footbridge obtained thanks to the CSI algorithm applied to the random excitation and those obtained for the sine signal applying the method described in [2].

One can see that the results for the modes shape obtained with the CSI algorithm are a bit offset compared with those obtained with the sine signal. However, the difference is small and the shape of conserved so that the results are considered to be consistent.

In conclusion, this part showed that the CSI algorithm allowed to obtain consistent results with less steps than the current identification method used by V2i, when there was no noise (induced by the pedestrians) in the system. This is quite convenient because doing a stepped-sine is costly in time since at each time step, the signal should be hold long enough to remove the transient effects. However, to obtain the most accurate results, one should determine the optimal position of the shaker for each mode to be determined and/or excite only one mode at a time.

3.2.1.5   Sine sweep excitation

Since the analysis of Section 2.3.2.3 showed that the sine sweep signal provided consistent results with the random signal, it will be tested in this real-life case since it was not used in the software before. Figure 64a and 64b show the power spectral densities of the signals applying a sine sweep around 1.59 and 3.68 Hz. Only the curves obtained with sensor 5 are shown for sake of readability. It should be noted that here the CSI algorithm has been applied to the whole signal. Indeed, there is no point in doing an average on portions of the signal as the frequency of the signal progressively increases until the end of the excitation.

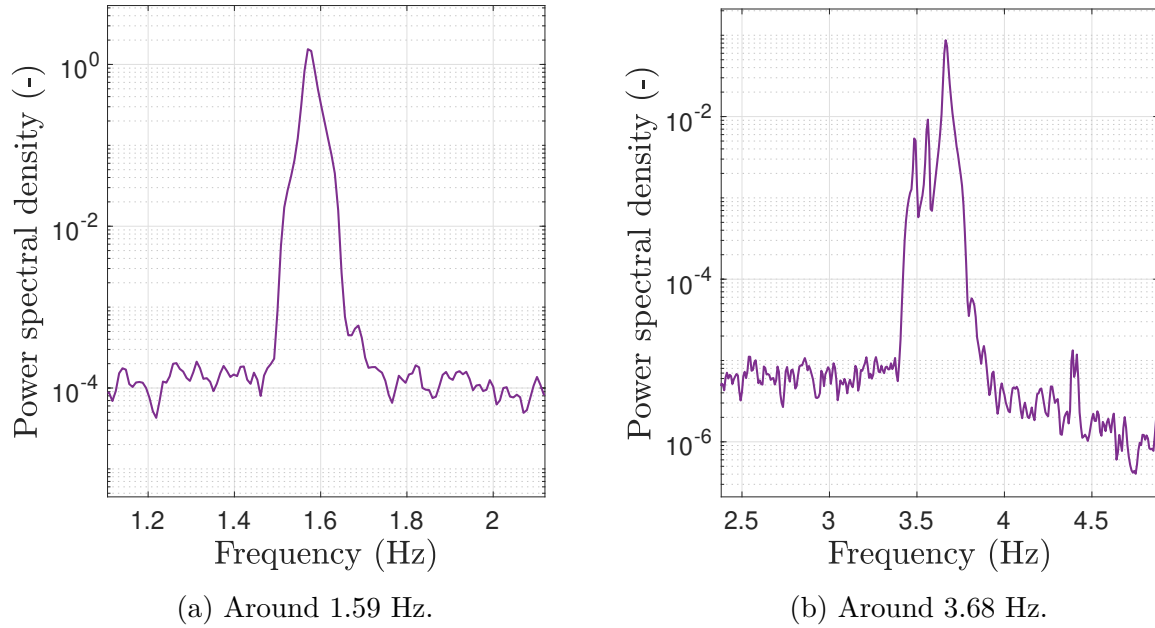(a) Around 1.59 Hz.

(b) Around 3.68 Hz.

Figure 64: PSD of the signals captured by accelerometer 5 for the sine sweep excitations.

It can be seen that the width of the peak is larger than with the random signal (compared to Figure 58). The problem when doing a sine sweep is that if the rate of change of frequency is too high, the system does not have the time to go into resonance. This will result into a different damping ratio than what is expected. Methods exist in order to simulate a slower sweep based on those data, but this is beyond the scope of this thesis. More information about those methods can be found in [25]. What is important to point out is that the speed of the sweep can affect the damping ratio. This is indeed what was observed with the simplified model in Figure 44.

Table 13 shows the modal properties of the footbridge obtained with the peak-picking method and CSI algorithm for the sine sweep signal. It should be noted that the signal did not have to be filtered as the excitation was already centered arount the frequency of interest.

	Peak picking		CSI	
Mode	f (Hz)	$\zeta(\%)$	f (Hz)	$\zeta(\%)$
1	1.57	0.82	1.58	0.63
2	3.67	0.36	3.66	0.32

Table 13: Modal properties of the structure obtained with the peak-picking method and CSI algorithm thanks to the sweep signals without pedestrians.

As expected, the wider peak leads to a larger damping ratio when comparing with Table 10 for the pick-picking method applied to the random signal and Table 12 for the CSI applied to the random signal. One can also have a look at the modes obtained with the CSI algorithm applied on the sweep signal in Figure 65.
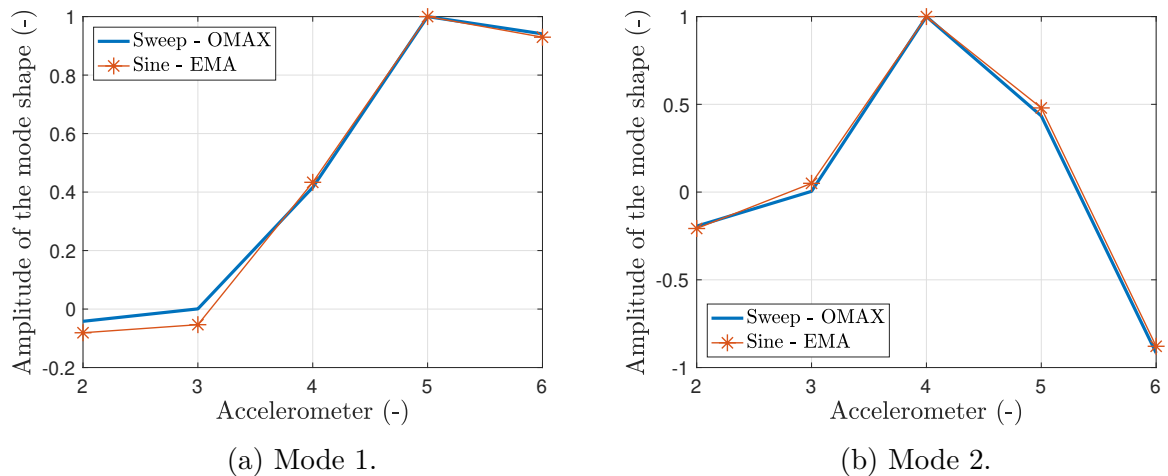
(a) Mode 1.

(b) Mode 2.

Figure 65: Comparison of the first two mode shapes of the Tilff cable-stayed footbridge obtained thanks to the CSI algorithm applied to the sweep excitation and those obtained for the sine signal applying the method described in [2].

Despite the overestimation of the damping ratio, the mode shapes are consistent with those obtained with the sined excitation.

What can be concluded is that the sweep could allow to have a close estimation of the frequencies and mode shapes. However, it should not be used to determine the damping ratios. In Section 3.2.2, it will be proven that it is better to avoid using a sweep signal.

3.2.2   Part 2: tests with pedestrians

In this section, a group of pedestrians was invited to walk back and forth on the footbridge in order to assess their influence on the modal properties of the footbridge. Figure 66 shows the characteristics of the group of pedestrians used for the tests.

Figure 66: Characteristics of the pedestrians used to perform the tests.

As it can be seen, the range of the pedestrians is wide (from young to elder people and from light to heavier people). As their weights and ages, their pacing rates will also be different. The pedestrians also had different types of shoes which can further modify their pacing rate and interaction with the structure. However, no device was used in order to measure the pacing rate of the pedestrians.

The tests consisted in applying different types of loading with the help of the shaker while a group of pedestrians crossed the footbridge from one side to the other. The group **tried** to stay as randomly distributed as possible. Figure 67 shows the scheme realised for the measurements and Table 14 shows the excitation range for each mode.
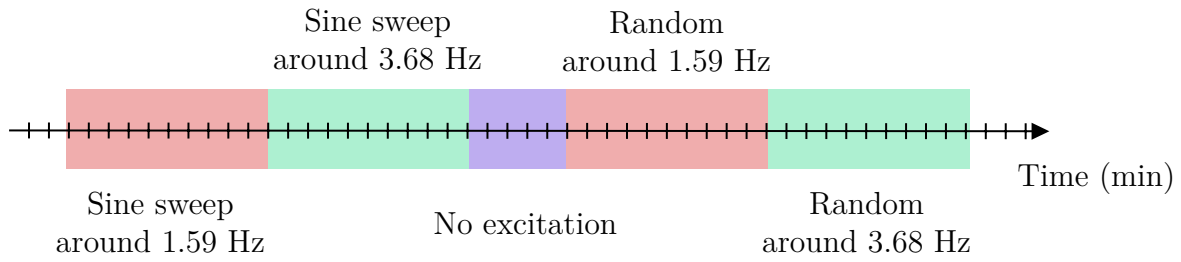
Figure 67: Timeline of the excitation applied with the shaker for the test with pedestrians. One graduation line represents one minute.

Mode	Excitation range
1	From 1.5 to 1.65 Hz
2	From 3.2 to 3.9 Hz

Table 14: Excitation range used for the signals.

The excitation range was chosen in order to be consistent with the tests made for the stepped-sine. However, as it was shown, the modes of the cables should not have been excited. These measurements were realised for 10 and 8 pedestrians while only the red and violet parts were realised for 5 and 1 pedestrians, due to a lack of time during the measurement campaign.

3.2.2.1   No artificial excitation

The first thing that can be analysed is the effect of the pedestrians without artificial excitation. This will allow to roughly determine the frequency content of the pedestrians. Figure 68 shows the acceleration profile and the PSD of the signals for different numbers of pedestrians.
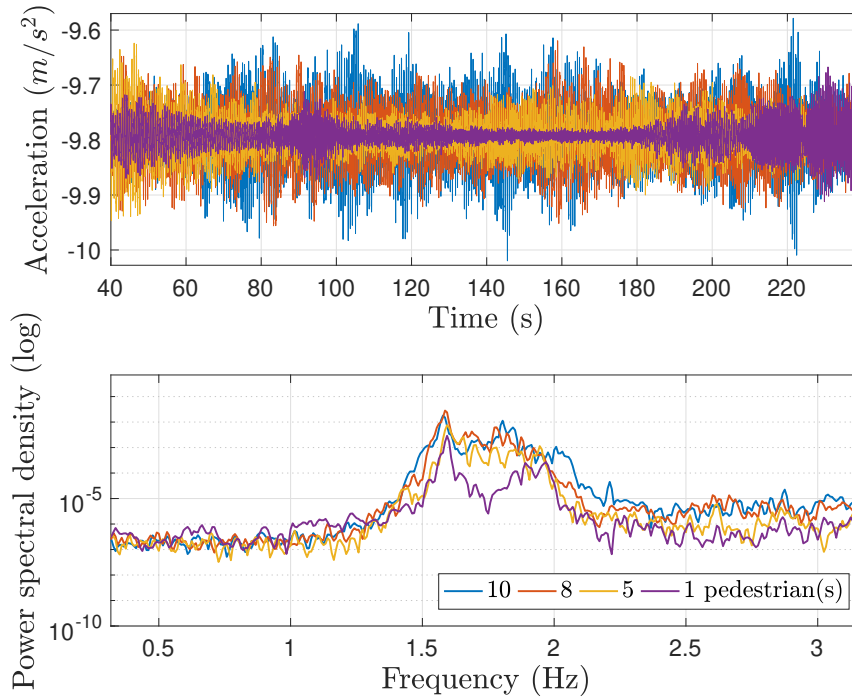

Figure 68: Acceleration profile of the signals and frequency content of the pedestrians for the detailed measurement campaign.

Several observations can be done concerning this figure:

- One can see that as the number of pedestrians is increased, the acceleration of the structure becomes higher and the frequency content of the signal widens and contains more and more frequencies (just as in Figure 46) in the range [1.3 - 2.2] Hz. However, in real-life, the PSD becomes higher as the number of pedestrians is increased (contrary to Figure 46). Nevertheless, as the number of pedestrians increases, the increase in PSD is less and less perceptible. The other difference with Figure 46 is that the PSD is not as smooth because other sources of noise may be present such as the wind, the water flowing underneath the footbridge... In conclusion, the frequency content of the pedestrians can be estimated to range about between 1.3 and 2.2 Hz in this case.

- It should also be noted that, contrary to the model, a real pedestrian never has a totally constant speed and thus pacing rate. This can be observed with the curve for one pedestrian showing several peaks between 1.7 and 2 Hz (2 Hz being the mean pacing rate for pedestrians [3]).

- The fundamental frequency of the footbridge can also be observed at 1.59 Hz, showing that even with the weak ambient forces, the frequencies of the footbridge can be detected. However, its amplitude is quite small and as more pedestrians are added, the less it is distinguishable. That is why a shaker is used, in order to emphasise the eigenfrequencies.

- One can also observe more consequent variations of the amplitude of the signal, especially for the purple curve at around 90 seconds and at the end of the signal. Indeed, as it was already mentioned, the pedestrians chosen for the study were not alone during the campaign. Sometimes, some cyclists, motorbikes and other pedestrians crossed the footbridge during the measurements which can cause variations in the results. The history of the perturbations is summarised in Appendix A.3.

Now that the frequency content of the pedestrians have been determined, one can have a look a the identified modal properties thanks to the CSI algorithm when noise (pedestrians) is present.

3.2.2.2 Artificial excitation around frequency 1

In order to identify the modal properties of the system, the CSI algorithm can be applied to the different signals of Figure 67. In this section, the results for the excitations (random and sine sweep) of mode 1 will be presented. Once again, the moving average technique explained in Figure 61 was realised for the random signal and the whole signal was taken for the sweep signal. However, the results are not filtered as the excitation is already around the frequency of interest.

The results for the modal properties obtained with the random excitation around frequency 1 thanks to the CSI algorithm are presented in Figure 69. As the moving average technique was performed, it is possible to obtain boxplots of all the estimations (obtained with the different portions of signal, see Figure 61) for each number of pedestrian.

(a) Illustration of the case tested. The green box shows the range of the known excitation and the orange one, the range of the unknown noise.
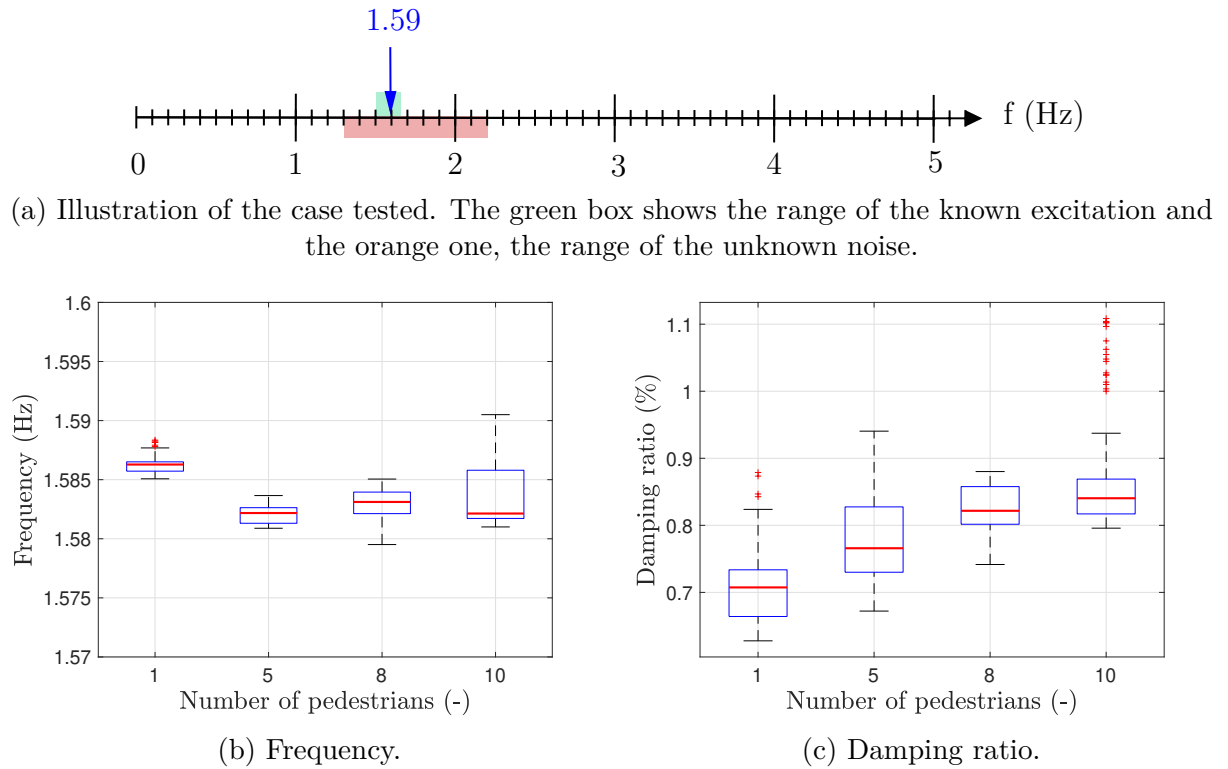

(b) Frequency.

(c) Damping ratio.

Figure 69: Results for the experimental identified modal parameters of the system computed with the CSI algorithm for a random signal ranging from 1.5 to 1.65 Hz.

By looking at Figure 69b, one can conclude that the frequency is quite close to the identified value with stepped-sine (exactly 1.5869 Hz). However, concerning the damping ratio (Figure 69c), it seems to increase as the number of pedestrians increases. However, the percentage of increase seems to be less and less consequent as more pedestrians are added, translating the saturation effect that was observed in Section 2.4.2 when noise was in the frequency range of interest. However, instead of evolving towards lower values as in Figure 48b for example, the median values of the damping now evolve towards higher values. This could be due to the fact that, as it is an old footbridge, damages such as cracks on the deck could be present. The pedestrians walking on the footbridge then allow the cracks to open and close so that friction between the sides of the cracks occur and the damping is increased. Other causes of friction can also be found. This is indeed, what is stated in [26]: "*In general, the amount of damping depends on the vibration level, as higher amplitudes of vibration cause more friction between structural and non-structural elements and bearings*".

Another possibility could be that the pedestrians damp out the vibrations by walking in opposition of phase with the vibrations leading to an increase in damping ratio. However, if the pedestrians start to walk in phase with the vibrations, the damping can decrease and the vibrations are amplified. This is called synchronisation. An example of synchronisation is the one that occurred on the Broughton Suspension Bridge in 1831 due to a military troop marching in phase with the vibrations of the bridge [27].

Unfortunately, these damping ratios cannot be compared with a reference value as no tests with a random excitation from 1.5 to 1.6 Hz without pedestrians was performed. The filtered random signal cannot be used either as the imposed level of shaker was not the same for the tests with and without pedestrians. However, the behaviour of the damping ratio is in accordance with the results in Figure 11c of [28].

Still in Figure 69c some outliers can observed for the boxplots of one and ten pedestrians. It can thus be interesting to look at the evolution of the frequency and damping ratio during the whole signal (thanks to the estimations obtained with the moving average technique). This can be seen in Figure 70.
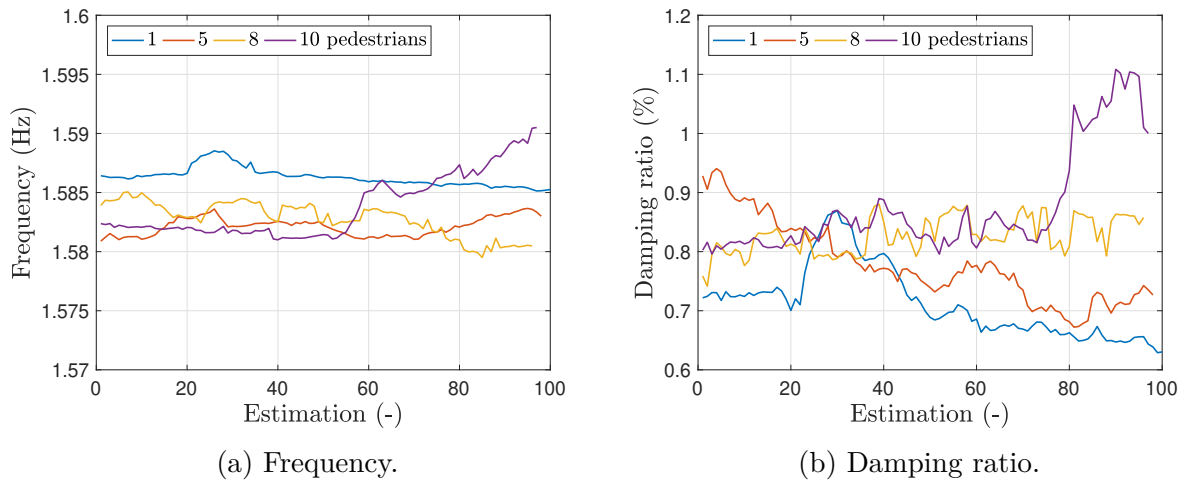

(a) Frequency.   (b) Damping ratio.

Figure 70: Evolution of the modal parameters of the first mode along the whole signal, obtained thanks to the estimations computed with moving average technique.

One can see that the parameters for one and ten pedestrians show consequent variations in some portions of the signal. Some hypotheses concerning those variations are given here after:

- As is was already mentioned, the pedestrians chosen for the study were not alone during the campaign. Sometimes, some cyclists, motorbikes and other pedestrians crossed the footbridge. This hypothesis can be confirmed by looking at the yellow curve for 8 pedestrians. Indeed, as it can be seen in Appendix A.3, in the history of the perturbations, no perturbations were recorded for 8 pedestrians. One can see that the corresponding curve for frequency and damping ratio does not show major peaks, which could confirm this hypothesis.

- The pedestrians of study tried to stay as randomly distributed as possible but sometimes groups would form so that 2 or 3 people walked together, at the same pacing rate. If a group starts to form and if they walk at the same pacing rate, as the vibration increases they can eventually start to walk at the eigenfrequency of the footbridge and enter into resonance with the footbridge. This is the synchronisation behaviour that was discussed here before. However, the peaks in damping ratio are always towards higher values so that the vibrations are more damped out than amplified.

- Other sources of noise other than the pedestrians can play a role as the wind, the flow of water underneath the footbridge, the temperature...

The modes shapes obtained are not shown as they do not differ from Figure 63a. Concerning the sweep signal around the first frequency, boxplots cannot be build as the CSI algorithm should be applied to the whole signal. The results can be observed in Figure 71.

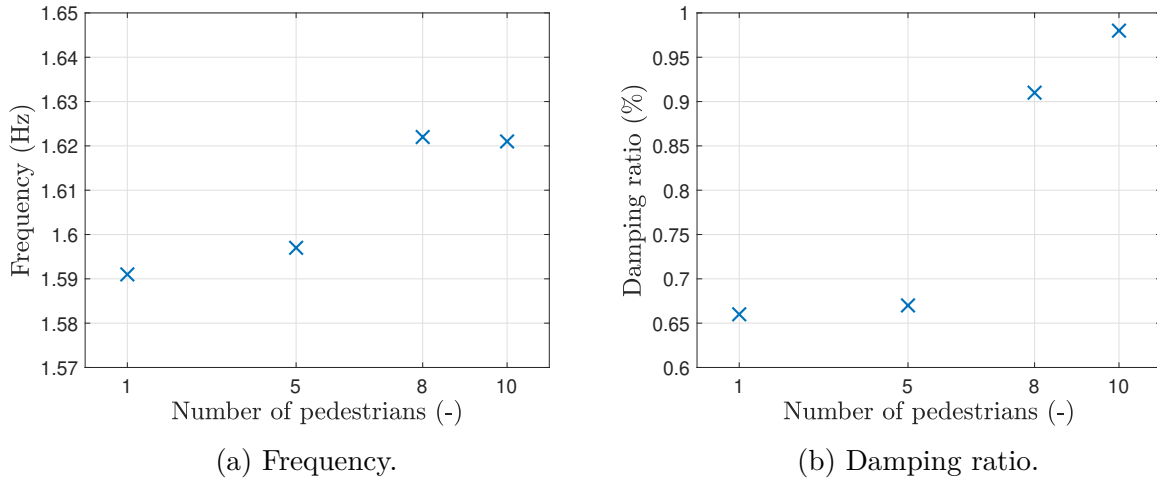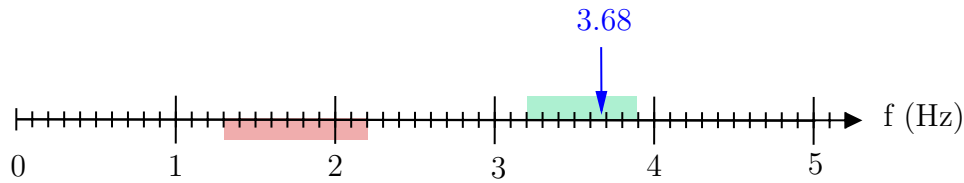(a) Frequency.

(b) Damping ratio.

Figure 71: Results for the experimental identified modal parameters of the system computed with the CSI algorithm for a sweep signal ranging from 1.5 to 1.65 Hz.

Concerning the sweep signal, it is not an optimal signal of excitation to apply in order to obtain the modal properties of the structure with the CSI method. Indeed, as the algorithm should be applied to the whole signal, only one estimation of the parameters can be obtained. However, as it can be seen in Appendix A.3, the sweep tests contained a lot of perturbations so that the evolution of the results for an increasing number of pedestrians cannot be properly analysed. In conclusion, if one wants to apply the CSI algorithm in a real life case, it should avoid using a sine sweep signal.

3.2.2.3 Artificial excitation around frequency 2

In this section, the results for the modal properties obtained with the CSI algorithm for excitations around mode 2 will be presented. The results for the random signal around frequency 2 are presented in Figure 72 (shown at the beginning of next page).

Once again, by looking at Figure 72b, the frequency is quite close to the one obtained with the stepped-sine (less than 1% error) and the modes shapes obtained are not shown as they do not differ from Figure 63b. However, no conclusion about the evolution of the damping ratio in function of the number of pedestrians can be can be drawn from the damping ratio curve (Figure 72c) as there is not enough data. However, it can be seen that the damping ratio shows a small variation between 8 and 10 pedestrians even if the noise is not in the frequency range of the excitation. Indeed, the pedestrians contribute to the damping of the structure by walking on it as previously explained, in addition to the other possible sources of noise.

(a) Illustration of the case tested. The green box shows the range of the known excitation and the orange one, the range of the unknown noise.
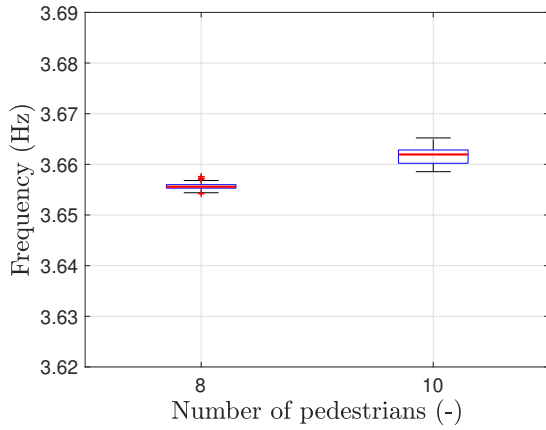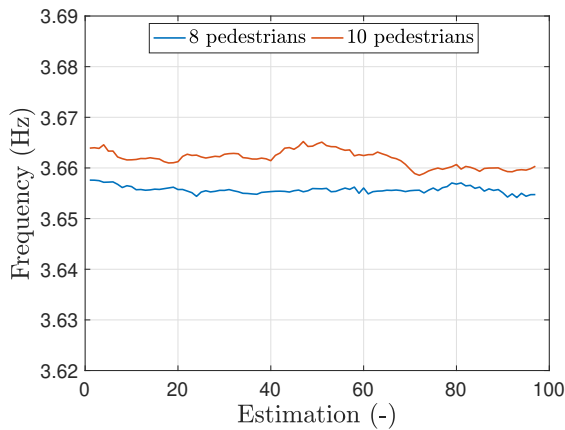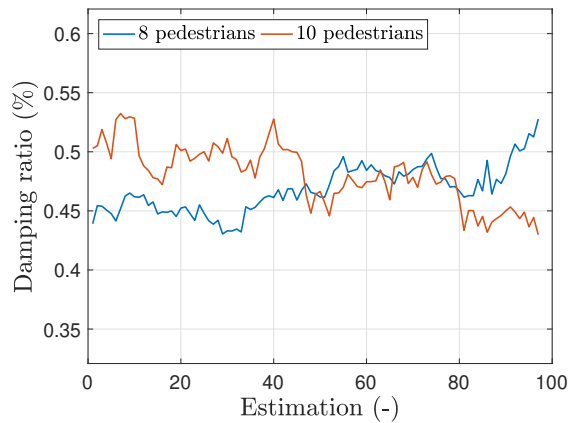

(b) Frequency.
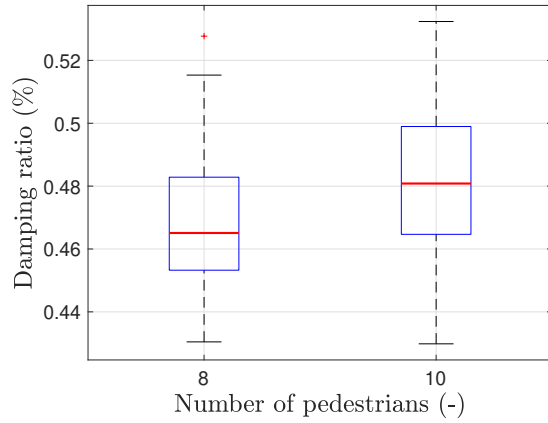
(c) Damping ratio.

Figure 72: Results for the experimental identified modal parameters of the system computed with the CSI algorithm for a random signal ranging from 3.2 to 3.9 Hz.

One can also have a look at the evolution of the estimation of the modal parameters obtained with the moving average technique. This is shown in Figure 73.

(a) Frequency.

(b) Damping ratio.

Figure 73: Evolution of the modal parameters of the second mode along the whole signal, obtained thanks to the estimations computed with moving average technique.

The hypothesis that the perturbations cause a change in the modal properties can also be confirmed here. Indeed, no perturbations were recorded when doing the random on the second frequency (see Appendix A.3). Moreover, it can be observed in Figure 73b that the variation in damping ratio is small (0.44 to 0.52 %) compared to the case in Figure 70b (variation from 0.6 to 1.1 %).

The results for the sweep for this case are not shown as it was determined that due to the lack of estimations and to the numerous perturbations it could not give analysable results. Moreover, as only the measurements for 8 and 10 pedestrians were performed, the analysis would be even more complicated.

3.2.3   Summary

In this section, the CSI algorithm was applied to experimental data. The first part **without pedestrians** allowed to compare the results obtained with the CSI algorithm and those obtained with the identification method currently used by V2i. It was shown that the results were **consistent** for all the modal properties (frequencies, damping ratios and modes) of the first two modes, excepted the damping ratio of mode 2. This can be explained by the fact that:

- The location of the shaker was not optimally chosen to capture this mode;
- There is a possible interaction between the cables and the deck;
- The signal was a wide band one so that it excited too much modes at a time.

Concerning the sine sweep excitation, it gave consistent results for the frequencies and mode shapes but the damping ratios were overestimated due to the fact that this type of signal does not allow to have steady-state configuration if the speed of the sweep is too high.

The second part of the tests were realised as several **pedestrians** (1, 5, 8 and 10) **crossed the footbridge back and forth**. The test only implying the pedestrians (no shaker) allowed to determined the **frequency content of the pedestrians**. As the number of pedestrians increased, the acceleration of the structure was higher and the frequency content of the signal widened. However, contrary to the numerical model, the signal looked more like a white noise sequence, as the speed of the pedestrians is not constant in reality and other sources of noise can be present as the wind, the water flowing underneath the footbridge, ...

By applying a random signal around the first frequency of the footbridge, as the pedestrians walked back and forth, one could see that the conclusions joined those made in Section 2.4.2: The **frequency** remained quite **stable** and the **damping ratio** showed an evolution leading to less and less variation as the number of pedestrians increased, translating the **saturation effect** observed in that same section. However, instead of evolving towards lower values, it evolved towards higher ones showing that the vibrations were damped out by the pedestrians. Concerning the second frequency, it was complicated to analyse the results as there were not enough data to analyse. However, a small variation between the damping measured with 8 and 10 pedestrians could be observed: this was due to the fact that in real-life, pedestrians contribute to the damping, even if they are not in the frequency range of interest. Concerning the mode shapes of both modes, they provided consistent results with those obtained thanks to the CSI algorithm applied to the random signal without pedestrians.

Finally, concerning the sine sweep excitations with pedestrians, they should be avoided as only one estimation can be done on the whole signal and the results are really sensitive to the perturbations.

Conclusion

The main goal of this thesis was to study the effect of an increasing noise level on the modal properties of a system identified thanks to the combined subspace identification algorithm. To do so, the CSI algorithm developed in [10] was applied to a numerical model and to experimental data.

In order to develop the simplified numerical model, a preliminary measurement campaign was held on the Tilff cable-stayed footbridge in order to roughly determine its first modal properties. The results obtained were only approximations as no shaker was used for this campaign and simple graphical methods were used in order to determine the modal properties. However, the goal was only to obtain estimations of the parameters in order to build a simplified model to test the CSI algorithm, not to represent the real structure. The model was designed on the BeamZ software, allowing to represent the structure as 2D beam elements. The stays were represented by a single element while the deck was composed of multiple elements. These assumptions were not a problem in this work as there was no interest in obtaining the mode shapes of the cables or the torsion ones of the deck. Thanks to the model, the reference modal characteristics (frequencies, damping ratios and mode shapes) were obtained.

In order to apply the CSI algorithm to the model, some artificial and ambient excitations were defined and imposed on the structure. The response of the structure to those excitations was computed thanks to a time integration method. In this work, the Newmark method was chosen for its high stability. Before applying the CSI algorithm some parameters had to be defined: the number of blocks rows used in the Hankel matrices i and the system model order n. The first one should be at least larger than the maximum order one wants to identify but not too large as the computational time is proportional to i^2 [10]. Concerning the model order, the eigenvalues were plotted in a stabilisation diagram in order to separate the real poles from the spurious ones and to chose the adequate order.

Two types of influence on the identified modal properties were investigated: 1) the influence of the type of excitation when the noise was a random white sequence and 2) the influence of the type of noise, when the noise was represented by pedestrians walking on the footbridge. Concerning the type of excitation, it was observed that when the noise was **outside** the frequency range of interest, all modal parameters (frequencies, damping ratios and modes shapes) were independent of the level of noise in the system and the variability of the results was very low. Indeed, as random signals were used, the simulations had to be repeated several times in order to build boxplots for each level of noise. The observation was even more true if the noise was in lower frequency range than the frequency range of the excitation. When the noise was **inside** the frequency range of interest, the same conclusion could be drawn concerning the frequencies. However, concerning the damping ratios, a progressive degradation of the results towards lower values (compared to the identified value at 0% noise) was observed as the level of noise increased up to 8%. Concerning the bandwidth of the excitation, it should be chosen large enough to cover all the resonance peak in order to correctly identify the damping ratio. However, taking a too large bandwidth is also not recommended as it is better to only excite one mode at a time in order to correctly identify its modal properties.

The OMAX method makes the assumption that the noise is a Gaussian white sequence. However, the force induced by the pedestrians on the footbridge can be described by a sum of sinusoidal forces. In order to determine what was the effect of not having a white noise, some pedestrians walking back and forth on the footbridge were simulated. The results showed that as the number of pedestrians increased, the imposed dynamic charge also increased and the frequency content of the signal widened. However, some dominant frequency components remained, so that the noise was coloured. When the noise was outside the frequency range of interest, the modal properties were close to the identified value at 0% noise, no matter the level of noise. However, when the noise was in the frequency range of interest, the damping also showed a progressive degradation towards lower values but as more pedestrians were added, the effect of the added pedestrian decreased. This can be called a saturation effect. A limit value of pedestrians beyond which the results overcome an acceptable percentage of error cannot be determined as it depends on the system, the frequency studied and the limit value that one wants to set. Concerning the frequencies, they depended on the level of noise contrary to the first case. This was the effect of having a coloured noise: when the white noise assumption is violated, the system considers the noise as poles of the state matrix A.

In order to validate the observations made with the numerical model, the CSI algorithm was applied to experimental data. They were obtained by performing a more detailed measurement campaign on the Tilff cable-stayed footbridge, with the help of a shaker. The first part of the measurements was realised without pedestrians in order to compare the results obtained with the CSI algorithm with those obtained with the method currently used by V2i [2]. The results (frequencies, damping ratios and modes shapes) were in agreement for both first modes excepted the damping of the second one. This can be explained by the fact that: 1) the shaker was not optimally located to capture mode 2; 2) there is a possible interaction between the cables and the deck for mode 2, making the identification more complicated; 3) the excitation was a wide band random signal (from 1 to 7 Hz) so that it excited several modes at the same time and the results must be filtered in order to obtain stabilisation at low orders. A sine sweep excitation was also realised. It gave consistent results for the frequencies and mode shapes but the damping ratios were overestimated due to the too high speed of the sweep.

The second part of the measurements was done by adding several (1 - 5 - 8 - 10) pedestrians walking back and forth on the footbridge in order to assess their influence on the modal parameters. Contrary to the numerical model, the recorded frequency spectrum for the pedestrians did not show major frequency components as a background noise was also recorded. This one could be due to the wind or the flow of water flowing underneath the footbridge. The same saturation behaviour for the damping ratio as in the simulations was observed. However, the evolution of the median values was towards higher values in this case. Indeed, the pedestrians can increase the damping ratio by walking in opposition of phase with the vibrations. However, they could also decrease it if they start to walk in phase with the vibrations. This behaviour is called synchronisation. Concerning the sweep signals, it is advised to not use them for experimental testing as several estimations cannot be obtained contrary to a random signal where several portions of the signal can be taken in order to realise a moving average.

Finally, the content of this thesis might be used as a basis for an article that will be written in the scope of the Eurodyn conference (Delft, 2023) [29].

Improvements and Perspectives

Here are some improvements and perspectives about what could be done in a future work:

- It could be interesting to study a footbridge whose finite element model is available. So that tests could be done numerically on an accurate model and be compared with the tests on the real structure. Moreover, if the mode shapes are known beforehand, it will be easier to define the setup for the measurement campaign.

- The accuracy of the modes could be assessed by computing the modal assurance criterion.

- To generate the pedestrians' weight, a normal distribution could be used and the pacing rate of the pedestrians could be changed along time to take into account the fact that a normal people does not always walk at the same speed. Moreover, concerning the dynamical load factors, many values exist. A summary of all the possible coefficient can be found in Table 11 of [30]. A more detailed description of the pedestrian loads can also be found in this thesis if needed.

- The simulations with the pedestrians could be redone but by adding an additional background white noise to take into account the other sources of noise such as the wind, the traffic or water under the footbridge, ...

- When the assumption of white noise is violated, the CSI algorithm can be modified in order to take the noise correlation into account by introducing some weights. However, in practical cases, this correlation is not known which makes the extent of the use of the method consequently reduced. More information can be found in [10].

- The experimental tests could be realised with the shaker only, then the pedestrians only and finally both excitations at the same time. Those measurements should all be realised with the same configuration and with the same imposed force by the shaker to be comparable. Only one mode at a time should be excited to obtain accurate results. This will allow to define the percentage of noise as in the simulations and to compare the three methods (EMA, OMA and OMAX).

- In the measurement campaign more accelerometers or more setups could be defined in order to obtain more accurate modes (higher density of measurement points on the footbridge).

- The experimental tests could also be realised with smartwatches to measure the average pacing rate of the pedestrians or by imposing a pacing rate thanks to a metronome, to assess its effect.

A   Appendices

A.1   Results for the modal properties of the third frequency when noise is a white random sequence

In order to validate the observations made in Sections 2.3.1.1 and 2.3.2.1, the tests were also performed for the third frequency of the system which was at 4.16 Hz with a damping ratio of 0.55%. Of course, the definition of noise and the time step had to be adapted to that case. Table 15 shows the parameters used for these tests and Figures 74 and 75 show the obtained results for the modal properties.

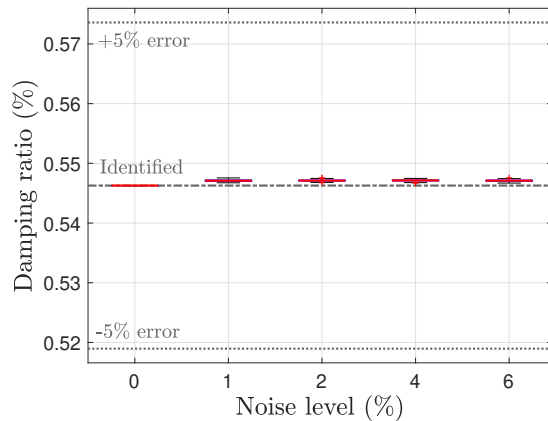| Parameters	Values
Low noise	2 to 3 Hz
High noise	4 to 5 Hz
Time step	0.008 s

Table 15: Parameters used for the identification of the third frequency of the system ($f_3 = 4.16$ Hz, $\zeta_3 = 0.55\%$).
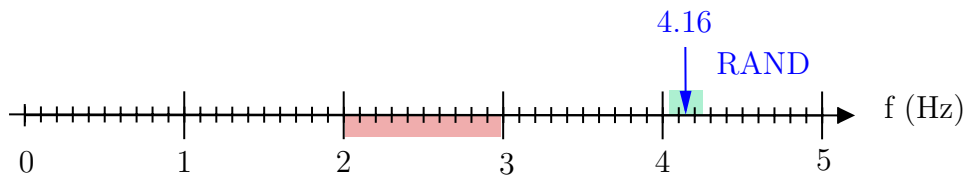
(a) Illustration of the case tested. The green box shows the range of the known excitation and the red one, the range of the unknown noise.
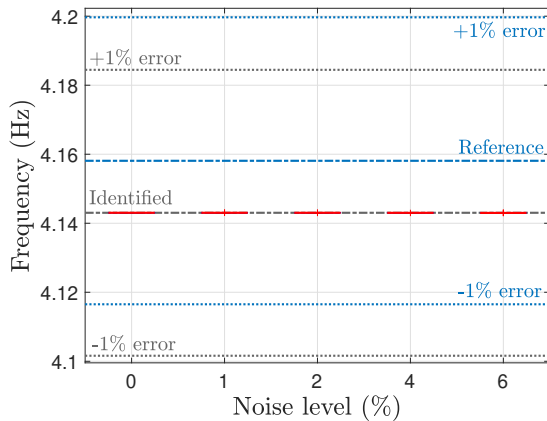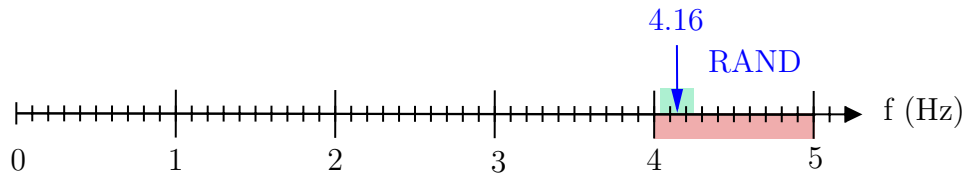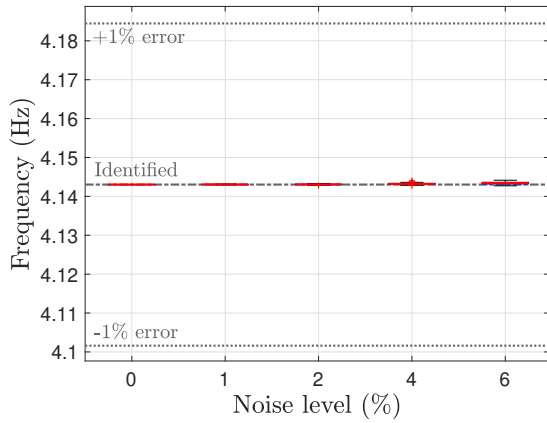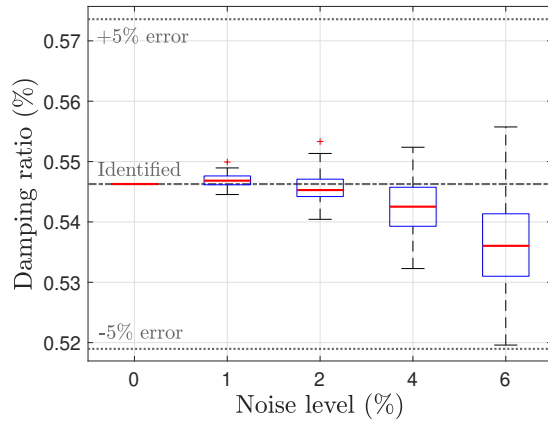

(b) Frequency.

(c) Damping ratio.

Figure 74: Results for the identified modal parameters of the system computed with the CSI algorithm for a low unmeasured noise outside the frequency range of interest and a known random signal of 0.2 Hz bandwidth around frequency 3 (4.16 Hz).

74

(a) Illustration of the case tested. The green box shows the range of the known excitation and the red one, the range of the unknown noise.

(b) Frequency.

(c) Damping ratio.

Figure 75: Results for the identified modal parameters of the system computed with the CSI algorithm for a high unmeasured noise inside the frequency range of interest and a known random signal of 0.2 Hz bandwidth around frequency 3 (4.16 Hz).

So that the hypotheses that:

- The frequency is stable no matter whether the noise is in the frequency range of interest or not;

- The damping is stable when the noise is outside the frequency range of interest;

- As the level of noise is increased, the damping ratio shows higher variability in the results and the medians converge towards lower values compared to the identified value, when noise is inside the frequency range of interest,

are confirmed.

A.2 Variation of the bandwidth and type of signal for the second frequency of the system

In order to validate the observations made for mode 1 concerning the change in bandwidth and in excitation type when the noise was inside the frequency range of interest (Section 2.3.2.3), the simulations were also performed for mode 2. Instead of a 0.2 Hz frequency band, the results will now be presented for an increased bandwidth (0.6 Hz) in Figure 76b. The signal can also be changed for a sweep and the results for the damping ratio can be observed in Figure 76c. Once again, the graph for the frequencies and mode shapes will not be shown as the conclusion does not change from the other graphs: they remain constant no matter the level of noise.
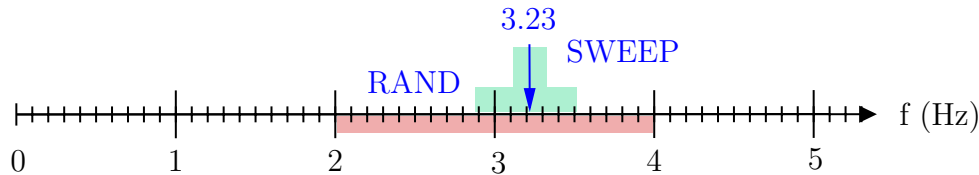
(a) Illustration of the case tested. The green box shows the range of the known excitation and the red one, the range of the unknown noise.
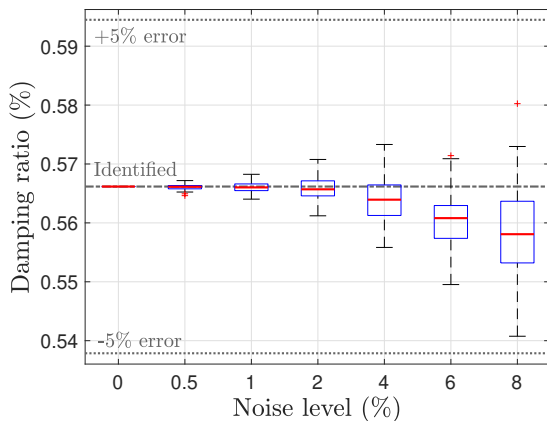
(b) Increased bandwidth.
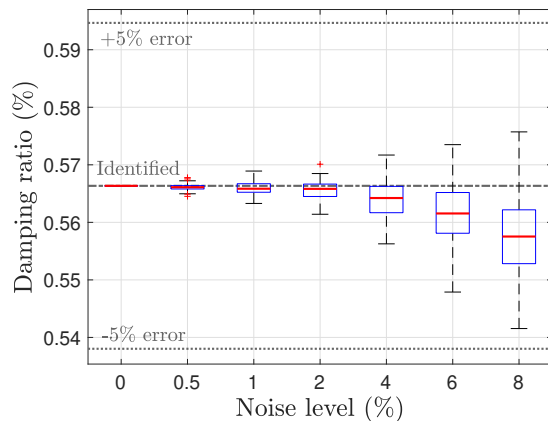
(c) Sweep signal.

Figure 76: Results for mode 2 when noise is in the frequency range of interest

The variability in the results decreases only for small percentage of noise but the difference is less and less perceptible as noise increases. Indeed, it can be seen that for a noise $< 2\%$, the median is more centered on the identified value but the difference is not really noticeable for a higher percentage of noise. Moreover, the difference between the medians for the case with a 0.2 Hz or a 0.6 Hz bandwidth are very small (of the order of 1% or less). The same is observed for the sweep signal.

A.3 History of the perturbations (for the tests with pedestrians)

Table 16 shows the history of the perturbations recorded for the tests with pedestrians.

Number of pedestrians	Starting hour	Tested signal	Perturbations
10 people	13:45	Sweep around 1.59 Hz	/
	13:55	Sweep around 3.68 Hz	Cyclists at 13:55 (1) and 13:59 (1) Pedestrians at 14:00 (1), 14:03 (1), 14:04 (1) and 14:07 (1)
	14:11	Random around 1.59 Hz	Cyclist at 14:17 (1)
	14:22	Random around 3.68 Hz	/
8 people	14:37	Sweep around 1.59 Hz	Pedestrian at 14:39 (1)
	14:48	Sweep around 3.68 Hz	Pedestrians at 14:48 (1), 14:56 (1) and 14:59 (1) Motorbikes at 14:58 (3)
	15:05	Random around 1.59 Hz	/
	15:15	Random around 3.68 Hz	/
5 people	15:30	Sweep around 1.59 Hz	Pedestrians at 15:30 (3), 15:32 (3), 15:36 (1), 15:37 (2) and 15:39 (2) Cyclist at 15:33 (1)
	15:45	Random around 1.59 Hz	Cyclist at 15:48 (1) Pedestrians at 15:48 (6)
1 person	16:02	Sweep around 1.59 Hz	Cyclist at 16:04 (1)
	16:18	Random around 1.59 Hz	Pedestrians at 16:19 (1), 16:23 (1) and 16:17 (2)

Table 16: History of the perturbations recorded for the tests with pedestrians. The numbers between parenthesis are the numbers of pedestrians/cyclists that perturbed the measurement at the given time.

References

[1] *V2i - From Vibrations to Identification (website).* Accessed on 27th of December 2022. URL: https://v2i.be.

[2] H. Güner et. al. *Dynamic identification of lightweight civil engineering structures using a portable shaker.* 2022.

[3] Groupe de travail SETRA / AFGC. *Guide pour la prise en compte du comportement vibratoire des passerelles piétonnes.* 2004.

[4] Edwin Reynders et. al. *Combined Experimental-Operational Modal Testing of Footbridges.* 2010.

[5] Edwin Reynders et. al. *Reference-based combined deterministic–stochastic subspace identification for experimental and operational modal analysis.* 2007.

[6] E. Parloo et. al. *Sensitivity-based operational mode shape normalization. Mechanical Systems and Signal Processing.* 2002.

[7] M. S. Cao et. al. *Structural damage identification using damping: a compendium of uses and features.* 2017.

[8] N. Barbieri and E. Caetano. *Operational Modal Analysis of a Footbridge.* 2019.

[9] A. Deraemaeker et. al. *Vibration-based structural health monitoring using output only measurements under changing environment.* 2007.

[10] Van Overschee P. and De moor B. *Subspace identification for linear systems: theory - implementation - applications.* 1996.

[11] Edwin Reynders et. al. *OMAX testing of a steel bowstring footbridge.* 2011.

[12] T. De Troyer et. al. *Combined use of FRFs and transmissbility functions in an OMAX framework.* 2010.

[13] ULiège. *MatheO: Master Thesis Online.* Accessed on 30th of December 2022. URL: https://matheo.uliege.be.

[14] Vincent Denoël. *Footbridge Vibrations Tilff.* Accessed on 30th of December 2022. URL: https://www.youtube.com/watch?v=AyxZPc3WvcY.

[15] Sinin Hamdan et. al. *Dynamic property analysis and development of composite concrete floor (CCF) and vibration serviceability: A review.* 2011.

[16] Vincent Denoël. *Notes de cours et syllabus (documents pédagogiques) - Analyse des Structures II.* Accessed on 31th of December 2022. URL: https://orbi.uliege.be/handle/2268/130616.

[17] Vincent Denoël & René Maquoi. *The concept of numerical admittance.* 2012.

[18] Functionbay. *What are the differences between the implicit method and the explicit method?* Accessed on 17th of December 2022. URL: https://support.functionbay.com/en/faq/single/263/differences-implicit-method-explicit-method.

[19] Jean-Claude Golinval. *MECA0029-1, Theory of vibrations, course notes.* 2019.

[20] Bart Peeters et. al. *Reference-based SSI for output only modal analysis.* 1999.

[21]   Mathworks. *Visualize summary statistics with box plot - MATLAB boxplot.* Accessed on 2nd of December 2022. URL: https://www.mathworks.com/help/stats/boxplot.html.

[22]   Jean-Claude Golinval. *MECA0062-2, Vibration testing and experimental modal analysis, course notes.* 2021-2022.

[23]   H. Bachmann and W. Ammann. *Vibrations in Structures: Induced by Man and Machine. Structural Engineering Documents.* 1987.

[24]   *Technical sheet of the wireless accelerometers G-Link-200 8G.* Accessed on 29th of December 2022. URL: https://www.mouser.be/datasheet/2/1083/g_link_200_datasheet_8400_0102_rev_h-2399698.pdf.

[25]   Luigi Carassale et. al. *Wavelet-based identification of rotor blades in passage-through-resonance tests.* 2017.

[26]   Christoph Heinemeyer et. al. *Design of Lightweight Footbridges for Human Induced Vibrations.* 2009.

[27]   Wikipedia. *Broughton Suspension Bridge.* Accessed on 31th of December 2022. URL: https://en.wikipedia.org/wiki/Broughton_Suspension_Bridge.

[28]   E. Shahabpoor et. al. *Effect of group walking traffic on dynamic properties of pedestrian structures.* 2016.

[29]   TUDelft. *EURODYN2023.* Accessed on 31th of December 2022. URL: https://eurodyn2023.dryfta.com.

[30]   Veronica Cancelinha Da Costa. *Identification of pedestrian loads on a very flexible footbridge.* 2020-2021.